AN ABSTRACT OF THE THESIS OF

Claudia Gabriela Mayorga Adame for the degree of Master of Science in Oceanography
presented on March 9, 2010.
Title: Development, Performance Evaluation and Application of a Physical Model of the Kenyan-Tanzanian Coastal Region.

Abstract approved:

_____

P. Ted Strub Harold P. Batchelder

A Regional Ocean Modeling System (ROMS) application for the coastal region of Kenya and Tanzania (0-10° S, 38.7-46.98° E) was developed with the aim of better resolving the circulation patterns in the coastal region that is poorly represented in global models. The model has a horizontal resolution of 4 km, and uses realistic time- and space-varying climatological forcing derived from the National Centers for Environmental Prediction (NCEP/NCAR) reanalysis daily product, and boundary conditions from the OFES global ocean general circulation model. To evaluate the performance of the model, results were compared with satellite sea surface temperature (SST) and altimeter products, as well as temperature and salinity profiles. The climatologically forced model does a reasonably good job of representing the hydrographic fields. Model fields show that there is strong seasonality in the nearshore

circulation, with generally sluggish flows and longer retention times during December, January and February, and strong northward alongshore coastal flow during the rest of the year. Lagrangian particle tracking experiments using the modeled circulation fields were conducted to quantify retention differences between seasons. The particle dispersion patterns observed have important implications for local environmental issues such as ocean disposal and discharge of pollutants and the ability of coral reef organisms to self-seed to local-scale coral reefs and to facilitate dispersal and connectivity among multiple coral reefs on the shelves of Kenya and Tanzania. In addition to the climatologically forced model, two specific contrasting years, 2000 and 2007, were modeled using year specific forcing to examine interannual variability in the hydrographic fields. High variability in the eddy field and SST was observed. The Kenyan-Tanzanian coastal model provides a framework for the study of more detailed physics, biology and chemistry processes of this region, and will enable examination of connectivity among coral ecosystems in East African coastal waters.

# Development, Performance Evaluation and Application of a Physical Model of the Kenyan-Tanzanian Coastal Region

by

Claudia Gabriela Mayorga Adame

A THESIS

Submitted to

Oregon State University

In partial fulfillment of

the requirements for the

degree of

Master of Science

Presented March 9, 2010

Commencement June 2010

Master of Science thesis of Claudia Gabriela Mayorga Adame presented on March 9, 2010.

APPROVED

_____

Co-Major Professor, representing Oceanography

_____

Co-Major Professor, representing Oceanography

_____

Dean of the College of Oceanic and Atmospheric Sciences

_____

Dean of the Graduate School

I understand that my thesis will become part of the permanent collection of Oregon State University libraries. My signature below authorizes release of my thesis to any reader upon request.

_____

Claudia Gabriela Mayorga Adame, Author

ACKNOWLEDGMENTS

I would like to thank Fulbright and COMEXUS for their financial support which made my studies possible. Thanks to NSF/NOAA for the additional support. And to the “Zanzibar Project” group for enriching this work with a field experience in Tanzania.

I am especially grateful to my co-advisors Ted Strub and Hal Batchelder, for their constant support, advice and mentoring. This work would have not been possible without their help. I also thank the members of my committee Yvette Spitz, Ricardo Matano and Staci Simonich for their feedback in the making of this manuscript.

I would also like to express my gratitude to:

- Those near and far, always available for a modeling conversation: Andrey Kough, Scott Durski, David Rivas-Camargo, Alexande Kurapov,Vincent Combes and Javier Zavala-Garay.

- The COAS community, especially my classmates, officemates and colleagues: Laurel Kellner, Ata Suanda, Brian Nelson, John Osborne, Dongwha Sohn, Alex Jonko Peter Gaube, Robyn Matteson, Diego Figueroa, Martin Hoecker-Martinez, Sangil Kim, Sam Kelly, Levi Kilcher, Satoshi Kimura, Amy Vendehey, Jacqui Tweddle, Emily Lemagie and Linda LaFleur. It was great to learn with you and thanks for helping me deal with this “North-American life”.

- All my professors at OSU for their efforts in sharing what they know. I appreciate what each of you taught me, and I am indebted to you for enriching my life with your knowledge.

- My lovely family, always with me despite the distance. A very special thanks to my mom for her eternal support, inspiration and encouragement to always continue farther.

- Italo Bravo Tapia, my dear husband, thanks for all your love, help and care, and especially for your patience in the stressful moments of this journey.

- And finally, to all my friends who have made Corvallis a nicer place to be.

TABLE OF CONTENTS

TABLE OF CONTENTS (Continued)

Page

LIST OF FIGURES

Figure Page

LIST OF FIGURES (Continued)

Figure Page

LIST OF FIGURES (Continued)

Figure Page

LIST OF FIGURES (Continued)

Figure Page

LIST OF TABLES

Table Page

**Development, Performance Evaluation and Application of a Physical Model of the Kenyan-Tanzanian Coastal Region.**

## 1. Introduction

The circulation in the Indian Ocean is different from that of the Pacific and Atlantic Oceans, due to its unique characteristics: it has a northern land boundary that restricts the northern extent to $26^{o}$N; and it is subject to an annual monsoon cycle characterized by surface winds that reverse seasonally north of $10^{o}$ S (Wiggert *et al*, 2006). The flow of equatorial-subtropical water from the Pacific into the Indian Ocean through the Indonesian passages, known as the Indonesian Through-flow, is also a distinctive characteristic of the Indian Ocean (e.g. Meyers, Bailey, & Worby, 1995 in Schott and McCreary, 2001). The Southern Indian Ocean has a dynamical connection with the Atlantic and Pacific Ocean through the Agulhas Current and the Antarctic Circumpolar Current (ACC), making it an important link in the global circulation (Mishra *et al*, 2007). Within this larger picture, the circulation along the East African coast modifies the regional water masses through interaction between coastal and inshore waters with the water masses of the large scale currents (Sen Gupta and Desa, 2001).

The large scale circulation in the Indian Ocean follows Sverdrup dynamics. In the northern hemisphere region of the Indian Ocean, the curl of the wind stress is negative during Boreal summer and positive during winter due to the reversal of the

monsoon winds. This causes a semiannual change in the direction of rotation of what would be the northern subtropical gyres on the Atlantic and Pacific Oceans. South of $10^{o}$S the general circulation is similar to that of the other oceans. The Southeast Tradewind regime is present year-round, with a significant annual cycle superimposed, allowing the South Equatorial Current (SEC), East African Coastal Current (EACC), Northeast and Southeast Madagascar Currents (NEMC and SEMC) and the Leeuwin Current (LC) to maintain their direction throughout the year. The semiannual change in direction of the wind forcing over the northern Indian Ocean generates a particularly dynamic circulation, characterized by the semiannual reversal of the East and West Indian Coastal Currents (EICC and WICC), the Southwest and Northeast Monsoon Currents (SMC and NMC). The Somali Current (SC), and the South Equatorial Counter Current (SECC) disappear during the southwest monsoon. This is known as the monsoon circulation and is predominantly wind-driven, although in some locations it is modified by heat and fresh-water fluxes. Figure 1a and 1b show a schematic representation of the circulation during the summer and winter monsoons (Schott and McCreary, 2001).

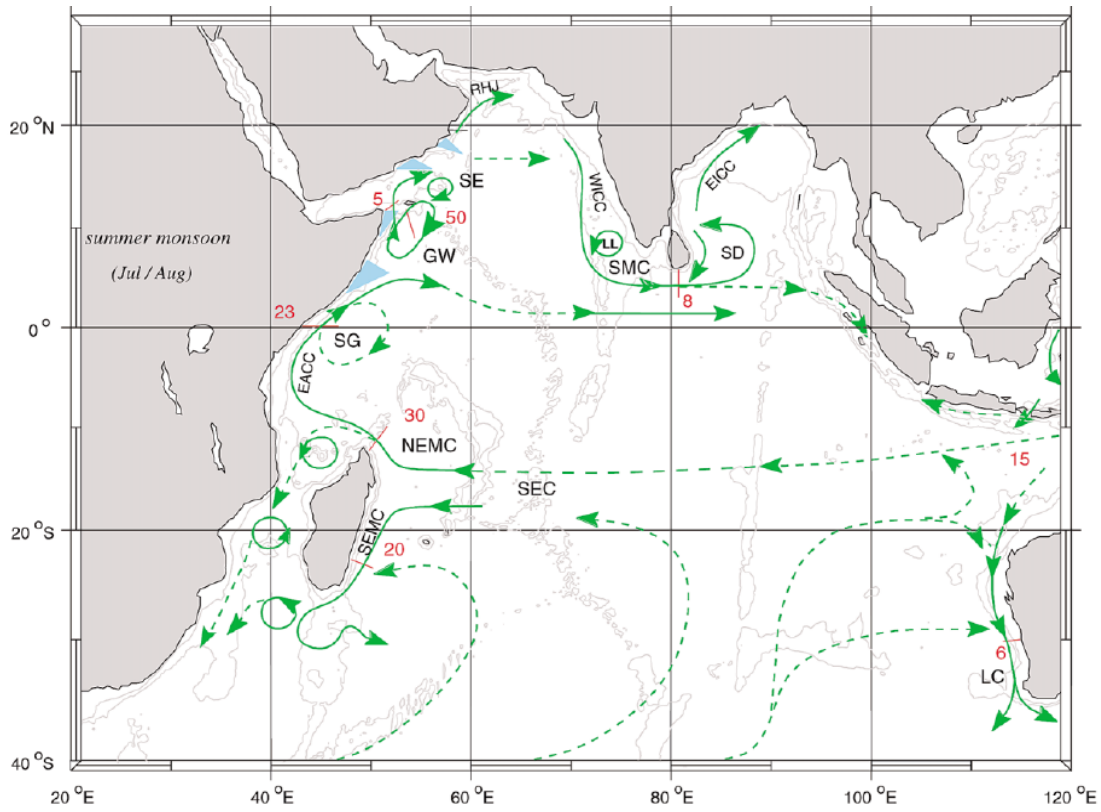


**Figure 1a. A schematic representation of identified current branches during the Southeast Monsoon (Africa) (SW monsoon for the Asian continent), including some choke point transport numbers (Sv=$10^6 m^3 s^{-1}$). Current branches indicated (see also Fig. 1b) are the South Equatorial Current (SEC), South Equatorial Countercurrent (SECC), Northeast and Southeast Madagascar Current (NEMC and SEMC), East African Coast Current (EACC), Somali Current (SC), Southern Gyre (SG) and Great Whirl (GW) and associated upwelling wedges, Socotra Eddy (SE), Ras al Hadd Jet (RHJ) and upwelling wedges off Oman, West Indian Coast Current (WICC), Laccadive High and Low (LH and LL), East Indian Coast Current (EICC), Southwest and Northeast Monsoon Current (SMC and NMC), South Java Current (JC) and Leeuwin Current (LC) (after Schott and McCreary, 2001).**

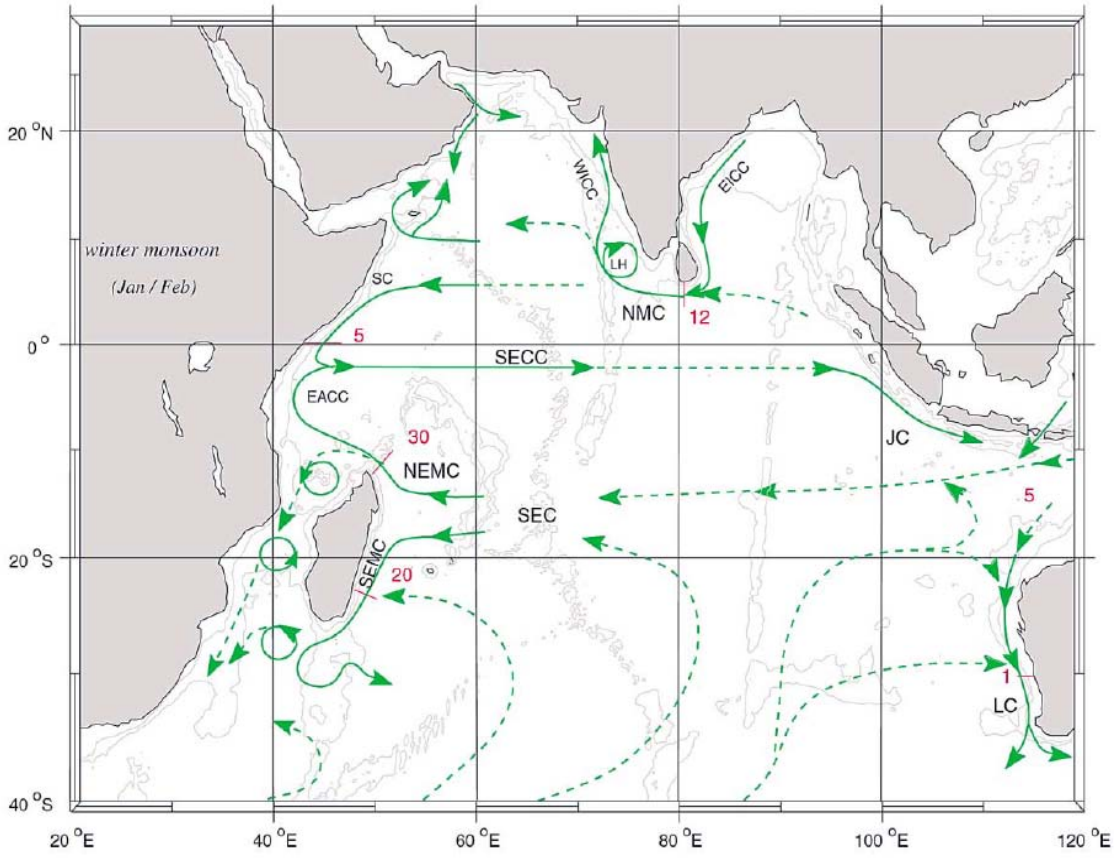


**Figure 1b. As in Fig. 1a but for the Northeast Monsoon.**

This study focuses on the coastal region of Kenya and Tanzania, which has been understudied in comparison to neighboring areas such as the Somali coast, the Arabian Gulf (e.g. Vimal-Kumar *et al*, 2008 , Smith, 1998, 1999, 2000), the Red Sea (e.g. Roman and Lutjeharms, 2009) and the Mozambique Channel (e.g.Van der Werf *et al*, 2010, Da Silva *et al*, 2009, Nauw *et al*, 2008, Matano *et al*, 2002). The coastal circulation off Kenya and Tanzania is mainly influenced by the northward flowing EACC and the seasonally reversing Somali current (Scott and McCreary, 2001). During the NE monsoon the SC flows across the Equator from the north to ~2$^{o}$S,

where it meets the northward EACC. During the SE monsoon the EACC and the SC create a continuous northward current next to the Tanzania and Kenya coast. Coastal water here is a mixture of the water masses of these two large-scale currents, modified by local coastal processes such as mixing with freshwater outflows from rivers, local precipitation, evaporation and solar heating (Sen Gupta and Desa, 2001).

The Tanzanian continental shelf is very narrow, with the 200m isobath approximately 4km offshore, except at the Mafia and Zanzibar Channels, where the shelf width extends 60km offshore. Several islands in Tanzanian waters are of particular importance due to their rich coral reef ecosystems. The Zanzibar Archipelago is composed of several islets and two main islands: Unguja (also known as Zanzibar Island), and Pemba. Mafia island is found farther south. Narrow channels (<60 km width) separate the main islands from mainland Tanzania; the Mafia and Zanzibar Channels are relatively shallow (<40m depth), while the Pemba channel is much deeper (300-500m depth). Kenya borders Tanzania to the north, its continental shelf is also narrow and protected by fringing coral reefs that stretch along the coast, except at the river mouths, where the continental shelf is wider (up to 15 km at the Tana River delta) (Fig 2 & 3) (Odido and Mazzilli, 2009).


**Figure 2. Map of the study area.**

The coastal regions of Kenya and Tanzania are influenced by rivers that supply water, sediments, nutrients and pollution to the ocean. Four main rivers discharge from Tanzania: the Pangani, Wami, Rufiji, and Ruvuma. In central Kenya, the Tana and the Sabaki rivers discharge north and south of Ungwana Bay, respectively (Fig 2). The volume discharge of these rivers varies strongly on seasonal and inter-annual time-scales fluctuating between several thousand $m^3s^{-1}$ to only 70 to 20 $m^3s^{-1}$ during the dry season for the Sabaki and Rufiji rivers (Temple and Sundborg, 1972, Snoussi *et al*, 2007).

The monsoons are the dominant influence on the climate of the region, affecting particularly wind direction and speed, air temperature and rainfall. The northeast monsoon during November to February is characterized by weaker winds

(~6m $s^{-1}$) and higher air temperatures (22-34$^{o}$C). The southeast monsoon from April to September brings lower air temperatures (19-29$^{o}$C) and stronger winds (up to 10m $s^{-1}$), The inter-monsoon periods: March/April and October/November are characterized by winds with lower speed and more variable direction (Odido and Mazzilli, 2009; Scott and McCreary, 2001). There are two rainy seasons: the long rains during March to May and the short rains during November and December, with the maximum precipitation (approximately 20cm/month) occurring during April and May (Odido and Mazzilli, 2009).

Coastal habitat types in Kenya and Tanzania are a mix of coral reefs, estuaries, mangroves and sea grass meadows. The intertidal zone is mainly sandy-muddy flats or rocky reef platforms, while the sublittoral zone consists of extensive seagrass beds and reefs (Odido and Mazzilli, 2009, Richmond, 1997). The coastal region of Tanzania contributes about one third of the national gross domestic product (GDP). Economic activities in the coastal area include subsistence agriculture, fishing, trade and tourism. Mariculture of pearl, fish and seaweed are starting to develop in coastal communities with support from local and international organizations, hoping to make these activities sustainable for the region (Whittick, 2007). In Kenya, coastal tourism accounts for 60-70% of the national tourism industry (~1/8 of the national GDP). Kenyan harbors represent the second most important economic resource after tourism. Some industries, including cement manufactures and petroleum refineries are located at the coast, taking advantage of the port locations. Unfortunately, the industries often

dispose of their sewage and industrial waste in the coastal ocean (Odido and Mazzilli, 2009).

Despite the importance of the marine resources to the economies of coastal communities, management is absent in most cases and detrimental usage is common. Coral stone is mined for building and mangrove forests are exploited for fuel wood and timber at rates that are not sustainable in both Tanzania and Kenya. Key issues affecting the coastal environment that have been identified by local marine science institutions are: 1) over-exploitation of fisheries and other living resources such as mangroves and coral stone, 2) modifications of ecosystems including community structure and/or species composition due to both environmental changes and direct anthropogenic activities, 3) coastal erosion, and 4) pollution from domestic and industrial sewage, solid wastes, and spills (Odido and Mazzilli, 2009).

There is uncertainty about the effects of climate change on the region. According to the International Institute for Environment and Development (IIED), East African temperatures are expected to rise 2 to $4^{o}$ C by 2100. Climatic patterns are becoming less predictable and more severe, with more extreme droughts and floods (Chambwera and MacGregor, 2009). Sea level rise has already had striking and irreversible effects in Tanzania, such as the complete submergence of Maziwi Island, famous for being the most important nesting ground for sea turtles in East Africa in the 1970s (Fay, 1992).

Local issues that impact the sustainability of marine resources along the East African coast need to be addressed promptly, despite the economic limitations of the countries directly involved. Issues such as sea level rise and coral reef conservation that are of global concern, are being addressed through international collaborative efforts such as the Coral Reef Targeted Research and Capacity Building for Management Program (CRTR) with benefits to all participants involved. A better understanding of the large-to-local scale circulation patterns and ocean dynamics of the region at high temporal and spatial resolutions will improve the assessment and the development of solutions to marine environmental problems in the Kenyan-Tanzanian region.

The lack of understanding of coastal dynamics at adequate temporal and spatial resolution makes it difficult to assess the environmental issues faced in the region. There are few studies that focus on coastal dynamics of the East African Coastal region, and they are based on few observations (Swallow *et al*, 1991, Shagude *et al*, 2002). The region is included in the domains of basin-scale modeling studies (Matano *et al*, 2008, Hermes and Reason, 2008, Mishra *et al*, 2007, Anderson *et al*, 1991) and global models (i.e. OFES[1(see Endnotes)], HYCOM[2]), but the spatial resolution is inadequate to give insight at a regional scale, since important topographic features are inadequately represented.

In this study, a modern ocean circulation numerical model is used to hindcast hydrographic structure and ocean circulation off East Africa. Ideally, the flow fields and hydrographic structure (temperature, salinity) produced by a model would be complemented by *in situ* observations of currents and ocean conditions, that would allow validation of model results or even the assimilation of data into models to increase their skill. However, observations of the ocean off East Africa are very sparse. The World Ocean Database[3] 2009 (WOD) shows only 460 vertical temperature profiles in our model domain for the period 2000 to 2007 (our period of study). The number of salinity profiles for the same period is only 38. The lack of continual, long-term records of hydrographic measurements makes it difficult to evaluate the performance of a model. Satellite derived observations of sea surface temperature (SST) and altimeter sea surface height (SSH) that have global coverage are an alternative for this propose, although they can only allow assessment of model performance in the surface layer.

A one-way, nested grid Regional Ocean Model System (ROMS) (Haidvogel *et al*, 2008) application for the Kenyan and Tanzanian region was developed in this study, we refer to it as Kenyan-Tanzanian Coastal Model (KTCM). It has a horizontal resolution of 4km, which allows the shelf circulation and coastal dynamics to be resolved, and a large enough domain (~1000 $km^2$) to capture the influence of large scale features that influence the model through boundary and initial conditions. The goal is to estimate the mean seasonal cycle of the circulation and water properties in

the region. WOD temperature and salinity profiles and satellite derived SSH and SST fields are used to evaluate the fidelity of the model fields. The objective of having a realistic model of the region is to gain understanding of the large-to-local scale circulation patterns and ocean dynamics of the region at high temporal and spatial resolutions and its possible impact on the environmental problems of the Kenyan-Tanzanian coast. After reproducing the climatology with relative success, two years that contrast in SST in the OFES output are modeled. Inter-annual variability is analyzed to characterize changes in the dynamics of the region in recent years. A preliminary investigation using Lagrangian particles is conducted to gain insight into the dispersion patterns produced by the circulation around the Tanzanian islands. Results are related to the circulation's effect on both pollutants and biological material. This 4km resolution regional model has a number of possible extensions that are beyond the scope of this thesis. First, it could be used to examine potential interactions among coral reef habitats in different locations off East Africa. Second, Theiss Research Group is planning to use this model to provide improved boundary conditions for local-scale models (0.5-1.0 km horizontal resolution), like those previously developed for the Zanzibar Channel (Mayorga-Adame, 2007, Moulton *et al*, 2010). These fine-scale models are expected to be more suitable to address environmental issues such as coastal erosion and pollutant dispersal.

## 2. Methods

### *2.1 Model set up*

The Regional Ocean Model System (ROMS) is a 3 dimensional, hydrostatic, terrain following, primitive equation model, described in detail by Haidvogel *et al* (2008). This model is used to simulate the circulation generated by local surface forcing (heat and fresh water fluxes and wind stress), and remote forcing from large scale circulation through boundary conditions (sea surface height (SSH), temperature, salinity and momentum fluxes at the boundaries) in the coastal region of Kenya and Tanzania. The model domain is a rectangular grid that extends from 38 to 47 $^{o}$E and from the equator to 10$^{o}$S (Fig 3). It has a horizontal resolution of 4km and 31 vertical stretched sigma levels.

A realistic bathymetric map for the region (Fig 3) was created by fusing ETOPO-02 data with information from digitized nautical charts of the region and depth measurements collected with sounders by local researchers of the Institute of Marine Sciences (IMS) of the University of Dar Es Salaam (Fig. 4c). It was necessary to include the local data, since ETOPO-02 and Smith and Sandwell 1997 global bathymetry datasets both underestimate the depth of the Zanzibar Channel, showing a depth of only 2m in its central part (Fig 4a). In the final bathymetry used for the modeling experiments the Zanzibar Channel has a more reasonable depth of 20m in its center (Fig 4c). In the eastern open boundary of the model domain, Aldabra and other

smaller islands of the Comoros Archipelago were flattened to 4000m depth to avoid numerical noise at the open boundaries of the model. The real effects of these islands on the circulation of the coast of Kenya and Tanzania are assumed to be negligible due to the distance between them (~1000km) and the shoaling of the ocean bottom towards the coast. The coast line was manually modified to keep the mean features allowed by the horizontal resolution. Only Zanzibar, Pemba and Mafia Islands were included as dry cells in the land mask.

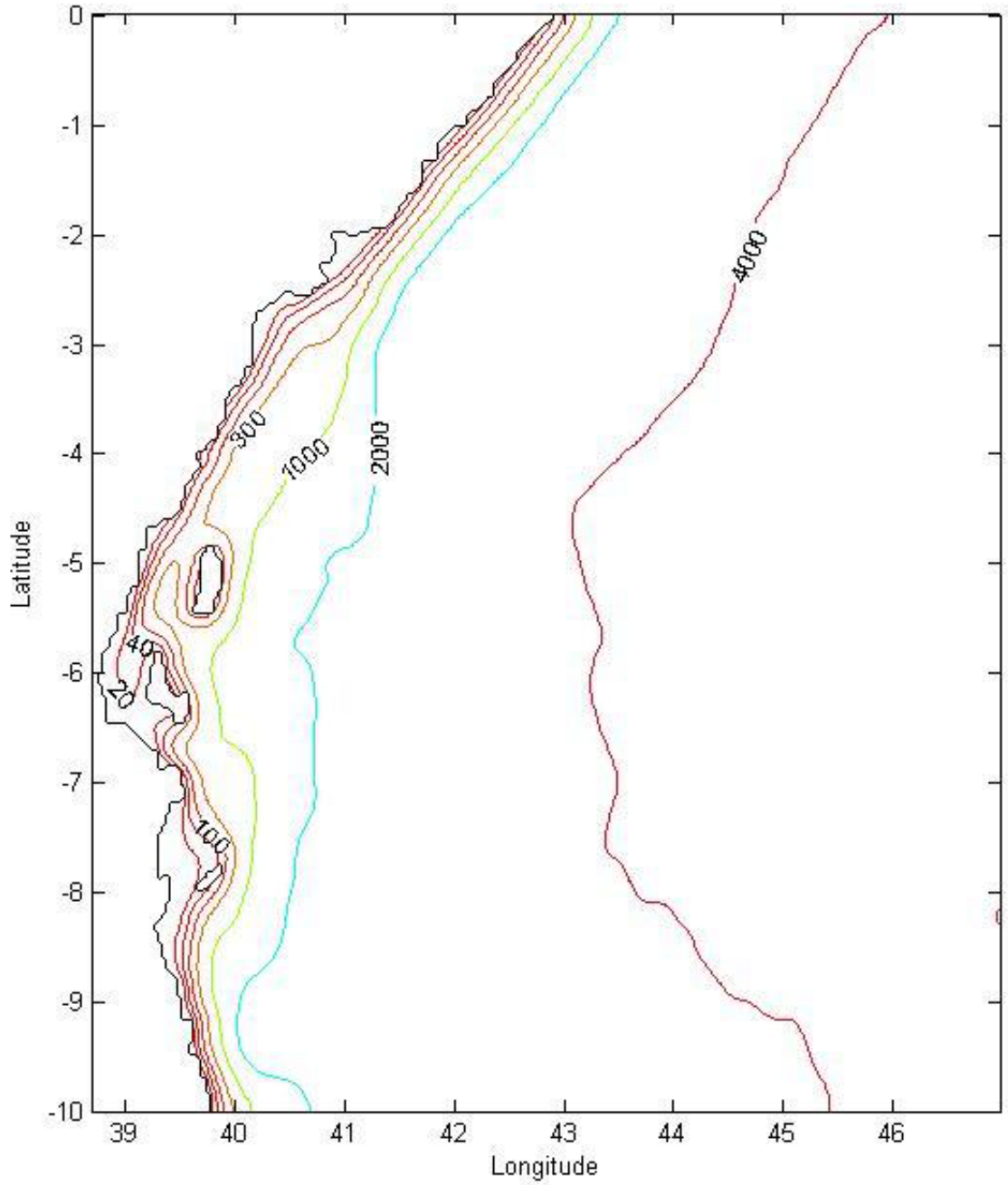


**Figure 3. Model domain with coastline and 20, 40, 100, 300, 2000 and 4000m isobaths. Islands from north to south are Pemba, Zanzibar and Mafia.**

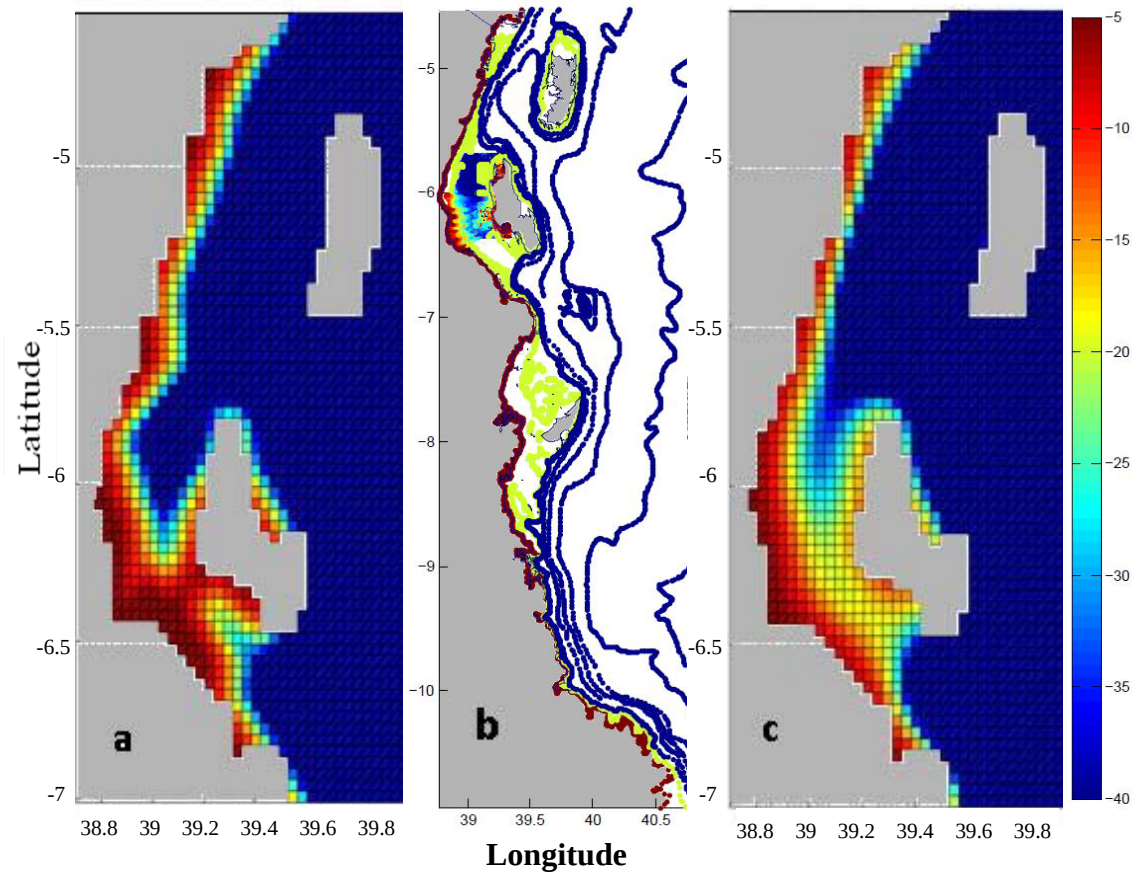


**Figure 4. a) Bathymetry data from Smith and Sandwell (1997) around the Zanzibar Archipelago interpolated to the model grid. b) Depth data provided by researchers from IMS. Isobaths are from digitized nautical charts. Measurements inside the Zanzibar Channel were collected with sounders. c) Final bathymetry of the KTCM model around the Zanzibar Archipelago. Color bar applies to all panels.**

A monthly climatology for the open boundary forcing and a daily climatology for surface forcing were generated taking the 8-year average of the variables from 2000 to 2007. Remote forcing was introduced in the model as monthly open boundary conditions for temperature, salinity, sea surface height, horizontal (u and v) and vertical (w) velocities. These variables were taken from the global Ocean General Circulation Model for the Earth Simulator (OFES) (Masumoto *et al*, 2004 in Aoki *et al*, 2007), which is based on the Geophysical Fluid Dynamics Laboratory's Modular Ocean Model (MOM3) and has a grid spacing of 1/10°. The OFES simulation was forced by daily mean QuickSCAT wind stress and NCEP/NCAR reanalysis atmospheric variables. The OFES simulation compares well with the general circulation of the region reported in previous studies (e.g. Schott *et al*, 2009, Reid, 2003, Schott and McCreary, 2001) and provides adequate resolution to downscale to the desired resolution.In order to use the OFES fields as boundary forcing for the ROMS domain, the fields were re-gridded using linear interpolation to the finer horizontal resolution of the ROMS grid and transformed from Z (constant depths) to sigma (terrain following) stretched coordinates.

Daily climatologies from NCEP/NCAR reanalysis variables were used as surface forcing. We examined differences between modeled SST and satellite observations using two model configurations that differed in the way the surface forcing was applied. In one configuration wind stress and total heat fluxes were provided as surface forcing. The heat flux was corrected by ROMS, to better

reproduce the climatological sea surface temperature (SST) of the OFES model. We refer to this model configuration as 'Qcorrected'. In the other configuration, daily fields of air temperature and pressure, precipitation rate, relative humidity, solar radiation, downward longwave radiation, and the two components of the wind velocity were used as surface forcing. Heat fluxes, fresh water fluxes and wind stress were calculated using ROMS atmospheric bulk formulation. We refer to this configuration as 'Bulk'. In both cases the surface fields were interpolated and re-gridded from their original resolution to the ROMS grid.

For the climatological runs, the model was initialized from an interpolation of the OFES fields corresponding to January 2000 to the ROMS grid and spun up for one year using climatological seasonal forcing. One year was chosen as the optimum period for spin up after examining the results from a four year simulation using repeated climatological forcing. Differences between the $2^{nd}$ , $3^{rd}$ and $4^{th}$ year fields were minor. Simulations using forcing from specific years (2000 & 2007) were initialized from the climatological solution. The 2000 and 2007 years were modeled because in OFES they showed the coldest and warmest spatially averaged SST of the 9 years analyzed, respectively.

Lagrangian particle tracking experiments used ROMS online float tracking code forced by climatological fields. The particles were advected only horizontally and were released weekly at the surface from 10 locations, corresponding to known

coral reefs, within the domain. Particle displacement is calculated from the modeled velocity fields every time step (400 sec), from the release moment until the end of the model runs (1 year). The position of each particle is stored daily.

### *2.2. Data*

In order to compare model results with observations, long-term seasonal climatologies were created from monthly fields for the 2000 to 2007 Pathfinder v5[4] satellite SST and AVISO[5] altimeter sea surface height anomalies (SSHa). Monthly anomalies of the model SSH were calculated by subtracting the annual average from each of the model monthly averages. To make the fields directly comparable, the model results were interpolated to the grids of the satellite products. In the case of SST the interpolation did not imply a change in resolution since both the model and the Pathfinder v5 SST have a grid spacing of 4km. The AVISO SSHa product has a grid spacing of $1/4^{o}$ (~40km) therefore the interpolation implied subsampling the model results at the coarser AVISO grid. Direct comparisons were done by subtracting the modeled SST and SSHa fields from the satellite observations.

The mean SST annual cycles for two regions of the study area were calculated from the OFES results and the two KTCM simulations and compared to the corresponding annual cycles of Pathfinder satellite SST. [Standard deviation and root mean squared error (RMS) of each data set was calculated. The modeled annual cycles were correlated to the satellite observations. The three statistical parameters are

compared in a Taylor diagram that summarizes how closely the patterns of the different models match the satellite observations (Taylor, 2001)]

Temperature profiles of the three models (OFES, 'Bulk' and 'Qcorrected' KTCM) were compared to the available World Ocean Database 2009 profiles, and statistical parameters plotted in a Taylor diagram. A similar comparison for salinity profiles was not possible due to the lack of data and the contamination of it. Since the quantitative comparison was unsatisfactory, we attempt a qualitative comparison with a vertical section of salinity reported in the literature.

# 3. Results

## *3.1 Comparisons to Observations*

### *3.1.1 Modeled Sea Surface Temperature vs. Satellite Observations.*

Temperature in the monthly climatology of the Pathfinder SST product (Fig 5a) ranges from 24 to 30.6$^{o}$C. We refer to temperatures$\leq$ 27 $^{o}$C as relatively cool, and greater than 27$^{o}$C as warm. There is a strong north-south temperature gradient during January and February with cooler temperatures in the north and warmer temperatures in the south of the studied area. Cooler temperatures at lower latitudes, especially extending southward along the coast, are due to the advection of upwelled water from the north by the Somali Current. More uniform warm conditions are observed during March to May and November to December (~inter-monsoon periods). Uniform cool conditions are observed from June to October. The warmest month is April and the coldest is August.

The spatial pattern of SST from the ~10 km OFES model agrees well with the satellite observations (Figs 5a and 5b). However, the OFES SST is always colder than the satellite observations with differences of up to 2.8$^{o}$C (Fig 6a). The differences (OFES-Pathfinder) are smallest during June to September (<1.5$^{o}$C) but never less than +- 0.5$^{o}$C.

Due to the higher spatial resolution, more small scale features are observed in KTCM SST for both the 'Bulk' and 'Qcorrected' configurations (Figs 5c and 5d). The horizontal patterns of the features are very similar in both configurations. The north-south gradient ($|\Delta T| > 1^{o}C$) is observed from December-February, and an east-west gradient with warmer temperatures towards the shelf is observed during May and November when the monsoon seasons are about to begin. The main difference between the results of the two KTCM configurations is that the 'Qcorrected' configuration SST is in general colder than the 'Bulk' configuration SST that is more similar to the satellite observations. This cold bias in the ‘Qcorrected’ simulation is expected from the correction applied to match the SSTs of OFES. Maximum differences between the KTCM 'Bulk' configuration and the satellite data are $\pm 2^{o}C$ compared to $\pm 3^{o}C$ for the 'Qcorrected' configuration (Figs 6b and 6c). The KTCM 'Bulk' model SST fields are within $\pm 0.5^{o}C$ of the satellite observations in much of the domain every month and in almost the entire domain during August to October. Some of the differences observed during the months with higher spatial variability in temperature (Dec to Mar) may be due to the ability of the KTCM model to resolve small scale features that are under-sampled by the satellite due to cloud cover or spatial smoothing when computing the climatological data set.

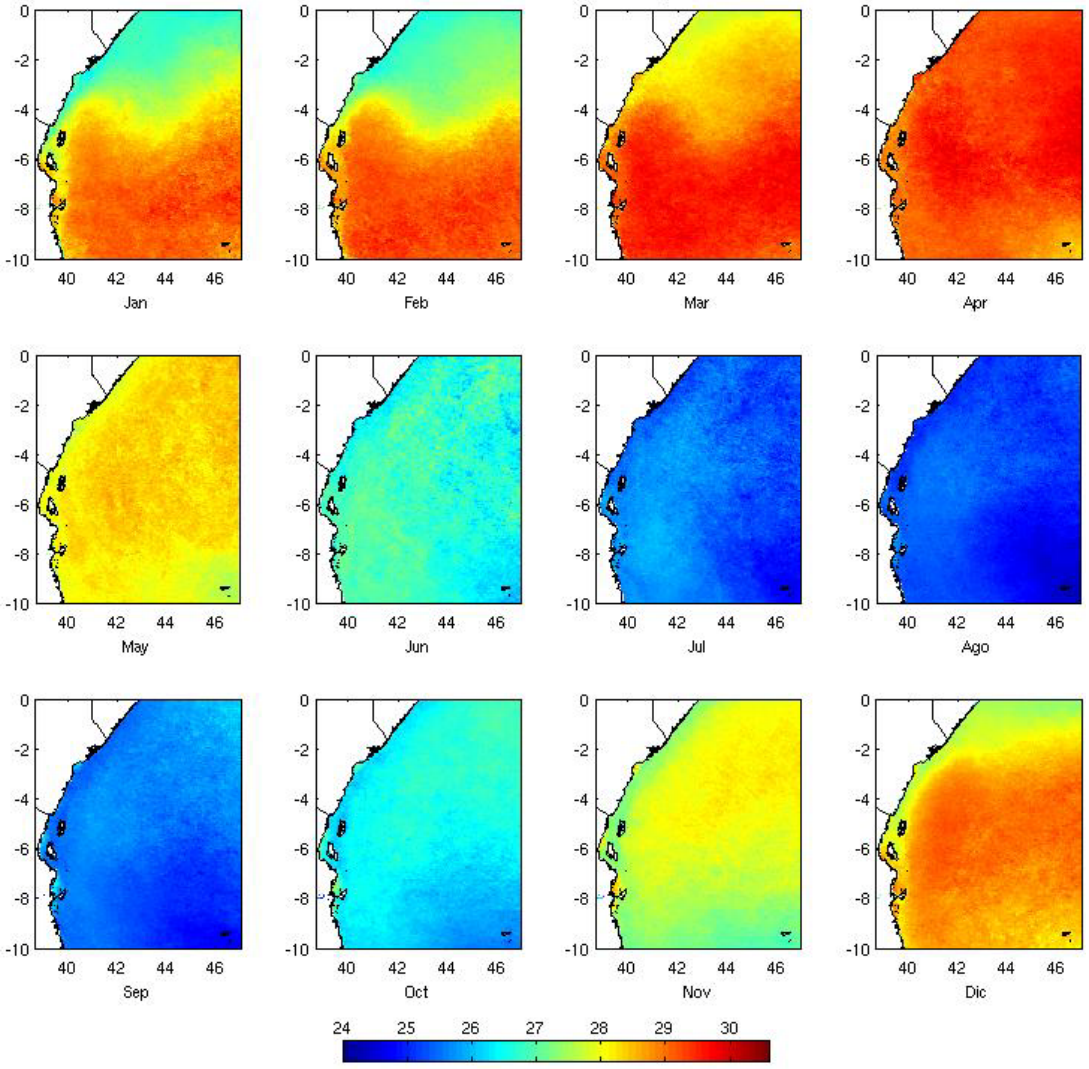


**Figure 5a. Pathfinder v5 monthly climatology of SST ($^{o}$C).**

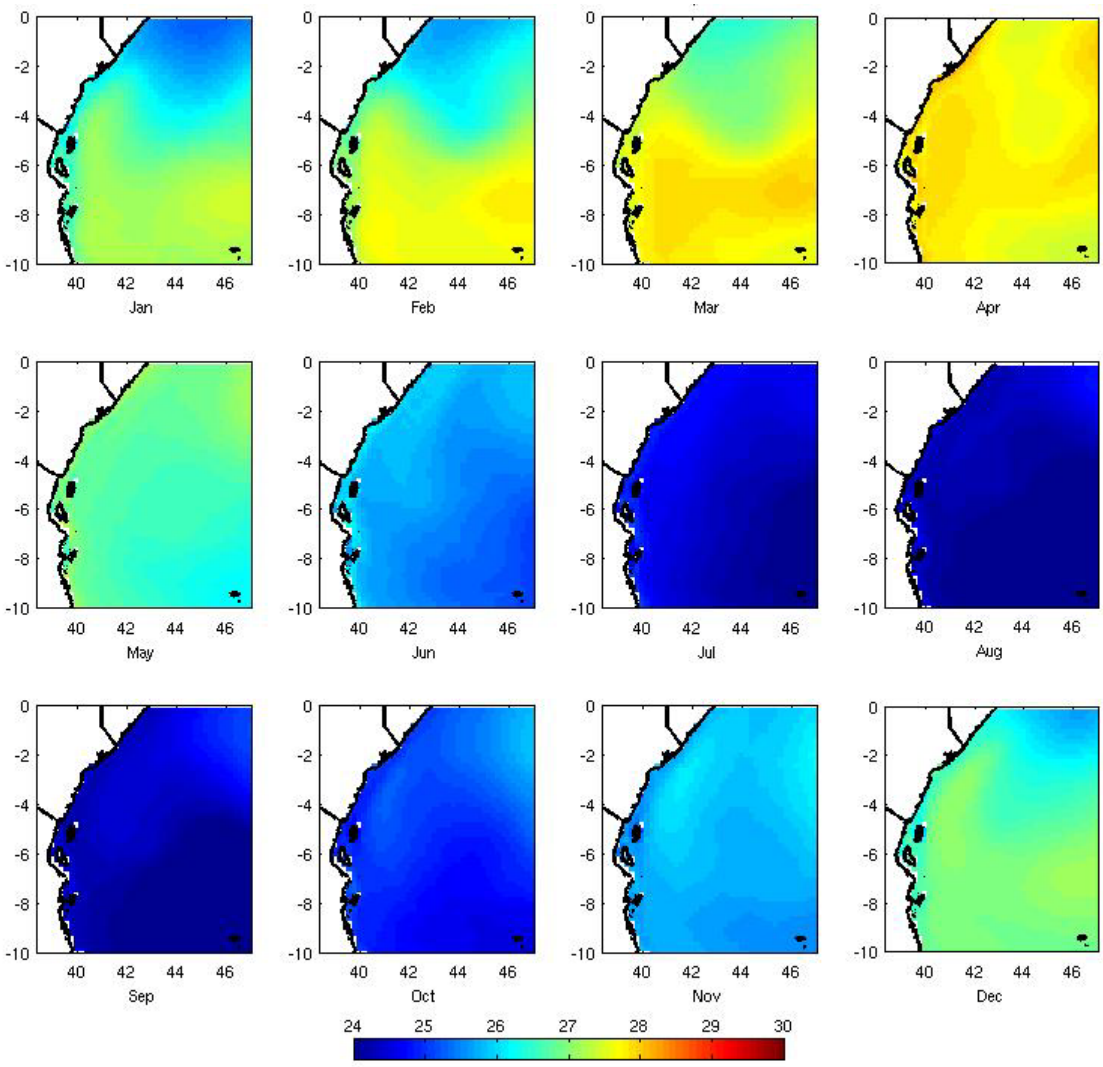


**Figure 5b. OFES monthly climatology of SST (°C).**

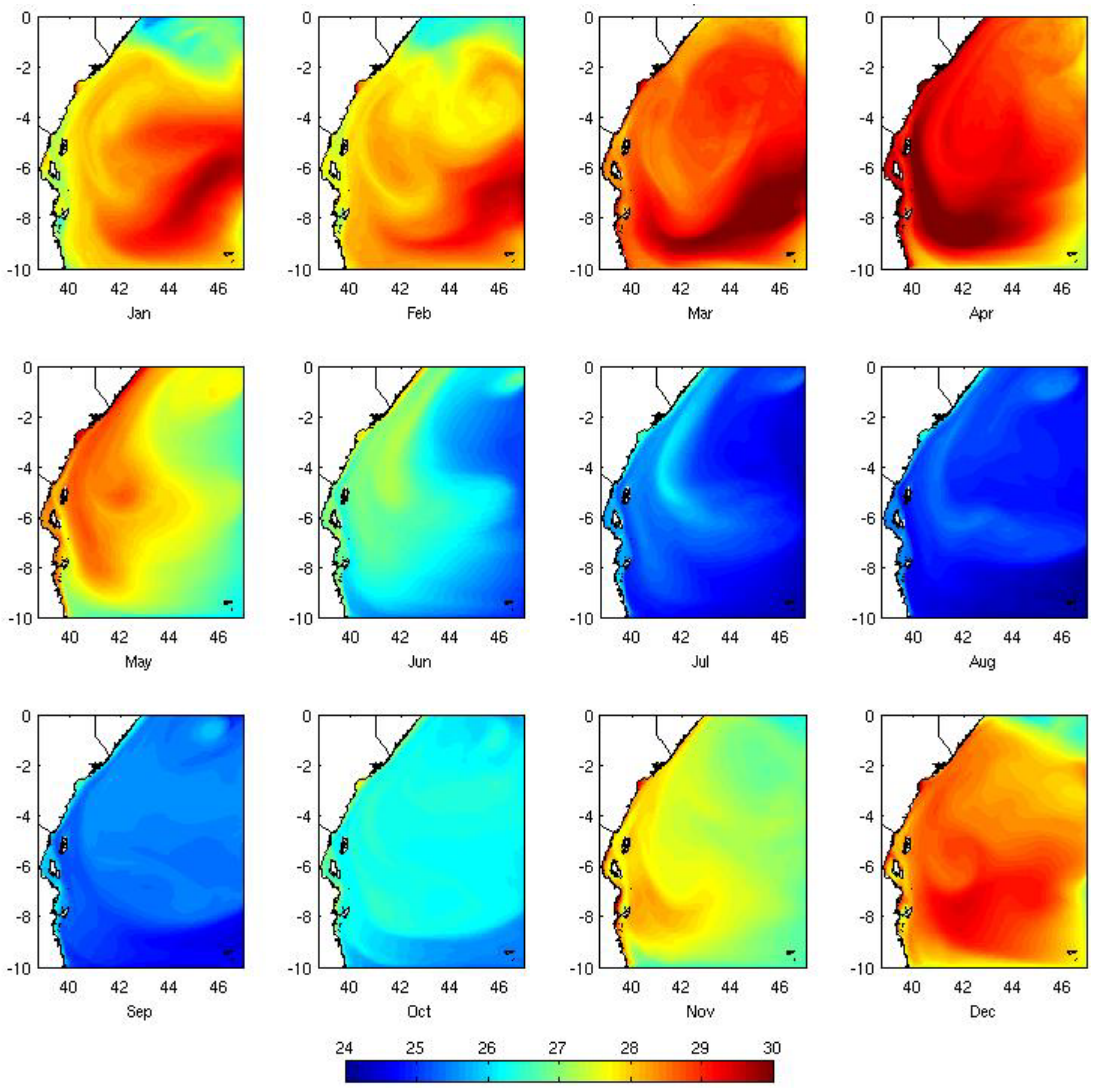


**Figure 5c. KTCM 'Bulk' monthly climatology of SST ($^{o}$C).**

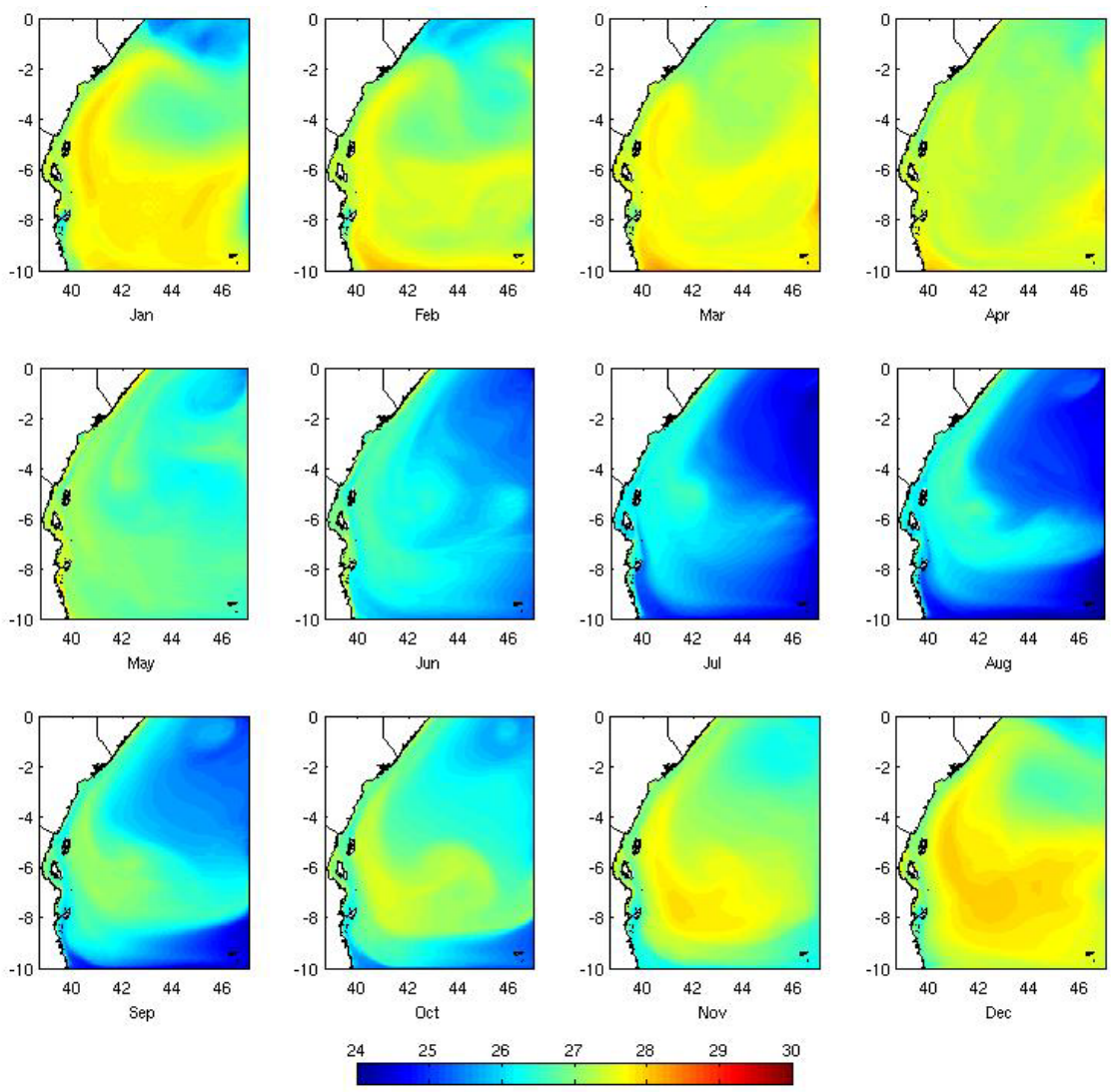


**Figure 5d. KTCM 'Qcorrected' monthly climatology of SST ( $^{o}$C).**

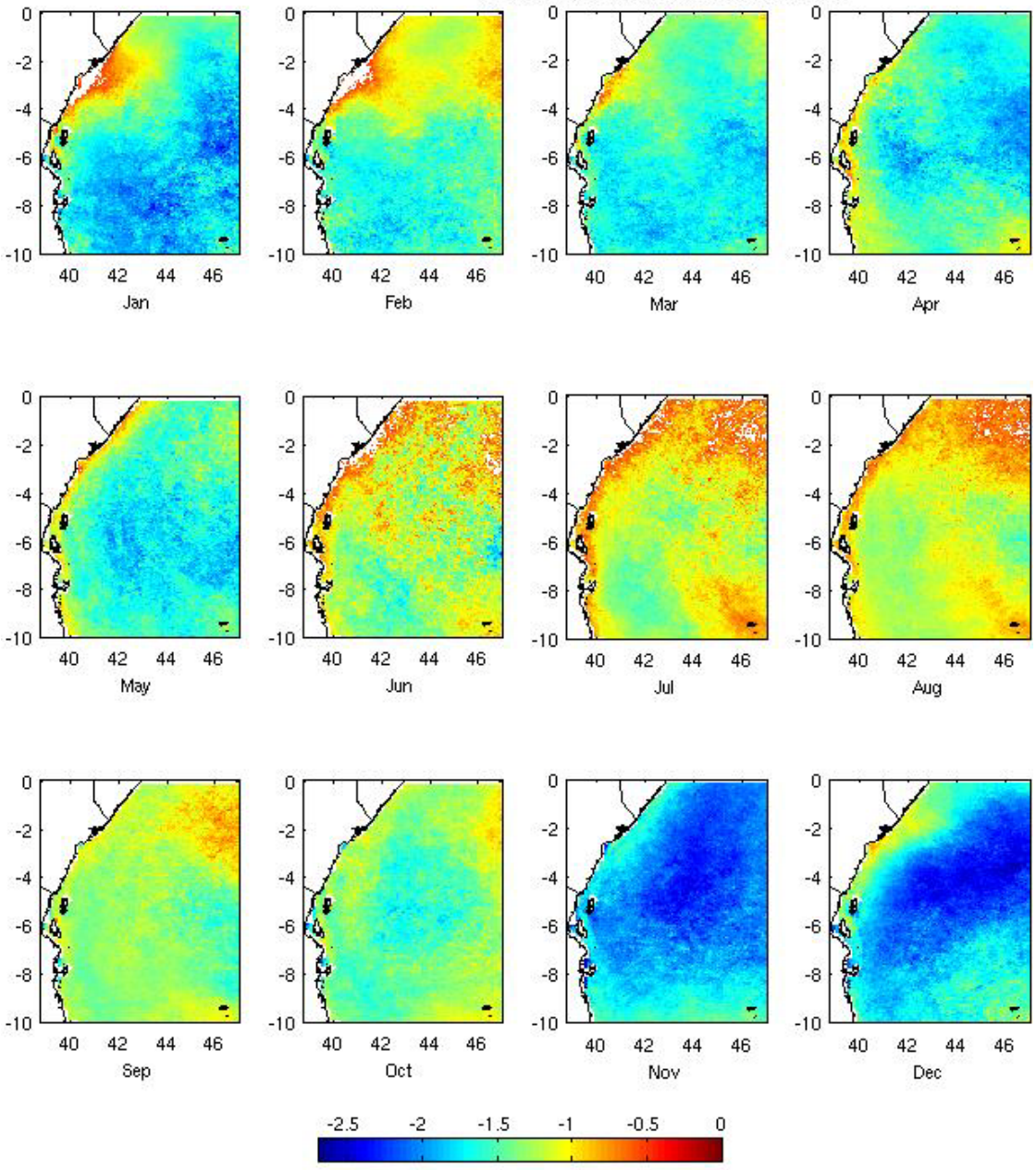


**Figure 6a. Monthly difference OFES-Pathfinder SST ($^{o}$C). Values with an absolute value smaller than 0.5 $^{o}$C have been blanked.**

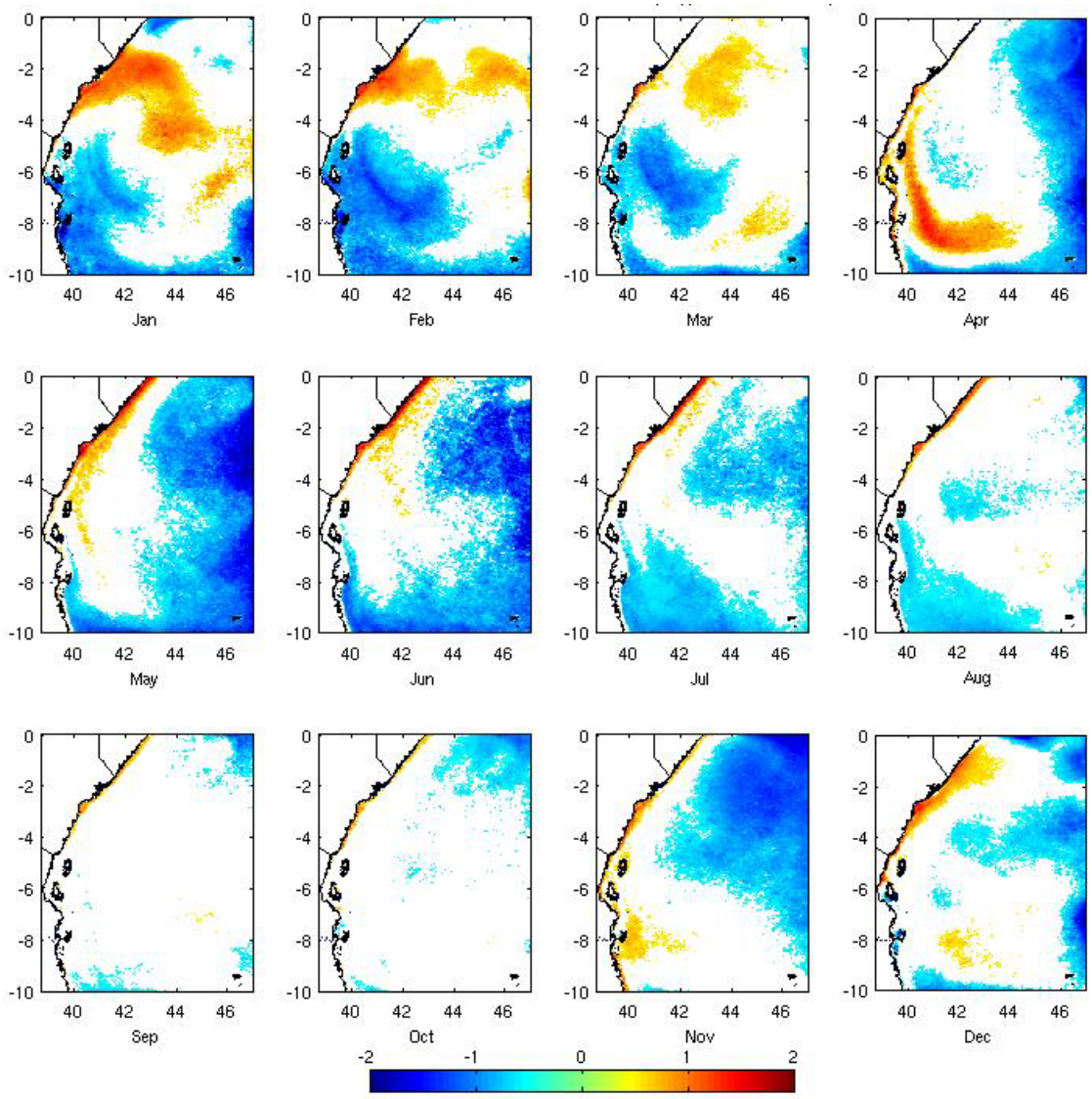


**Figure 6b. Monthly difference KTCM 'Bulk'-Pathfinder SST ($^{o}$C). Values with an absolute value smaller than 0.5 $^{o}$C have been blanked.**

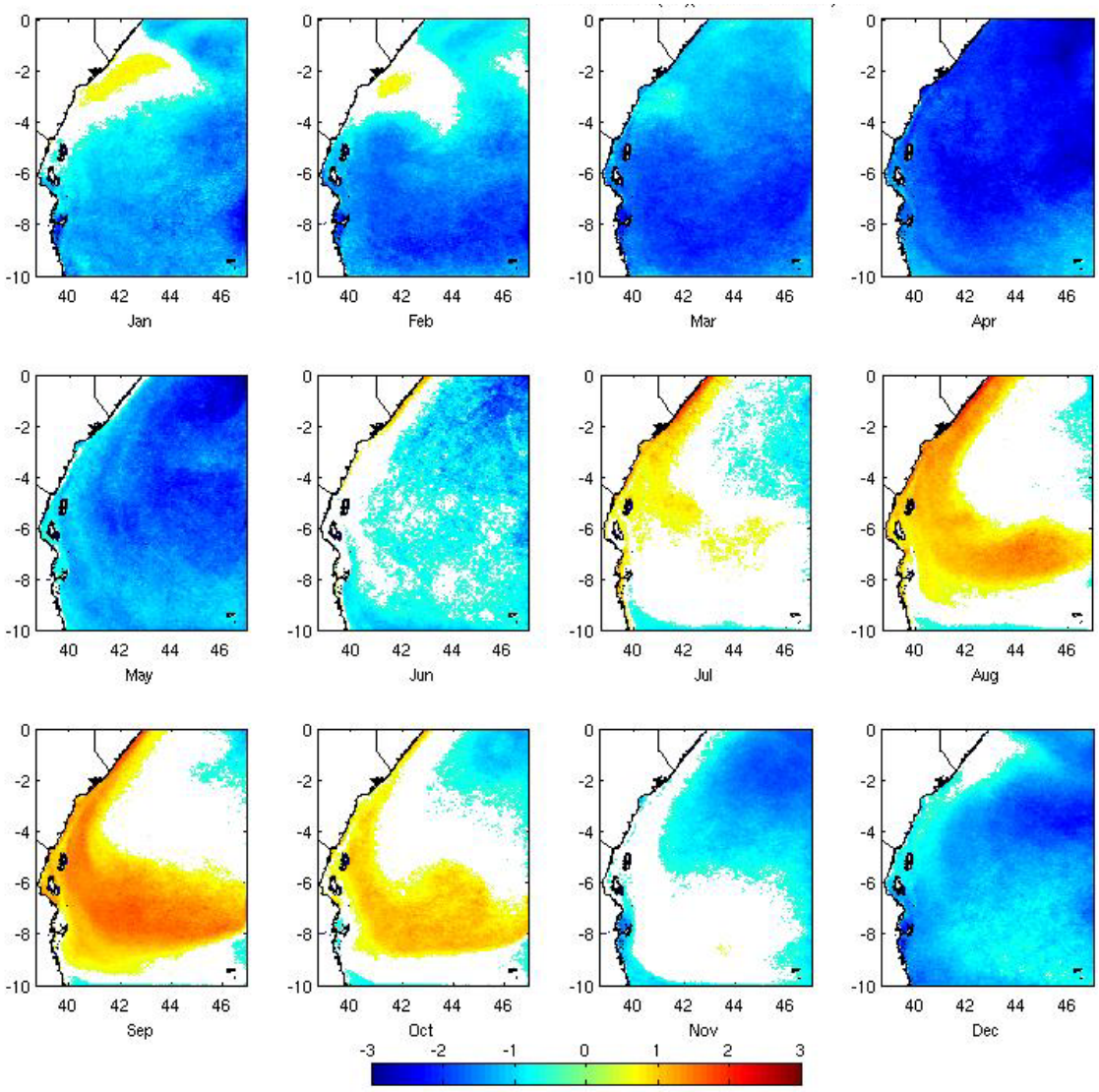


**Figure 6c. Monthly difference KTCM 'Qcorrected'-Pathfinder SST ($^{o}$C). Values with an absolute value smaller than 0.5 $^{o}$C have been blanked.**

To make an overall comparison of the different model's skill to represent SST, separate inshore and offshore SST annual cycles were calculated by taking the spatial averages of the monthly mean SST for the regions inshore and offshore of the 300m isobath for the three models (OFES, 'Bulk' and 'Qcorrected' KTCM) and the Pathfinder satellite data. The standard deviation and root mean squared error (RMS) were calculated for each annual cycle and normalized dividing by the standard deviation of the correspondent Pathfinder annual cycle. The correlation between each of the models inshore and offshore SST annual cycles and the inshore and offshore annual cycles from Pathfinder was also computed. The three statistical parameters are compared in a Taylor diagram that summarizes how closely the patterns of the different models match the satellite observations (Taylor, 2001) (Fig. 7). The diagram shows that the Bulk KTCM and OFES have similar skill, while the Qcorrected KTCM has significantly less skill at representing the pattern of SST in both the inshore and offshore regions. The variability of the Bulk KTCM model SSTs is very similar to the satellite observed SST and correlation coefficients are higher than 0.95.

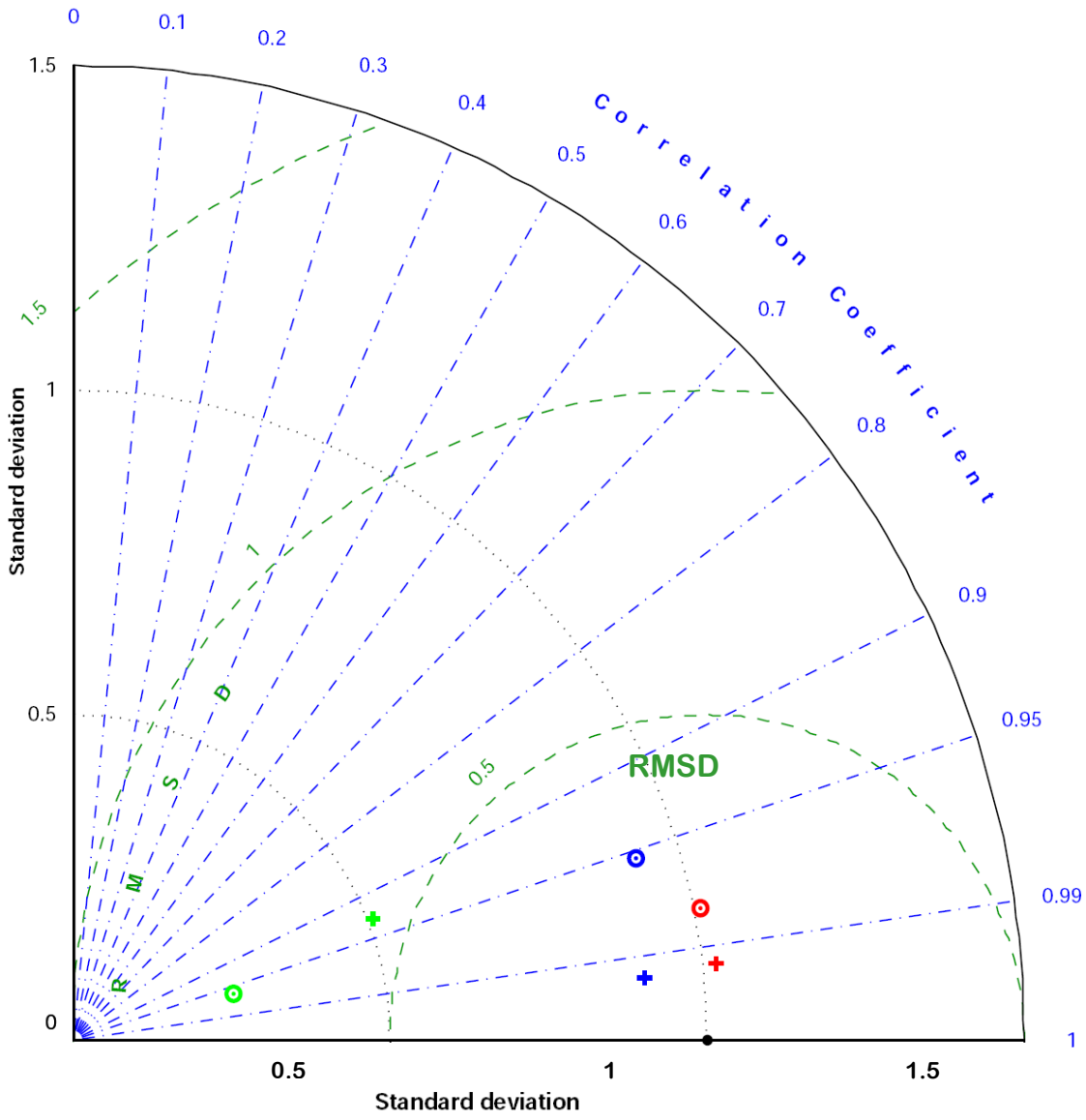


**Figure 7. Taylor plot showing correlation coefficients, normalized standard deviation, and root mean squared difference (RMSD) between the SST annual cycles of Pathfinder (black dot) and OFES in blue, KTCM Bulk in red and Qcorrected in green. The plus symbols are the comparisons for the inshore region (depth≤ 300m), and the circles are the comparisons for the offshore region.**

### *3.1.2. Modeled Sea Surface Height Anomaly vs. Satellite Observations*

The AVISO satellite product (Fig 8a) shows a negative SSH anomaly (SSHa) in the northern part of the domain during May to July and again during November and December. The northeast region has a positive SSH anomaly from February to April and during August-September. This is a reflection of the wind curl that presents a biannual sign change due to the monsoonal atmospheric circulation. The SSH anomaly is positive along the coast from 2 to 10$^{o}$S with a south-north gradient (higher in the south) during most of the year. The exception is January-March, when the positive anomaly in the south is almost absent. The large-scale circulation is responsible for this SSH feature; it is a reflection of the strength and northward extension of the EACC. The SSH anomaly is relatively uniform everywhere during the summer inter-monsoon (October).

Qualitatively, the SSH anomaly patterns of all three models (OFES, KTCM 'Bulk', and 'Qcorrected') agree with the observed AVISO SSH anomaly in the sense that positive and negative features are found in roughly the same areas. There is some exceptions for example during February and September in OFES and January and September for the KTCM models (Figure 8a-d). The magnitudes of the SSH anomalies are greater in the KTCM runs with a range from -11.2 to 13.7 cm for the Bulk configuration and -12 to 16.2 cm for the Qcorrected configuration, while OFES (-8.8 to 11.5cm) and AVISO (-8.2 to 10.6 cm) have more similar ranges. Quantitative differences between the AVISO and modeled SSHa fields (Figure 9a-c) are similar in

magnitude to the SSHa field because features are shifted in space. OFES SSHa is in general more similar to AVISO than either of the KTCM model configurations. The difference in resolution of KTCM and AVISO could be responsible for some of the differences. KTCM better represents the bathymetry, and therefore resolves in greater detail the circulation around the islands that is the region of interest on this study. We consider that despite the observed differences with satellite observed SSHa, KTCM results are still valuable since both OFES and AVISO are unable to resolve features at the scale of interest.

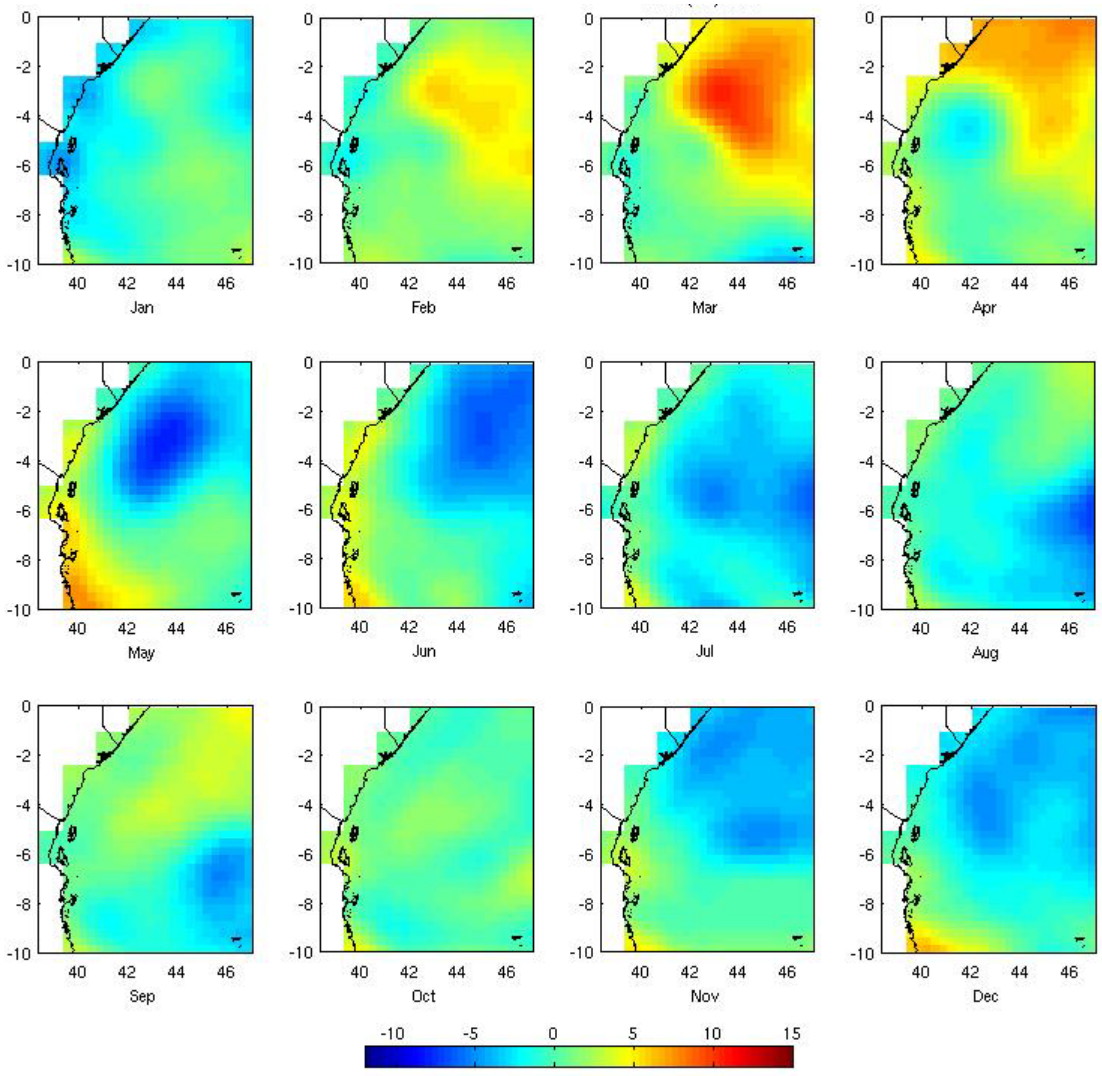


**Figure 8a. Monthly AVISO sea surface height anomaly in centimeters.**

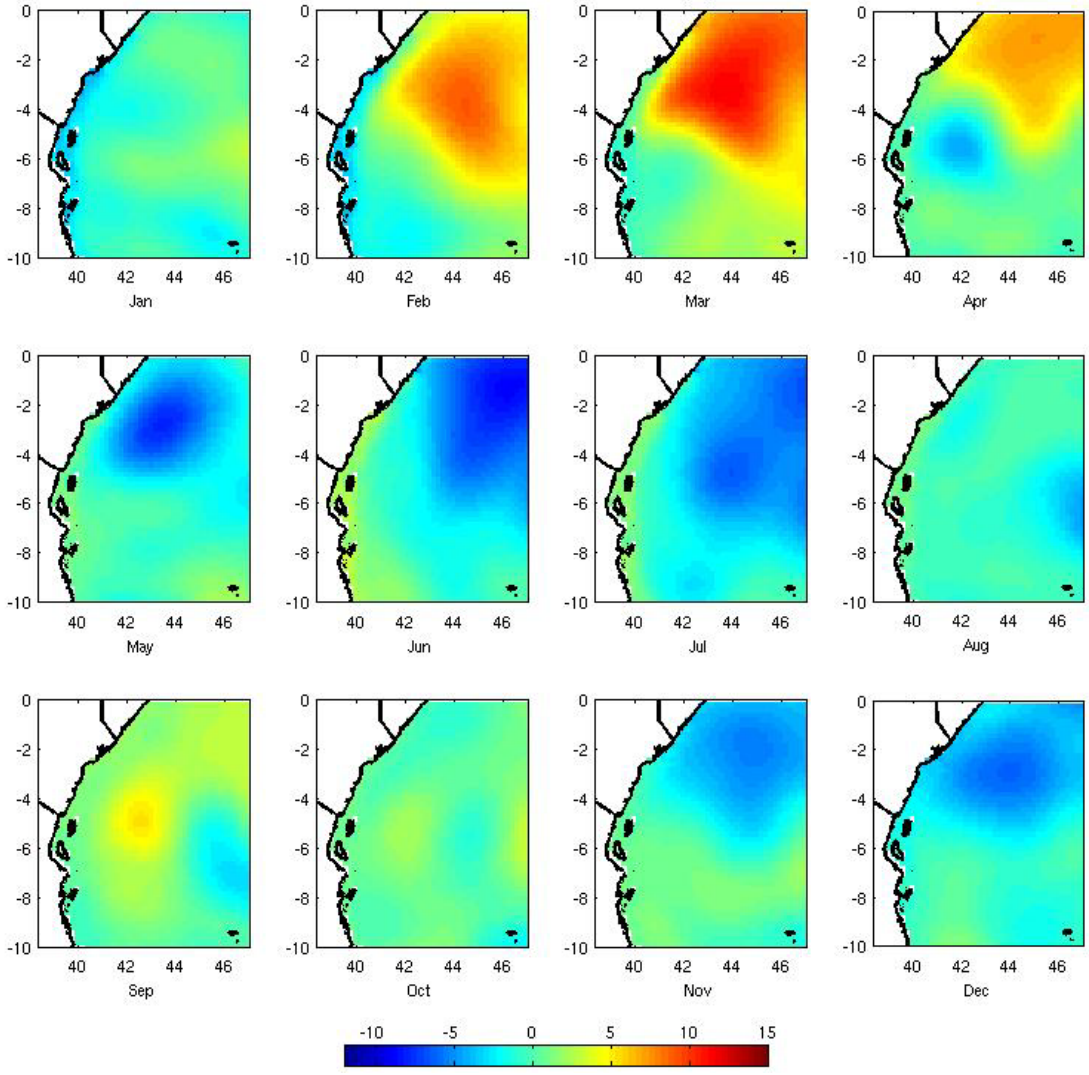


**Figure 8b. Monthly OFES sea surface height anomaly in centimeters.**

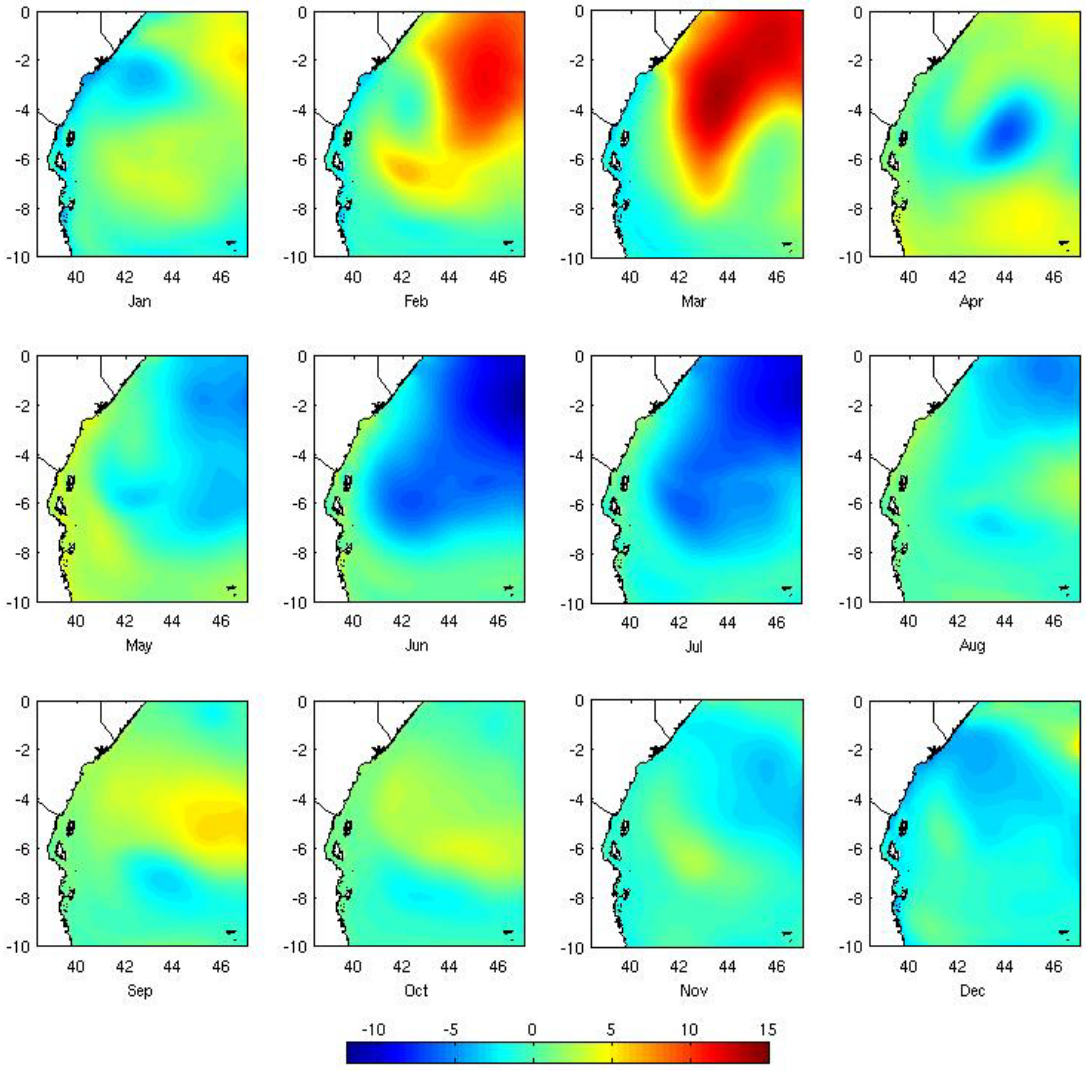


**Figure 8c. Monthly KTCM 'Bulk' sea surface height anomaly in centimeters.**

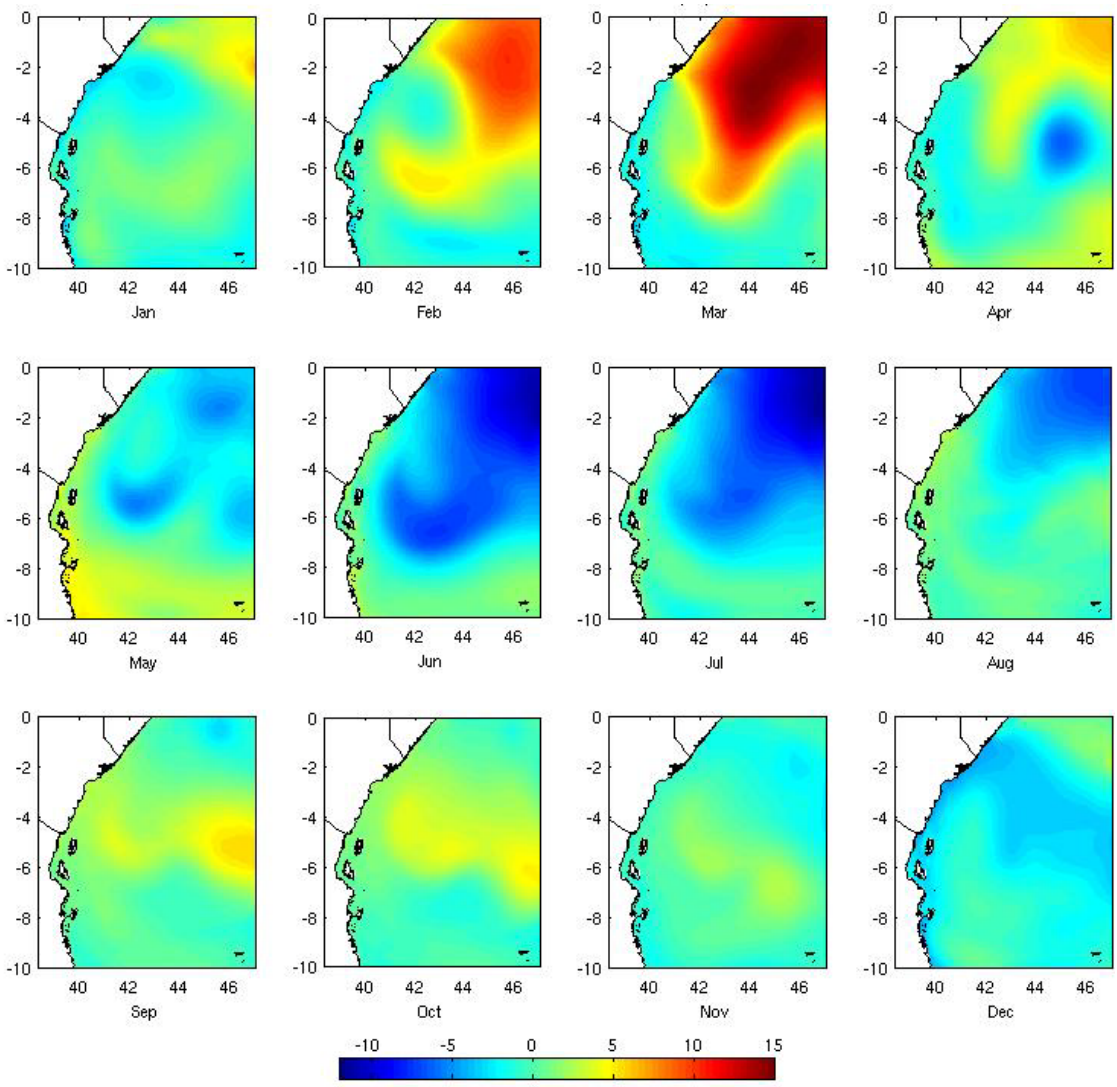


**Figure 8d. Monthly KTCM 'Qcorrected' sea surface height anomaly in centimeters.**

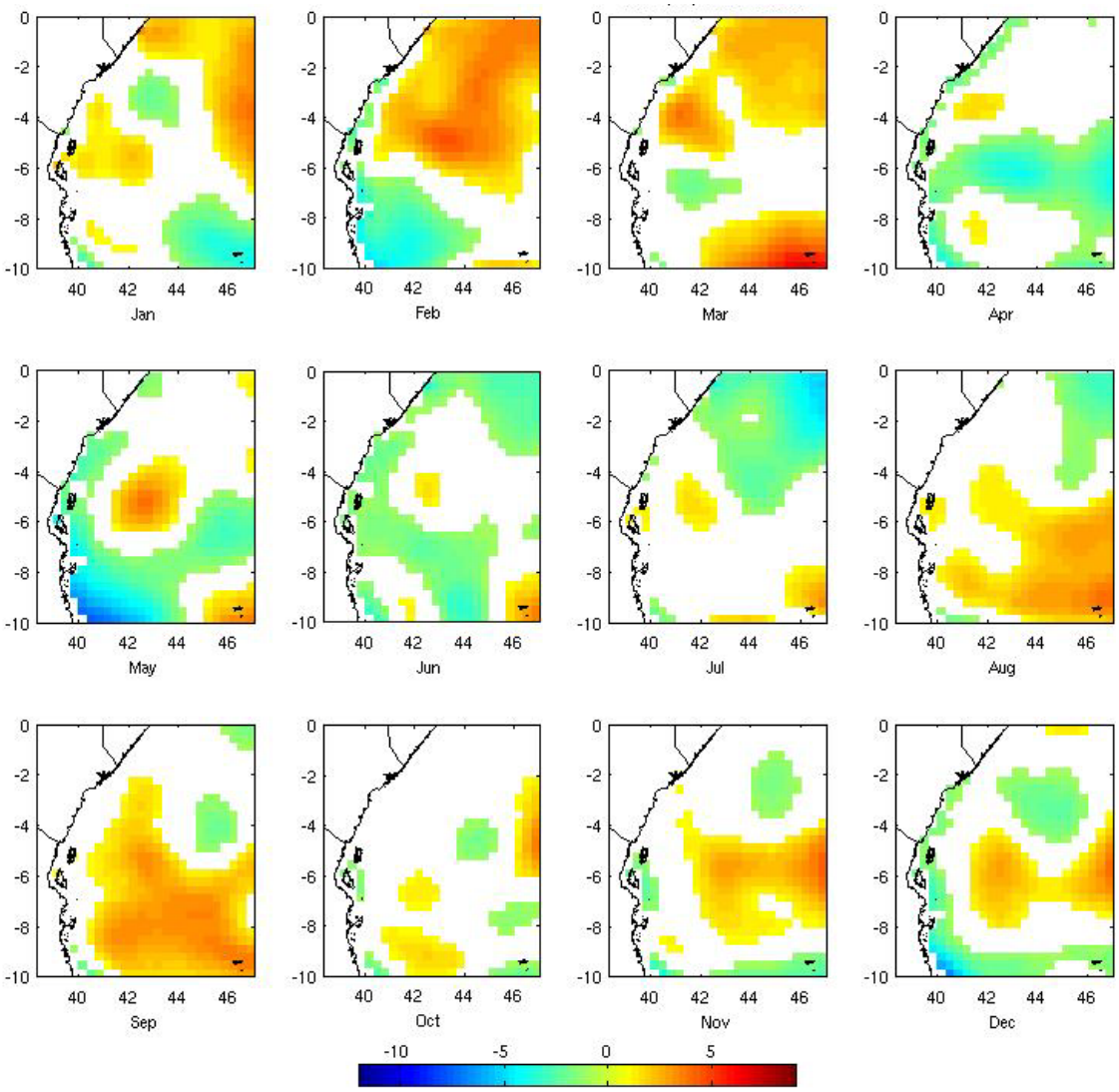


**Figure 9a. Monthly difference OFES-AVISO SSHa in centimeters. Values with an absolute value smaller than 1 cm have been blanked.**

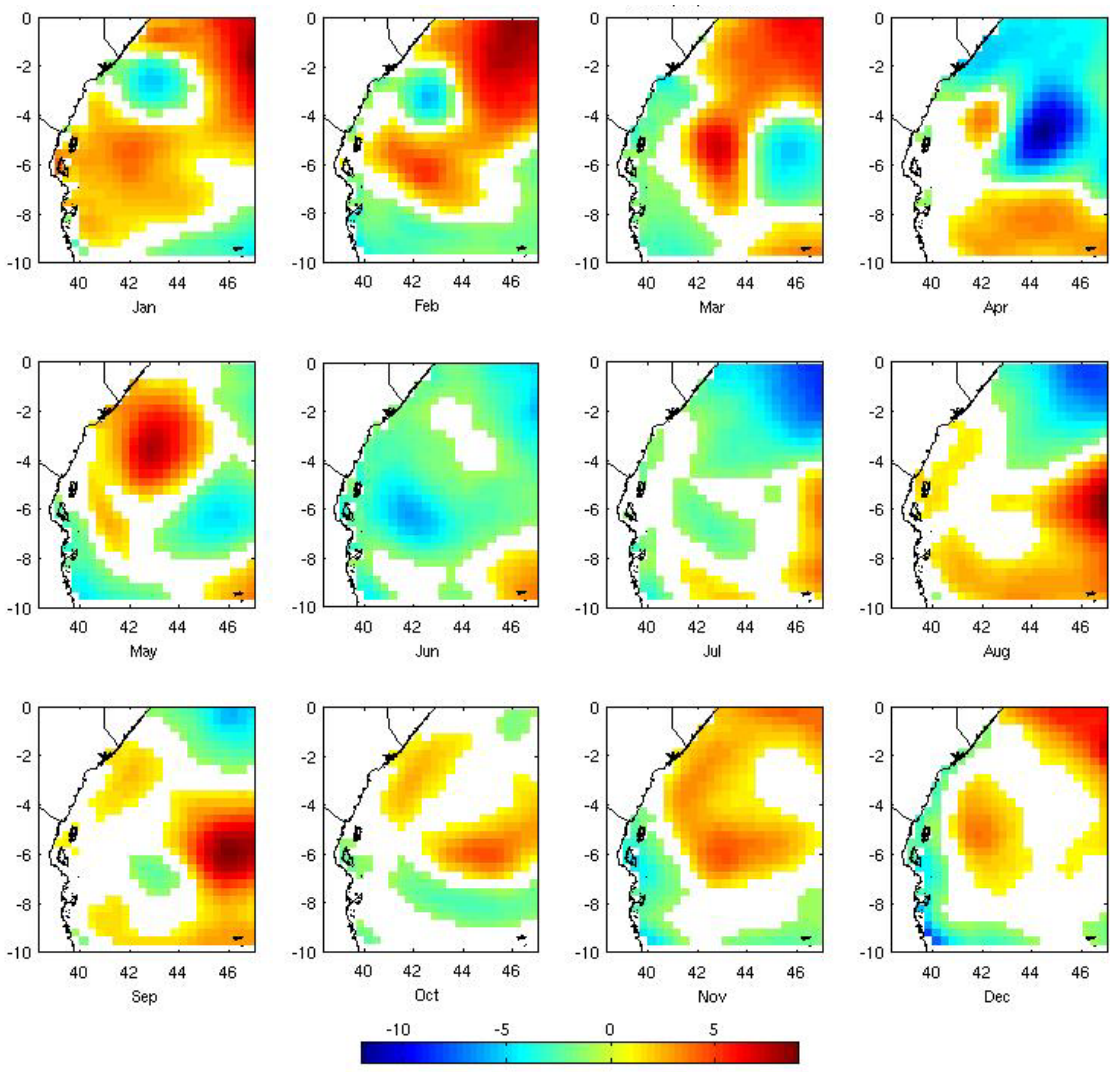


**Figure 9b. Monthly difference KTCM 'Bulk'-AVISO SSHa in centimeters. Values with an absolute value smaller than 1 cm have been blanked.**

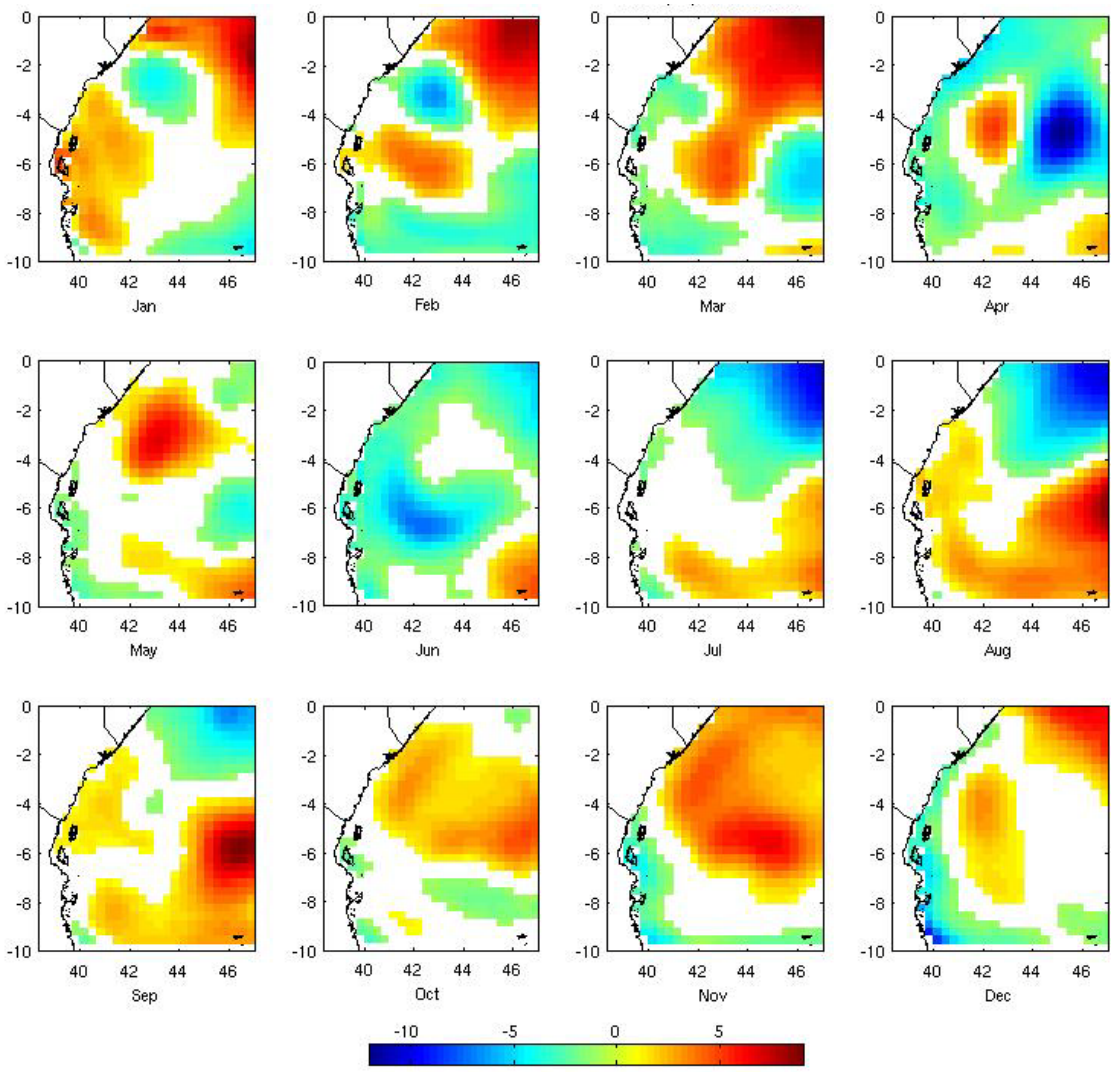


**Figure 9c. Monthly difference KTCM 'Qcorrected'-AVISO SSHa in centimeters. Values with an absolute value smaller than 1 cm have been blanked.**

### *3.1.3 Modeled vs. Measured Temperature and Salinity profiles*

To assess the performance of the subsurface structure of the KTCM and OFES models, 460 temperature profiles from the model domain (all that were available) were extracted from the World Ocean Database (WOD) for the period 2000 to 2007. These were compared with profiles extracted from the models for the same location and day of the year as the WOD profiles. For OFES, since we only have access to monthly means, the profiles were extracted from the month when the observations were made. Modeled and measured temperatures were interpolated to the same depths. The profiles were classified by month. Standard deviations and RMS values were calculated for the monthly profile groups of the three models (OFES, Qcorrected and Bulk) and the WOD observations and normalized by dividing by the standard deviation of the WOD data. The correlation between the monthly groups of WOD profiles and each of the models was also computed.

Figure 10 shows the comparisons between the OFES, Bulk and Qcorrected KTCM temperature profiles and WOD observations on a Taylor plot. It shows that all three models represent the temperature at depth as measured by the WOD profiles, with correlation coefficients >0.85 in all months except January, when the correlation coefficients are smaller (~0.65). It is not too surprising that all three models have fairly high correlations with the WOD temperature, because all depths have been included, and it would be unusual for a model not to have a warm surface to cold deeper gradient in temperature profiles. A more thorough analysis of spatial

agreement on specific depth horizons might be possible, but is not attempted here. All three models slightly overestimate the temperature variability during January (normalized standard deviation ~1.2), with relatively large differences between model and observed temperatures underneath the surface during that month (RMS ~0.8). There is no significant difference in the skill among the 3 models for any month.

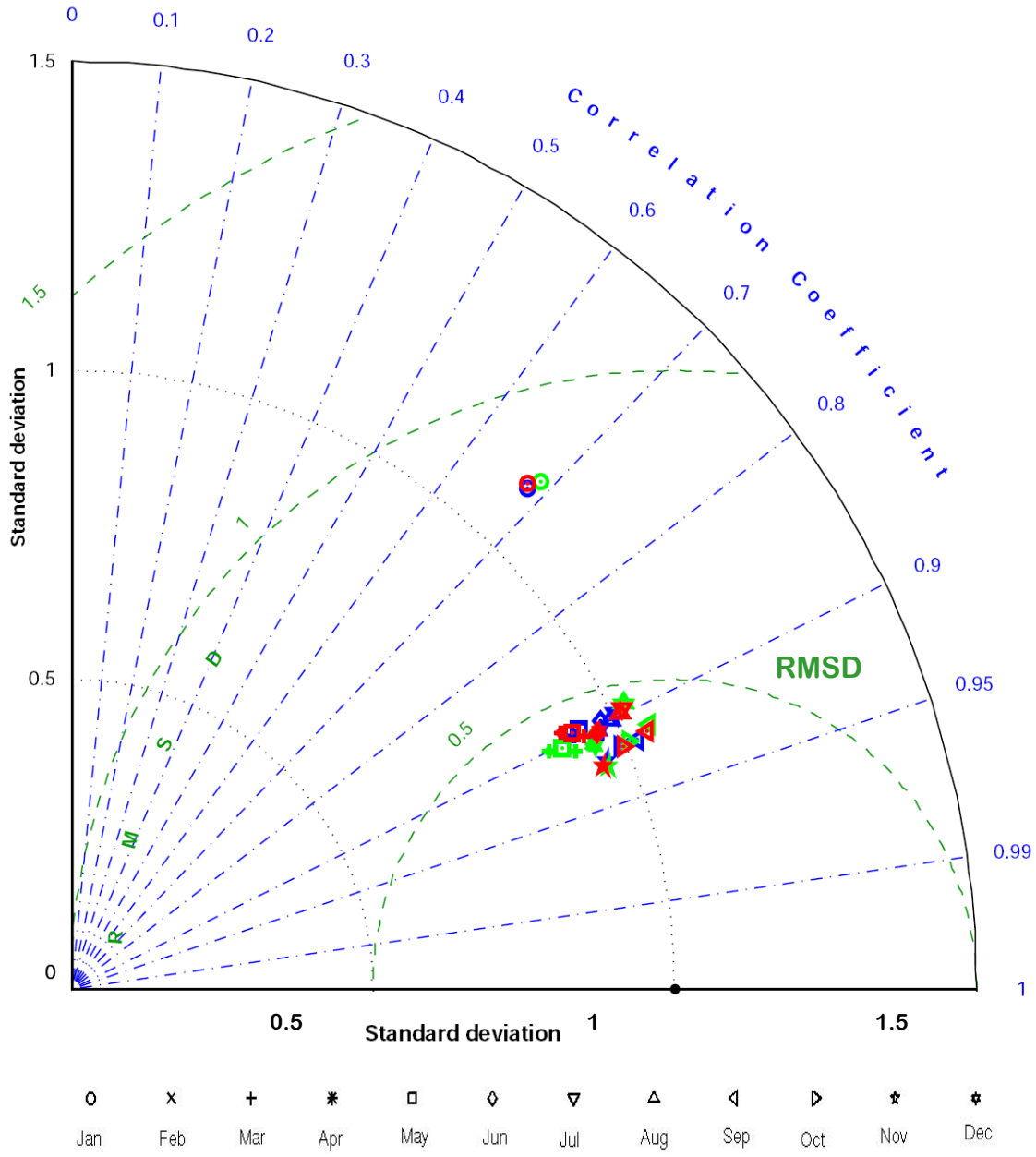


**Figure 10. Taylor plot showing monthly correlation coefficients, standard deviation, and mean root squared difference (normalized) between the temperature WOD profiles available for each month (black dot) and profiles extracted from OFES (blue), KTCM 'Qcorrected'(green), and KTCM 'Bulk' (Red). Every symbol represent a month as indicated by the symbol key above.**

A quantitative comparison for salinity profiles similar to the one done for temperature profiles was not possible as there were only 38 profiles with salinity from 2000 to 2007 available in the WOD. We expanded the time frame and extracted 1841 WOD salinity profiles from the domain from 1929 to 2009. Salinity profiles were extracted from the models at the time and location of the WOD profiles, and statistics were calculated following the same procedure described above for temperature profiles. However there was no significant correlation between the observed and modeled salinity profiles. Errors in the observations may also be a factor affecting the statistics, as suggested by the fact that several profiles of both temperature and salinity showed extreme spikes, despite the quality filters in the WOD. Profiles with obvious outlier values were discarded, but the possibility remains that profiles with salinity errors remain in the data set. The salinity range in the profiles is very small ($\Delta S \approx 1$PSU), making it possible for a few erroneous values in the observations to alter the statistics dramatically. The salinity section reported by Swallow *et al* (1991) (Fig 11, Top) based on observations taken at $5^{o}$S by the *Marion Dufresne* in April 1985, were compared to April salinities from the KTCM Bulk climatological run (Fig 11, Bottom). The main features are: Low salinity surface water inshore, a strong halocline between 50 and 100 m depth, and an offshore core of high salinity that extends towards the surface in both figures. Qualitatively there is good agreement, despite the fact that the observations were taken two decades before the beginning of the period used to calculate the climatological forcing of the model.

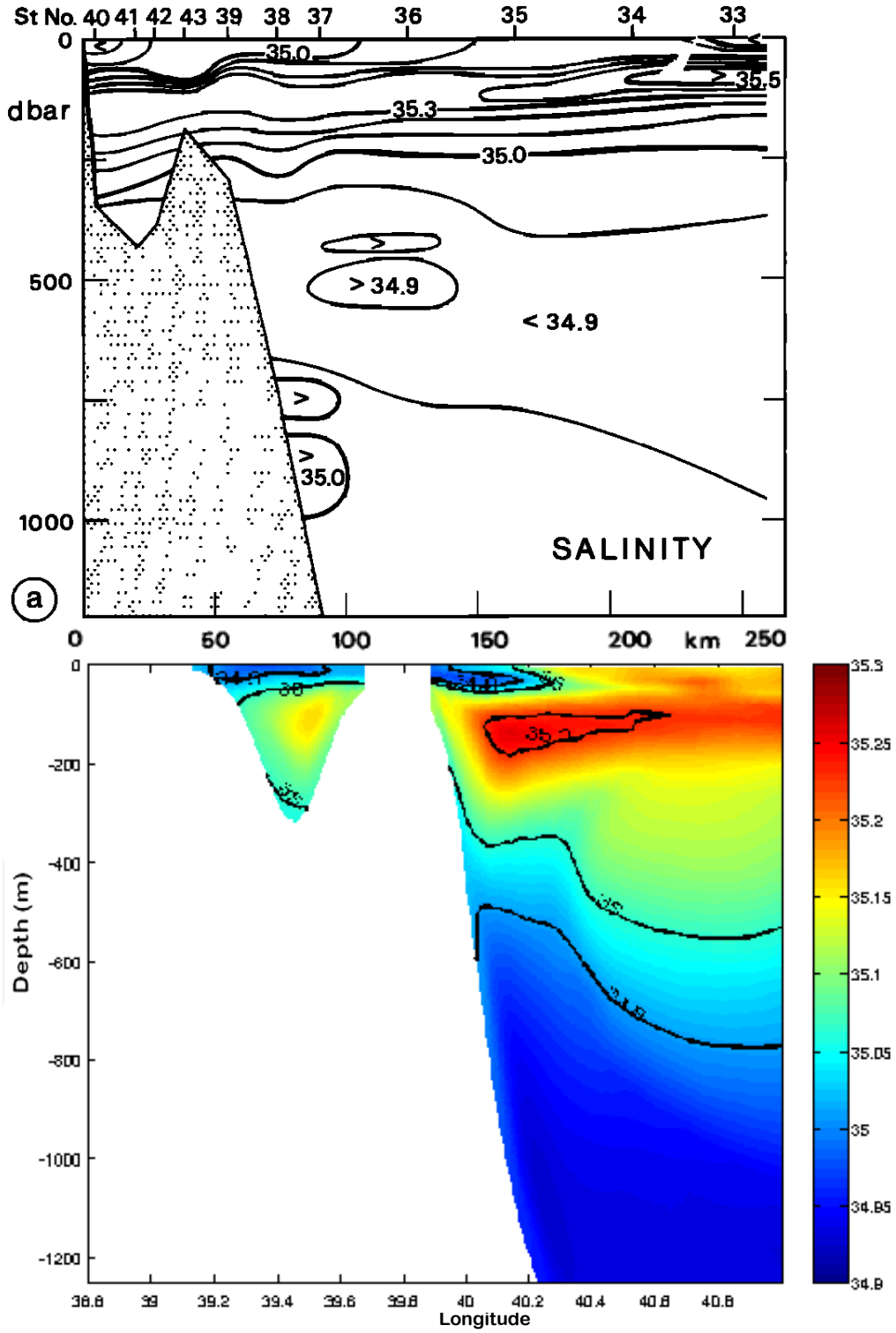


**Figure 11. Salinity contours on a vertical section at ~5°S. Top) Based on ship observations made in April 1985 (after Swallow *et al*, 1991). Bottom) KTCM Bulk simulated April salinity for the same section.**

### *3.2. Climatological Circulation, SST and SSS Patterns.*

Results of the climatological KTCM Bulk model are used to describe the seasonal variability in the SST and SSS patterns. Near-shore and large-scale circulation patterns are also described. Figure 12 shows the monthly mean wind stress climatology at the original NCEP resolution. The strongly seasonal reversal of the monsoon winds is observed, with strong southward winds (upwelling favorable) in January and February, and strong northward winds during April-October. Winds in March, November and December are weak and less oriented alongshore.

Figure 13 shows the volume transport across the north, south and east open boundaries of the model domain. Transport into the domain is shown as positive values. The inward flow through the southern boundary of the domain is relatively constant throughout the year, fluctuating between 25 and 10 Sv. The main contribution to this transport is the northward flowing EACC. Flow through the northern and eastern boundaries is more seasonally variable. Transport through the northern boundary varies from 30 Sv inward during December to -60 Sv (outward) in August; its variability is related to the presence or absence of the southward flowing Somali Current.

The transport through the eastern boundary is inward (westward) from June to November and outward the rest of the year. The flow through this boundary is governed by the complex equatorial dynamics affecting the model domain. Both the

Wyrtki jet and the SECC are responsible for the outward flow in the eastern boundary of the domain. During the inter-monsoon periods (Mar-Apr and Nov), the eastward flowing Wyrtki jet is present at 2-3$^{o}$S. During the NE monsoon period (December, January and February) the offshore jet generated by the convergence of the SC and the EACC forms the SECC that flows offshore between 2$^{o}$S and 8$^{o}$S. The transport into the domain through the eastern boundary is due to the SEC that flows westward year round to the south of our domain but reaches its maximum northward extent (~8$^{o}$S) during July and August (Fieux, 2001, Schott and McCreary, 2001).

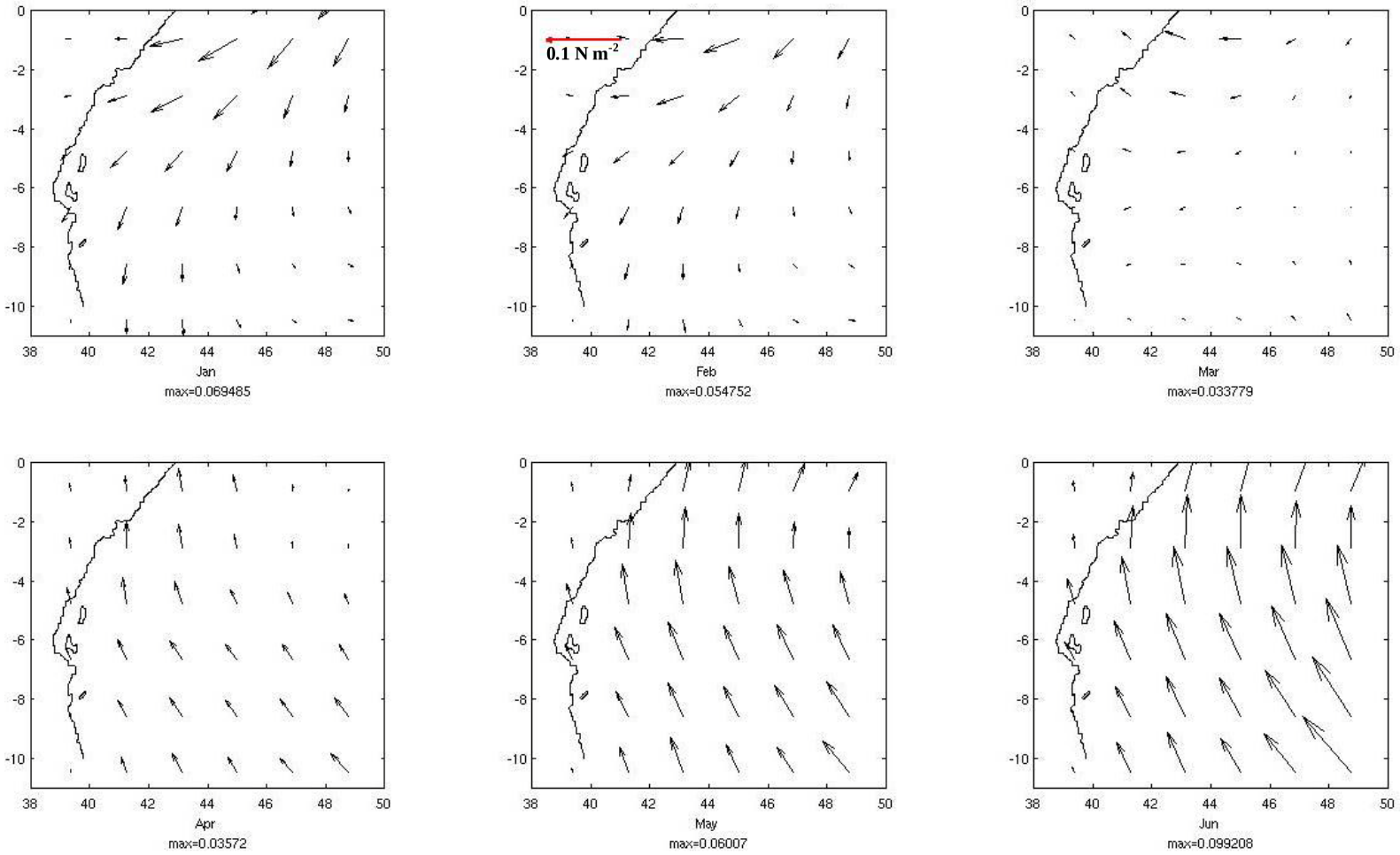


**Figure 12a. Monthly mean NCEP wind stress climatological forcing for January to June, calculated from the years of 2000-2007. The number below each panel is the maximum of the wind stress magnitude for each month in N $m^{-2}$. Scale vector in February panel applies to all panels.**

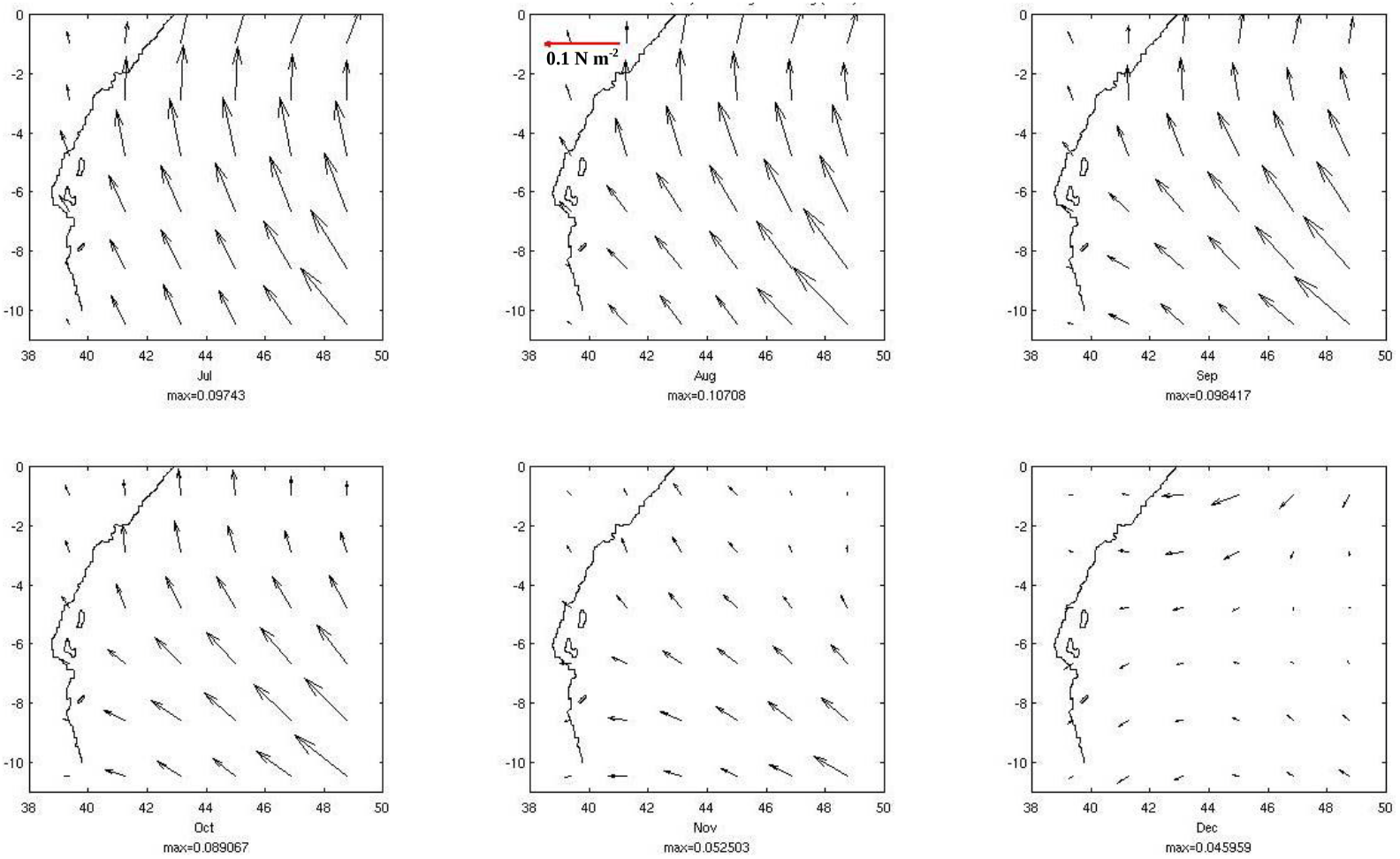


**Figure 12b. Monthly mean NCEP wind stress climatological forcing for July to December, calculated from the years of 2000-2007. The number below each panel is the maximum of the wind stress magnitude for each month in N $m^{-2}$. Scale vector in August panel applies to all panels.**

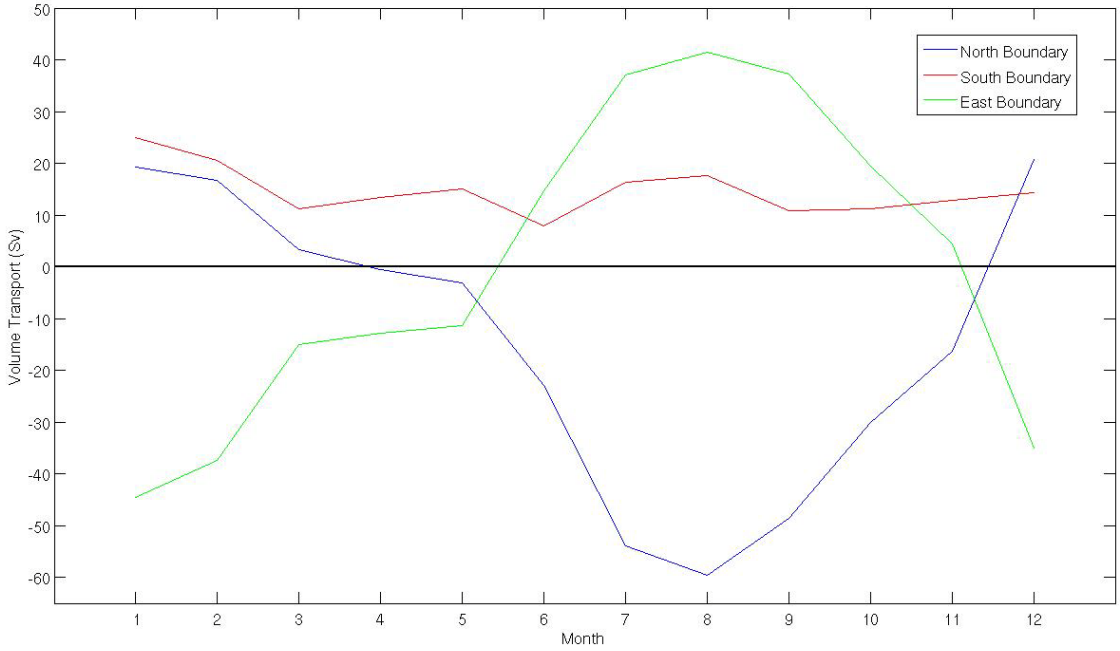


**Figure 13. Volume transport in Sverdrup's ($Sv=10^6 m^3 s^{-1}$) across the 3 open boundaries of the model domain. Positive (negative) values represent transport into (out of) the domain.**

### *3.2.1 Main Circulation Features*

From November to March the Somali current flows southward and meets the northward flowing EACC (Fig 14b & 14a). The latitude where these currents meet varies from north of the equator in November to ~2$^{o}$S in March. Where the currents meet, the offshore jet that forms the SECC develops. It flows eastward in November but tilts southward through time until it ends aligned in the north-south direction in March. A dipole is associated with the SECC jet, with an anticyclonic eddy to its north/east side and a cyclonic eddy to its south/west side. The dipole moves onshore and southward, and by March the cyclonic eddy is compressed against the coast. In

April as the southward flow of the Somali current disappears, continuous northward flow along the East African Coast is established. With the onset of the southeast monsoon, both the dipole and jet disappear. The dipole is fully inside the domain only during January to March.

A weak anticyclonic eddy centered approximately at $6^oS$, $42^oE$ is present during November and December. The southward flow on its western flank ~$41^oE$ is replaced by northward flow in the EACC at ~$40^oE$, offshore of the islands of most interest here.

During the SE monsoon season the EACC flows northward all along the coast of the domain. The incoming flow through the eastern open boundary north of $8^oS$ has a southwest direction. The southward component is stronger north of $4^oS$ and the shear with the northward flowing EACC produces a permanent cyclonic feature in the NE corner of the domain known as the Southern Gyre (SG) (Fig 1a Schott and McCreary, 2001).

During January and February, the wind blows southward along the coast south of Zanzibar Island (Fig 12a), however the EACC continues to flow northward against the prevailing winds (Fig14a). This indicates that the circulation at this regional scale is dominated by remote forcing from the large-scale circulation patterns rather than local wind forcing. Local winds may affect the strength and vertical extent of the

EACC (discussed in section 3.2.4). The shelf circulation (see detailed description in section 3.2.5) that tends to respond faster to the local forcing is also affected. Flow inshore of the Zanzibar and Mafia Islands follows the wind direction during December to March (Figs 19a & 19b).

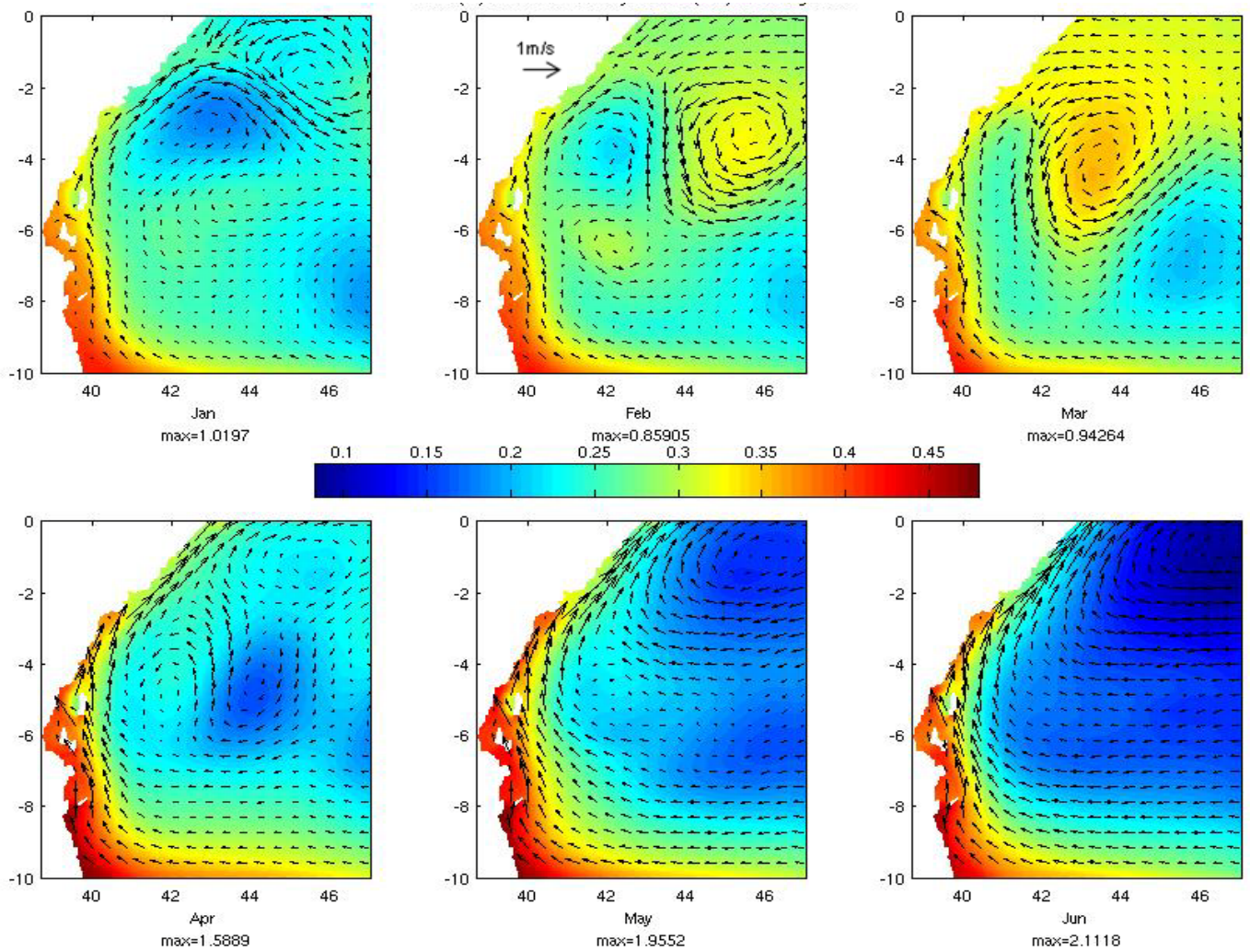


**Figure 14a. KTCM Bulk configuration monthly climatology of SSH (m) with vectors of surface velocity for Jan to Jun. Maximum speed in $ms^{-1}$ for each month is at the foot of each panel. Scale vector on Feb apply to all panels.**

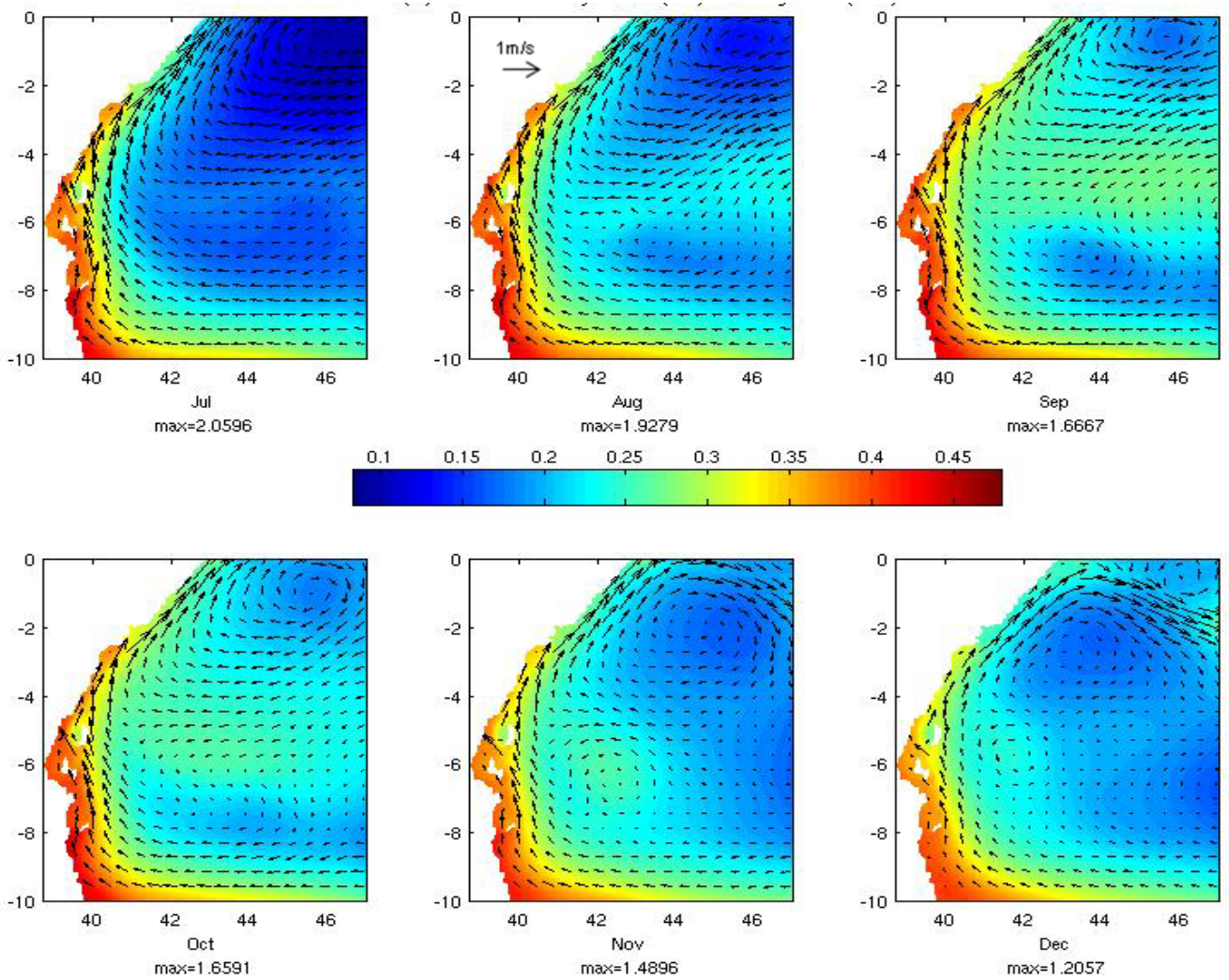


**Figure 14b. KTCM Bulk configuration monthly climatology of SSH (m) with vectors of surface velocity for Jul to Dec. Maximum speed in ms$^{-1}$for each month is at the foot of each panel. Scale vector on Aug apply to all panels.**

### *3.2.2. Sea Surface Temperature Seasonality*

A strong north-south SST gradient (of up to 3$^{o}$C) is observed from December to March (NE monsoon) (Fig 5c). Warm water is advected into the domain from the south (which is austral summer) and east (south of 8$^{o}$S) by the EACC and SEC respectively, while the SC brings cold water from the northern hemisphere (which is in boreal winter and strong coastal upwelling is occurring). Outflow from the model domain occurs through the NE corner of the domain in the SECC.

From April to July (Fig 5c) the warm water is pushed towards the coast, as colder water starts to advect into the domain through the south and east open boundaries. In May, warm water occurs along the coast and in offshore features (centered at 6.5$^{o}$S, 43$^{o}$E) associated with sluggish flows. By June the warm water (>28$^{o}$C) has been flushed out by the EACC through the northern open boundary. A uniform cold SST (~24$^{o}$C) is observed during the southeast monsoon season (Jun-Oct). In November warm water is observed along the coast. This warming is due to solar heating of sluggishly-flowing (e.g., long residence time) waters during the intermonsoon period. By December the north-south gradient has been established.

### *3.2.3. Sea Surface Salinity Seasonality*

The modeled mean annual salinity is 34.9 PSU and the overall range goes from 34.7 to 36.7 PSU. Higher salinities are observed in shallow areas especially during the NE monsoon season when the circulation is slower. The salinity concentration in East African coastal areas is strongly influenced by river runoffs and estuarine dynamics that are not represented in the model; therefore good agreement with observations in the inshore region is not expected. Offshore, vertical sections showed qualitatively good agreement with the values reported by Schott *et al* (2001), for the EACC (34.8 to 35.3 PSU). Higher sea surface salinity (SSS) is observed in the northern coastal part of the domain during the NE monsoon (Fig 15, Jan, Feb and Mar), when the SC is advecting upwelled water from the north. That water is expected to be slightly saltier due to its contact with the Red Sea and the fact that was bottom water recently upwelled. Maximum SSS is found in the near shore areas of the continental shelf that have sluggish circulation during December to March. Off the shelf there is a band of relatively low salinity along the coast in all months, although this is less obvious in November and December. It is associated with the EACC water mass. SSS along the southern boundary of the domain is also relatively low from January to August, due to the influence of the SEC.

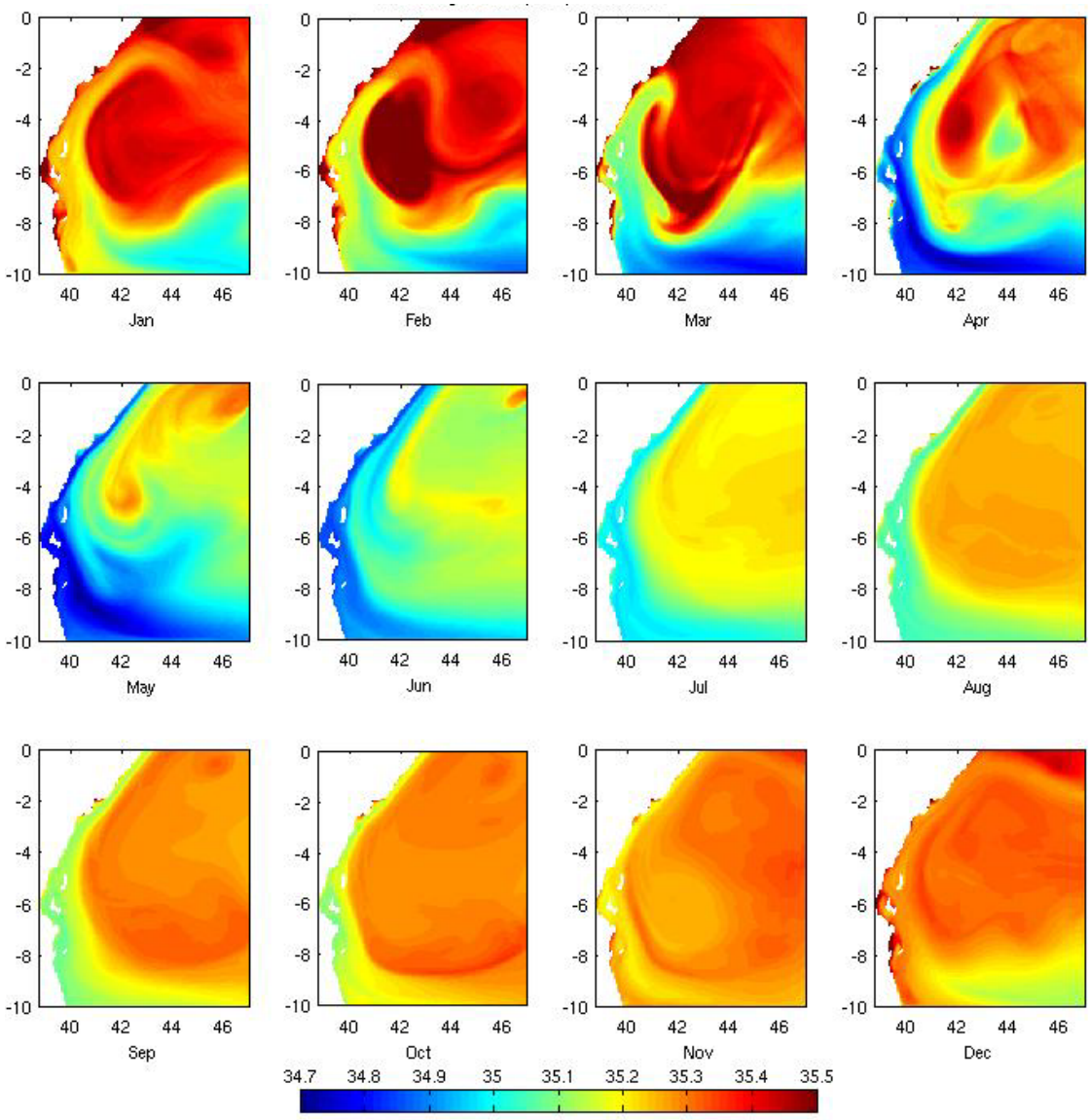


**Figure 15. KTCM 'Bulk' Sea Surface Salinity in PSU. The higher end of the color scale is clamped to 35.5 to be able to observe small gradients, the actual range of the data is 34.7 to 36.7 PSU**

### *3.2.4 EACC seasonality and spatial variability.*

The northward flowing EACC shows seasonal and spatial variation of its speed, depth and offshore extension. A north-south gradient of the alongshore velocity is observed year round, with slower velocities in the southern region of the domain and stronger velocities in the northern part (Figs 16 a to c). The flow divergence is stronger during the SE monsoon season and is compensated by the westward flow of the SEC through the east open boundary of the domain.

In the northern half of the domain the EACC shows a strong seasonality (Figs 14, 16a & 16b). It reaches a maximum speed of 1.45 m $s^{-1}$ during the SE monsoon (May to August), at the $1^{o}$S section (Fig 16a). It is weaker during the northeast monsoon and north of $2^{o}$S appears in the subsurface, overlain by the southward flowing Somali Current in the upper 60m. Strong shear develops between the upper layer, flowing south, and the underlying 200m layer that flows northward (Fig 16a).

The core of the EACC (with speeds greater than 0.8m $s^{-1}$) is wider in the north showing a maximum offshore extent of 100 km at $1^{o}$S, while the 0.1m $s^{-1}$ isotach extends to 200 km offshore (Fig 16a). At this latitude the core stays above 200m depth all year round, however northward velocities exceeding 0.1 m $s^{-1}$ are observed deeper than 1000m from August to December (Table 1).

At 6$^{o}$S, where the shelf is wider, the offshore extension of the EACC beyond the shelf break is minimum. The core extends to less than 50 km offshore and the 0.1m s$^{-1}$ isotach is within 100 km most of the time (Fig 16b). Northward flow extends deeper than 1000m from February to April (Table 1).

At 9$^{o}$S the EACC is slower (maximum speed 0.5m s$^{-1}$) and shows very little variability. The 0.1 m s$^{-1}$ extends approximately 150km offshore, a little bit farther than at 6$^{o}$S, but it does not extend as deep (Fig 16c and Table1). An interesting pattern is observed during December when the deepest part of the EACC jet is about 100 km offshore reaching down to 950m, while at the shelf break it only reaches to 300m.

Northward current speeds inshore of the Islands are much smaller than offshore. Maximum speeds in the Zanzibar channel are 0.25m s$^{-1}$, about 20% of the offshore velocity (Fig 17). However the seasonality of the speed of the northward flow inside this Channel agrees with the seasonality of the core of the EACC at this latitude (~6$^{o}$S) (Fig 16b). This suggests a direct influence of the offshore current on the near-shore circulation.

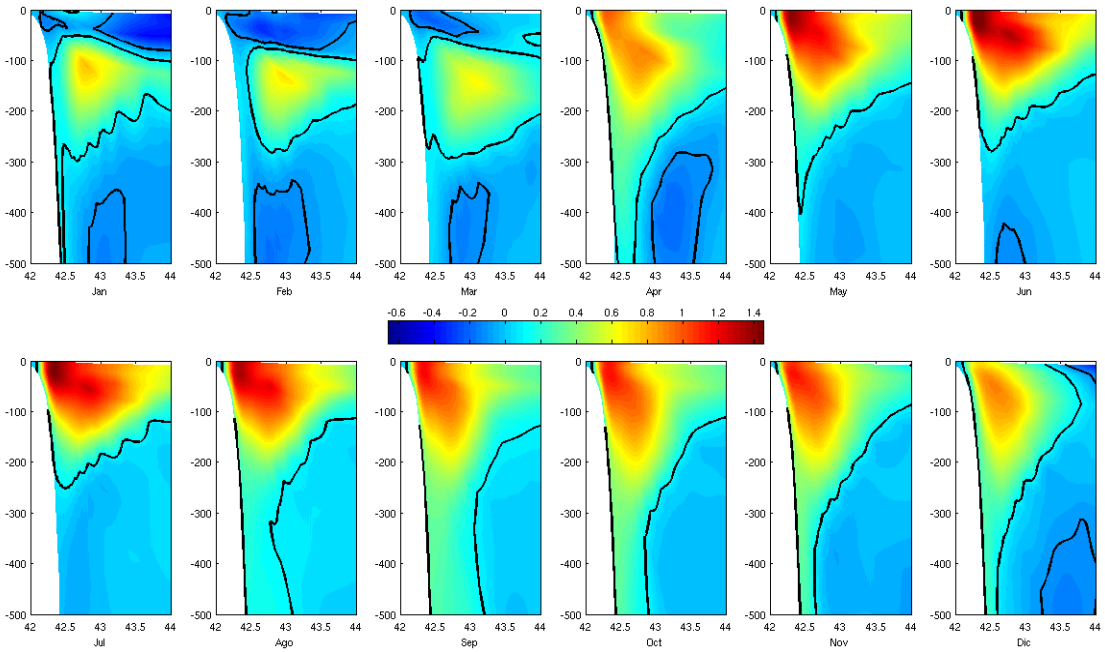


**Figure 16a. Across shore section of north-south velocity at 1°S. The black contour is the +-10cm.s$^{-1}$ isotach.**

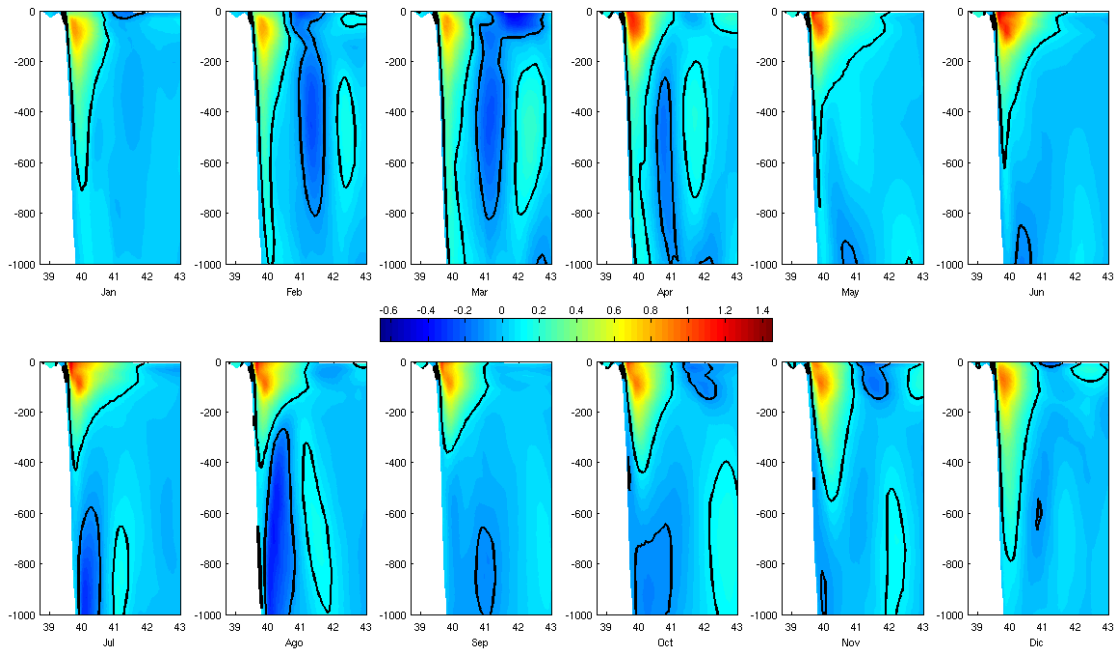


**Figure 16b. Across shore section of north-south velocity at 6°S. The black contour is the +-10cm.s$^{-1}$ isotach.**

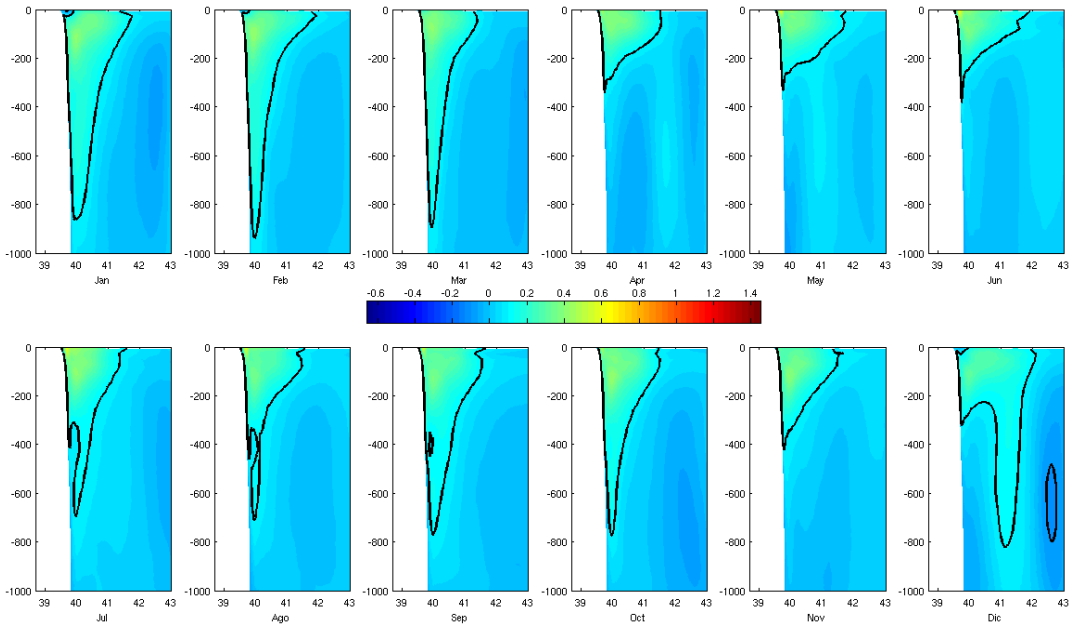


**Figure 16c. Across shore section of north-south velocity at 9°S. The black contour is the +-10cm.s$^{-1}$ isotach.**

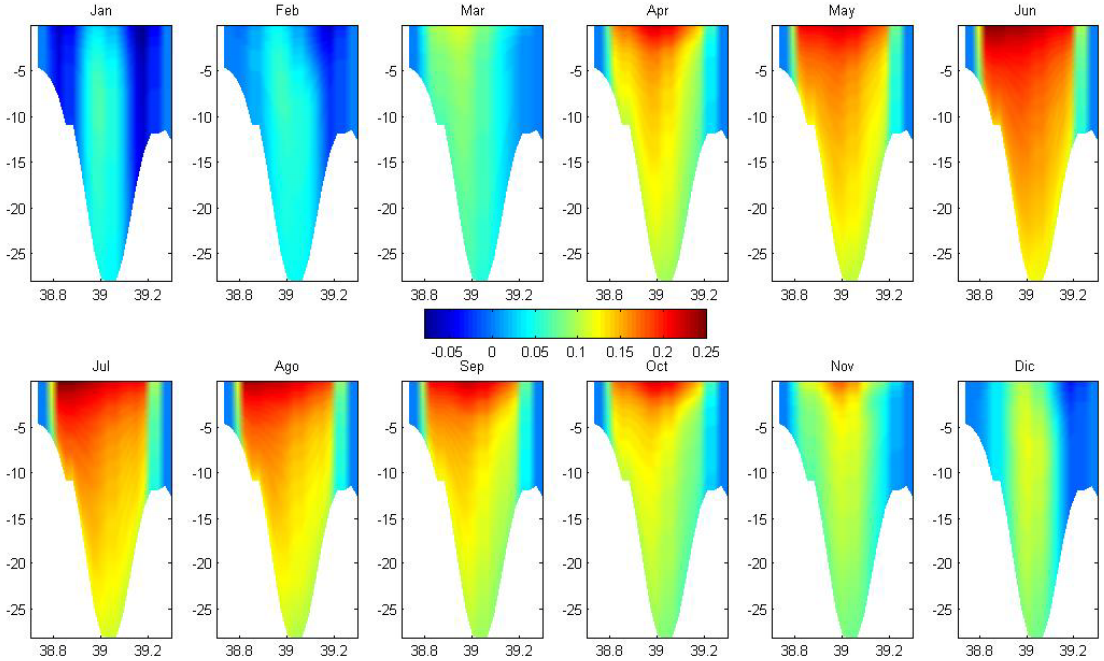


**Figure 17. Cross section of north-south velocity at -5.96°S (north Zanzibar Channel).**

**Table 1. Maximum depth in meters of the 0.10m.s$^{-1}$ northward velocity isotach of the EACC at 3 different latitudes by month.**

| Latitude / Month | 1°S | 6°S | 9°S |
|---|---|---|---|
| **January** | 580 | 700 | 850 |
| **February** | 280 | 1020 | 940 |
| **March** | 300 | 1650 | 890 |
| **April** | 540 | 1400 | 340 |
| **May** | 400 | 780 | 330 |
| **June** | 280 | 630 | 380 |
| **July** | 250 | 430 | 690 |
| **August** | 3000 | 420 | 710 |
| **September** | 2350 | 360 | 770 |
| **October** | 1440 | 440 | 770 |
| **November** | 1130 | 550 | 420 |
| **December** | 1130 | 790 | 820 |

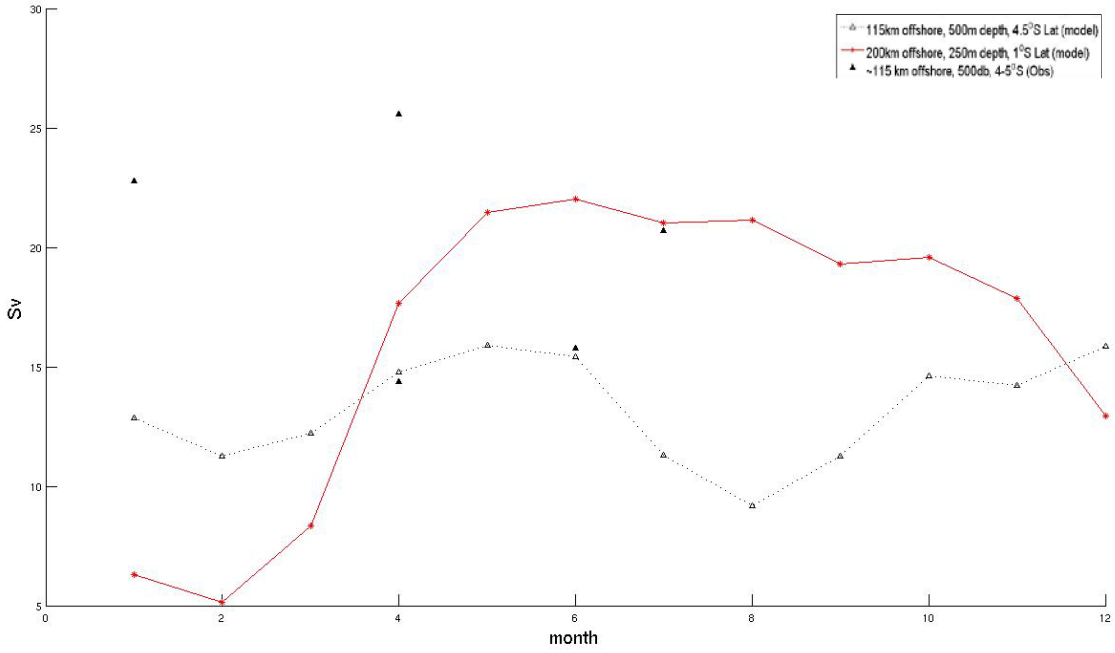


**Figure 18. Volume transport in Sv calculated from the surface to 250 or 500 depth and from the coast to 115 and 200 km at two different latitudes. Lines correspond to modeled climatological values and symbols to observations.**

To look at the seasonality of the EACC the monthly averaged KTCM 'Bulk' volume transport was calculated for two different sections. The section at 1oS was intended to show the strong seasonal variability of the EACC at northern latitudes. The second section at 4.5$^{o}$S was meant to have some values comparable to available observations. Volume transport at 1$^{o}$S was calculated for the upper 250m through a transect from the coast to 200 km offshore (Fig 18. red line). The depth and offshore extent of the section were chosen to encompass the core of the EACC during all months. It fluctuates from ~5 Sv in February to 22 Sv in June, with an annual mean of 16 Sv. For the section at 4.5$^{o}$S a depth of 500m and an offshore extension of 115km

was chosen to match the observations. This section showed much less variability and a mean annual volume transport of 13.5 Sv. Swallow *et al* (1991), report a mean northward transport of 19.9 Sv in the upper 500 dbar, from the coast out to ~115 km offshore from 5 transects between 4$^{o}$S and 5$^{o}$S. The five observational transects were sampled during July 1964, January and April of 1965, June 1979 and April 1985. Transport was calculated as the sum of geostrophic transport calculated from salinity and temperature profiles and the Ekman transport from observed winds, fitted to the corresponding transports calculated from observed velocities. The observations show little seasonality and a positive offset on the magnitude of the transport of around 10 Sv compared to the modeled values. Inter-annual variability may be responsible for the difference between the model annual mean (13.5 Sv) and the mean of these five transects (19.5 Sv). A longer time series of more frequent observations (at least monthly transects throughout the year) at different latitudes is needed to corroborate the seasonality shown by the model at northern latitudes.

### *3.2.5. Shelf Circulation Seasonality*

The effect of the islands on the coastal circulation depends on the intensity of the EACC and the depth of the channels between the islands and the continent. Therefore the circulation patterns around the islands vary both temporally and spatially along the Kenyan-Tanzanian shelf.

During the NE monsoon period, when the EACC is slower, the three islands have a similar effect on the coastal flow. Friction with the coast causes an across-shore gradient on the northward velocities, with a positive curl. This causes a small portion of the northward flowing EACC to turn southward into the channels after it passes the obstacle that the islands represent (Figs 19a-e). This return flow is observed year-round in the north tip of Pemba Island and from December to March in the north of Zanzibar and Mafia Islands (Figs 19a-b). The concave shape of the east coast of the Zanzibar Island has a similar effect, and the return flow establishes a small permanent anticyclonic eddy inside the bay on the east coast of the island (Fig 19a, $6.5^{o}$S, $39.6^{o}$E).

During the SE monsoon, the fast flowing EACC overcomes the obstacles that the shallow channels represent and shelf flows are northward all along the coast (Figs 19c-f; Apr-Nov). The northward flow both inside and outside the channels minimizes the curl caused by friction with the east coasts of the islands and the southward return flow inside the Zanzibar and Mafia channels disappears.

Shelf flow at the southern entrances of the channels is different among the islands, and depends on the channel depth. The shallow southern entrance of the Zanzibar channel acts as a barrier to northward shelf flow during December and January, forcing it to turn southward (Fig 19a). From January to February the northward flow that gets into the southern entrance of the Zanzibar channel meets the

return flow coming from the north, causing sluggish circulation inside the channel, mainly with an eastward component. The waters of the Zanzibar channel are nearly isolated during this period, and residence time is much longer. By March (Fig 19b) northward flow through the Zanzibar channel restricts the southward return flow to the northern entrance. In April (Fig 19c), as its speed increases, the EACC is able to force itself into shallow regions and northward flow through the Zanzibar Channel is established.

Unlike the channel inshore of Zanzibar, the wider and deeper Mafia channel only completely blocks the northward flow during January and partially during December and February (Figs 19a & b). The deeper (>100m) Pemba channel allows the EACC to continue northward through it all year round (Figs 19a-e).

The east-west gradients of temperature in the near shore areas are remarkable, with up to $1^{o}$C horizontal differences in January (Fig 5c). The circulation is less intense on the continental shelf of Tanzania, inshore of the 300m isobath, due to the blocking effect of the islands and the barrier that shallower bathymetry represents to geostrophic currents. Temperatures in the shallow regions evolve differently than in the rest of the domain. During the onset of the monsoon periods (Apr-Jun and Nov-Dec) the near shore regions are warmer than the offshore and a band of warm water is observed along the coast. During this time of the year wind forcing is at its minimum and local solar heating is more likely to have an effect on shallow, slow motion areas.

During the peak of the NE monsoon (January and February) the inshore region (Fig 5c, west of 40.5$^{o}$E) is colder than the rest of the domain. This cooling is due to coastal upwelling, caused by the northeast monsoon winds blowing southward along the coast (Fig 12), opposite to the EACC direction. Upwelling velocities in the inshore region are of the order of 6m.day$^{-1}$. There is southward flow in the inshore region, south of Zanzibar Island allowed by the slow EACC (Figs 19a & b).

The flow over the shelf in the southern part of the Zanzibar Archipelago has a northwest direction all year round. Cooler areas observed to the west side of Mafia and Zanzibar Islands (i.e. Dec to Mar and Nov; Figs 19 a, b, f) may be associated with localized upwelling due to the island mass effect (Hamner and Hauri,1981).

As previously shown in section 3.1.1, in general the 'KTCM bulk' SST exhibits less cold bias than OFES. At the scale that emphasize the islands region (Figs 19a-f, and A1-A6) spatially averaged SST of KTCM bulk better matches the Pathfinder SST. Although the bulk spatial mean is similar to Pathfinder, the spatial patterns are not always in agreement. We discuss only the contrasts of the water surrounding Zanzibar Island for the months of December and October (Fig 20). When the Zanzibar Channel is "isolated" from the outside ocean (during the NE monsoon e.g. December) there is a greater difference between the SST within the channel and the SST to the east of the Island. The KTCM model and the satellite observations agree as to whether the SST is different within the channel than east of the island or not. In October (Fig 20, Top)

for example, there is continuous flow northward along the Zanzibar Channel, both Pathfinder and KTCM show little difference between the SST inside and outside the channel with the SST being slightly warmer inshore. The OFES model shows no gradients. In December (Fig 20, Bottom) when the circulation across the Zanzibar Channel is blocked by the cyclone and anticyclone at the north and south ends of the channel, respectively, there is a greater difference between temperatures inside and outside the channel. However the detailed spatial SST patterns inside the channel in the model and observations show opposite trends: KTCM shows cooler water SW of the island, and warmer water NW of the island, whereas the satellite shows the warmer water SW of the island. The pattern in OFES is similar to KTCM but the magnitude of SST is cooler by $2^{o}$C. The SST pattern in KTCM suggest localized upwelling SW of the island; the westward flow is pushing the warm surface water to the NW. Strong mixing due to tides and high frequency wind fluctuations may prevent this pattern if it occurs in nature from persisting in the satellite SST.

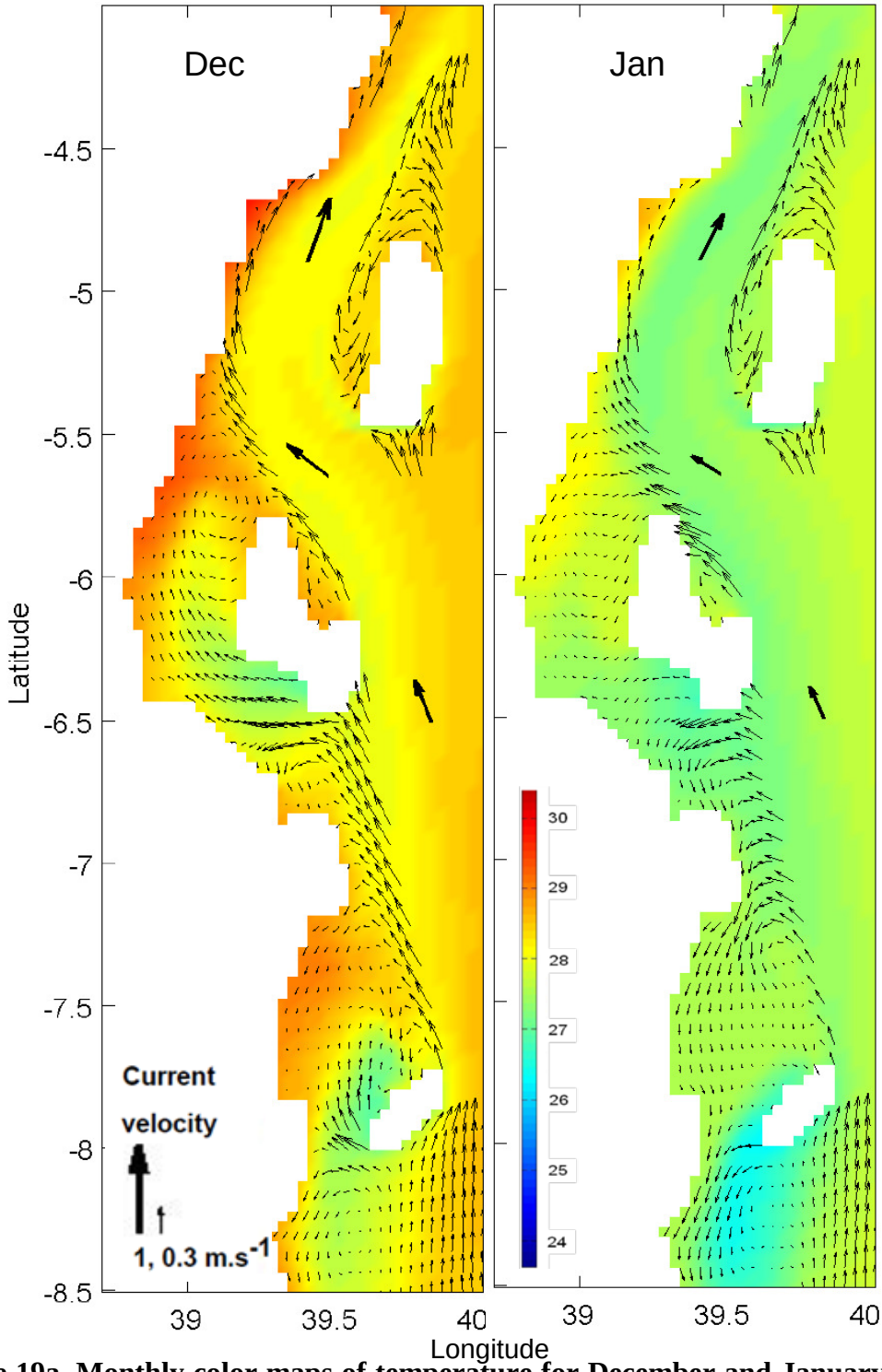


**Figure 19a. Monthly color maps of temperature for December and January with surface velocity vectors. The islands from north to south are Pemba, Zanzibar and Mafia. Velocity vectors with a speed greater than 0.4m.s$^{-1}$ were removed for clarity. The thicker arrows represent the flow of removed vectors.**

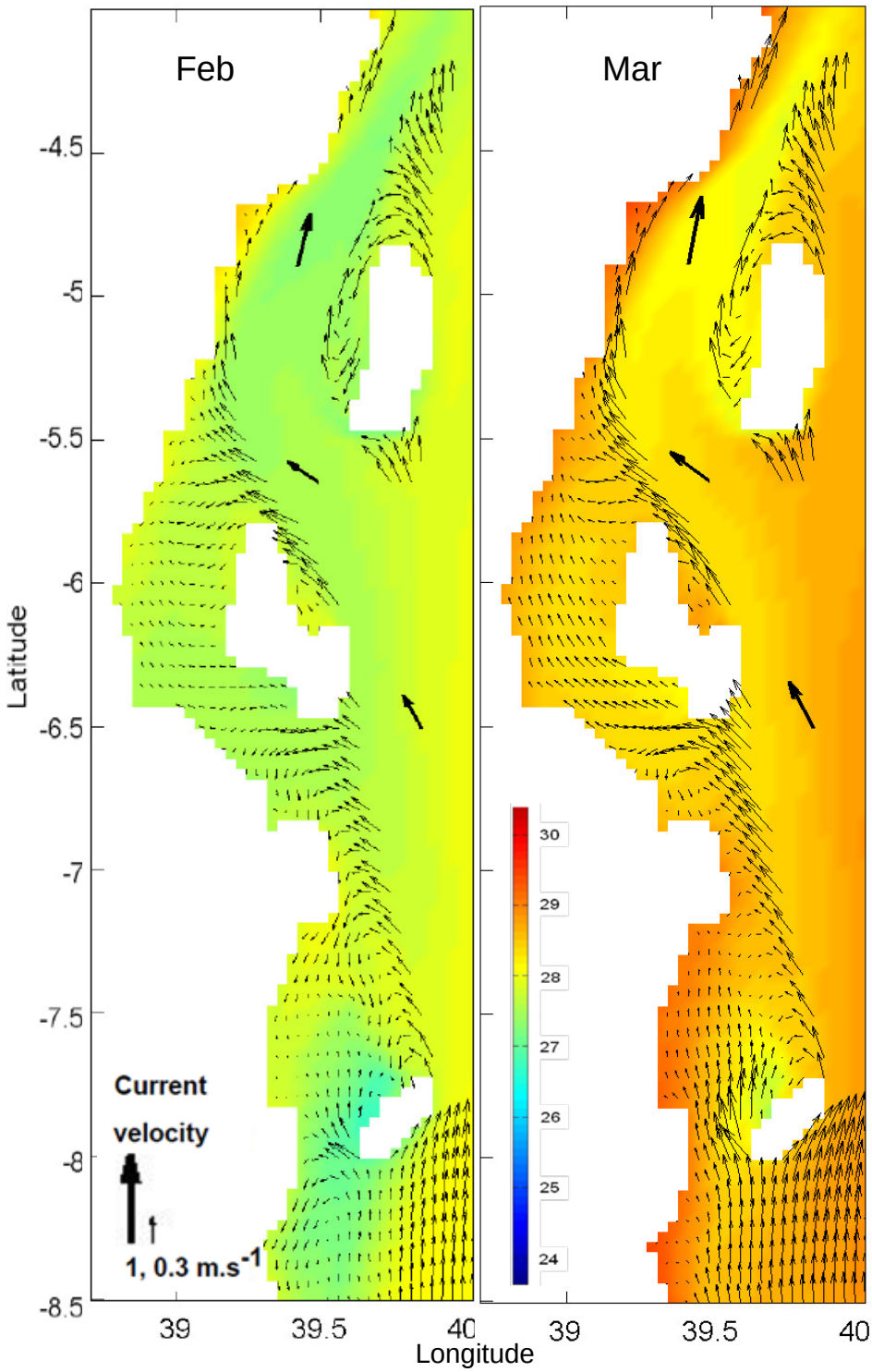


**Figure 19b. Monthly color maps of temperature for February and March with surface velocity vectors. Velocity vectors with a speed greater than 0.4m.s$^{-1}$ were removed for clarity. The thicker arrows represent the flow of removed vectors.**

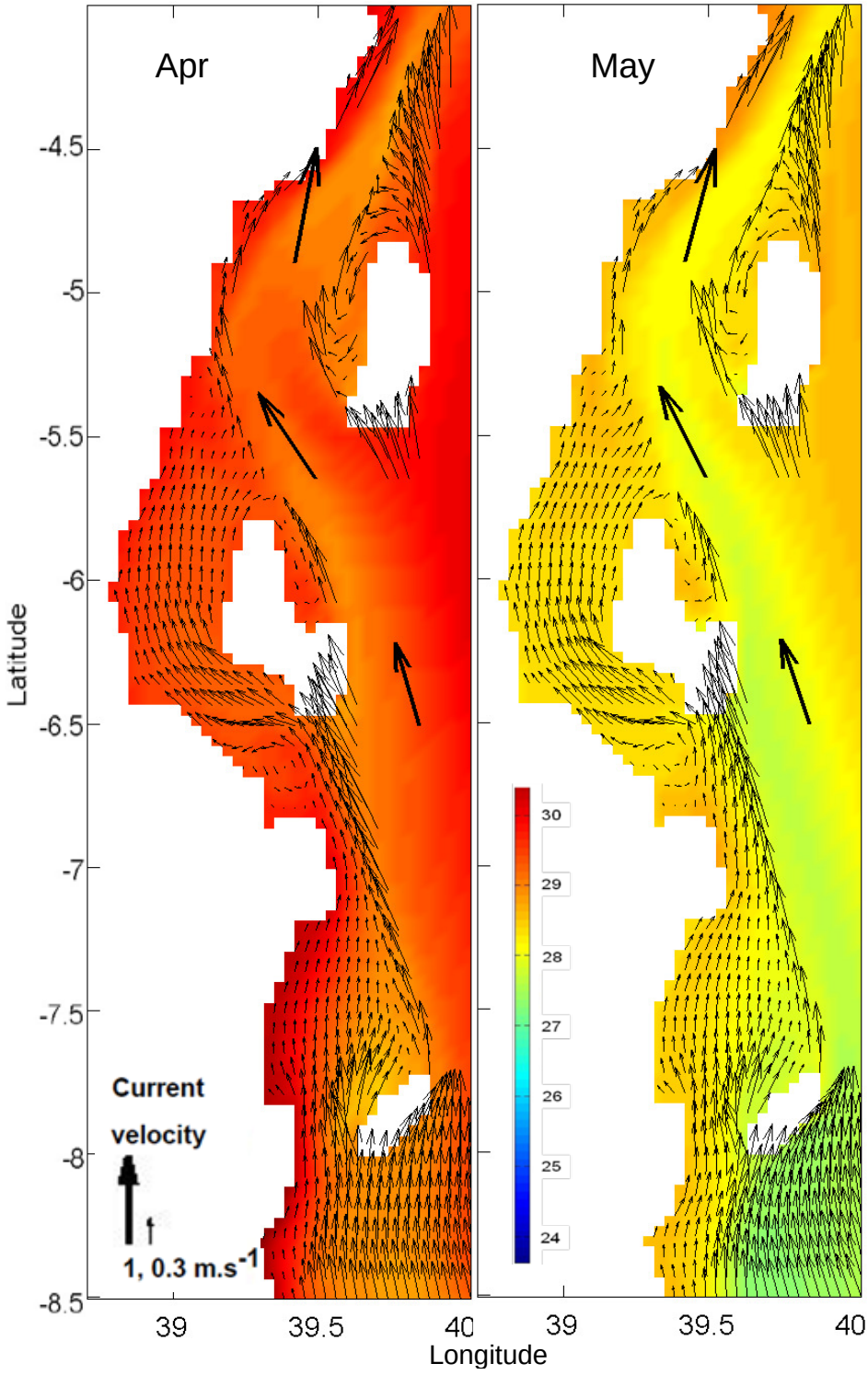


**Figure 19c. Monthly color maps of temperature for April and May with surface velocity vectors. Velocity vectors with a speed greater than 0.4m.s$^{-1}$ were removed for clarity. The thicker arrows represent the flow of removed vectors.**

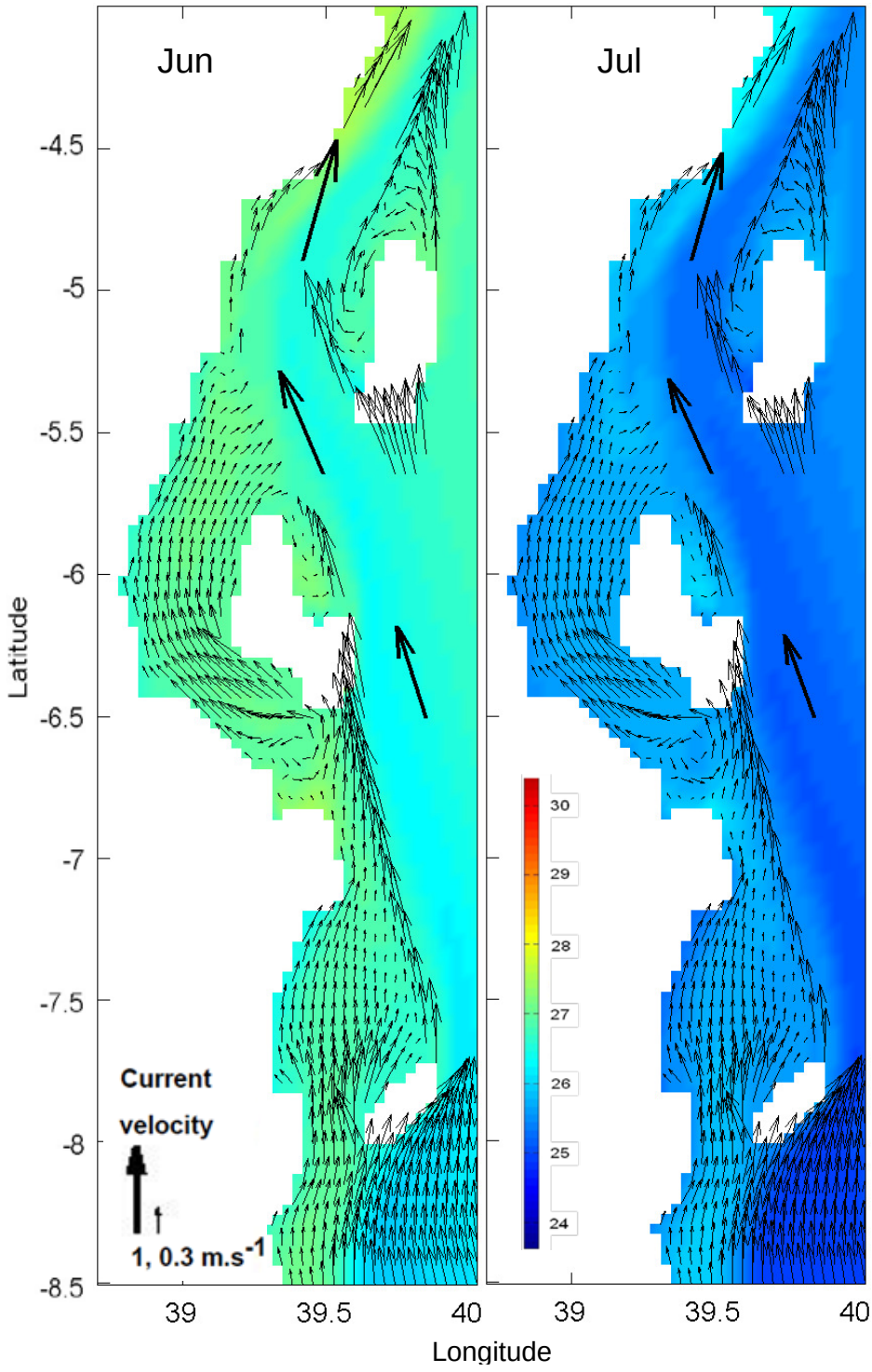


**Figure 19d. Monthly color maps of temperature for June and July with surface velocity vectors. Velocity vectors with a speed greater than 0.4m.s$^{-1}$ were removed for clarity. The thicker arrows represent the flow of removed vectors.**

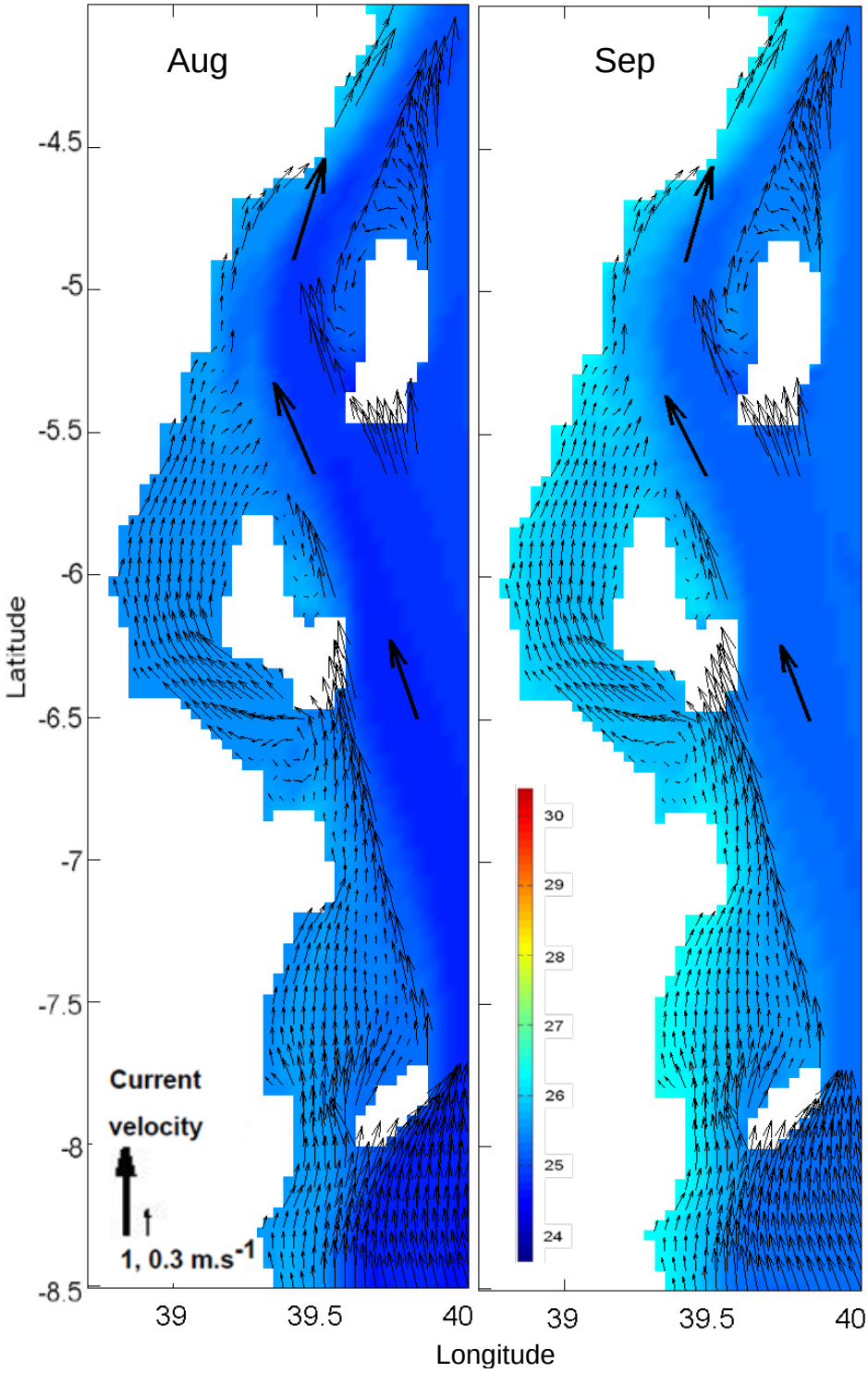


**Figure 19e. Monthly color maps of temperature for August and September with surface velocity vectors. Velocity vectors with a speed greater than 0.4m.s$^{-1}$ were removed for clarity. The thicker arrows represent the flow of removed vectors.**

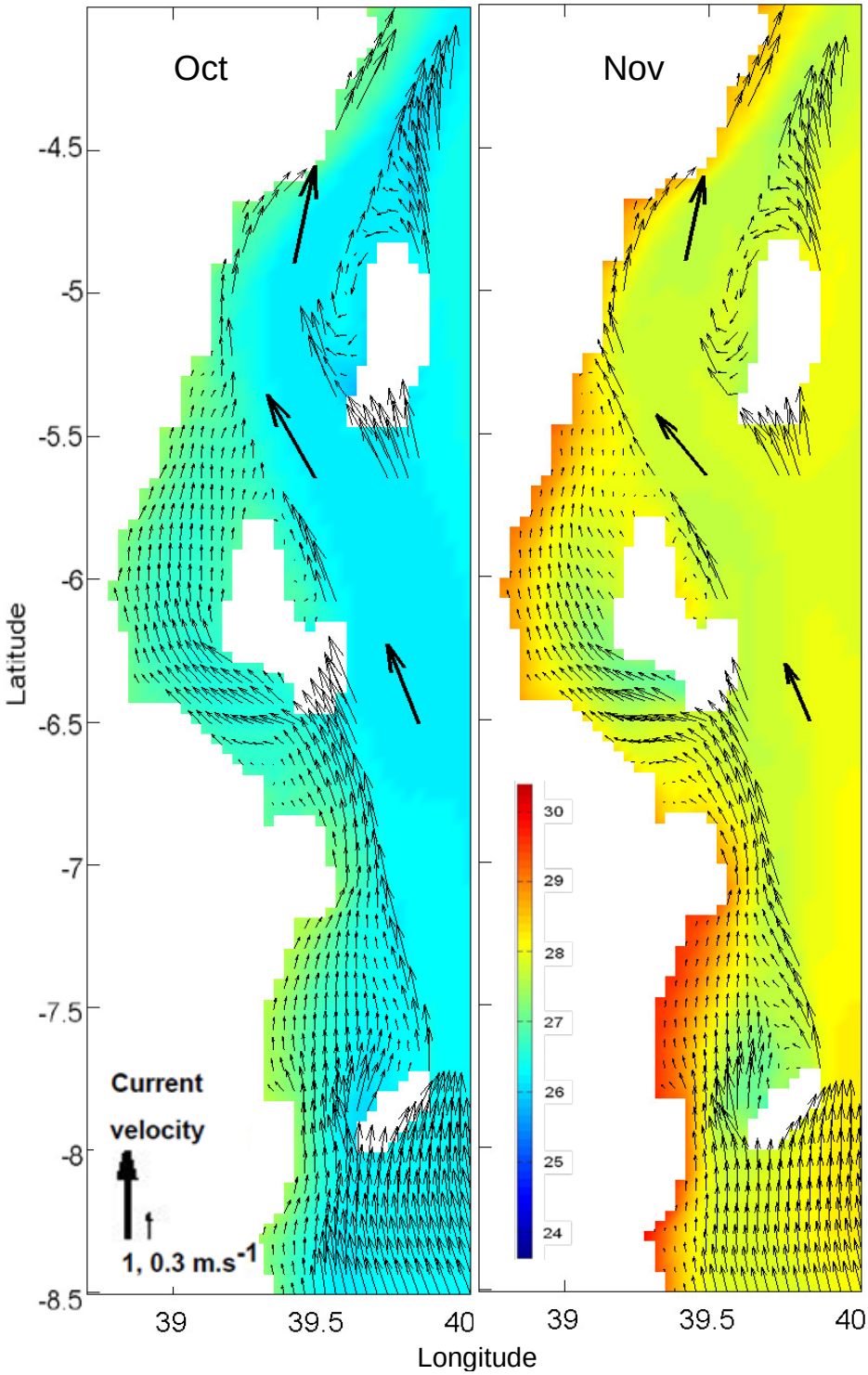


**Figure 19f. Monthly color maps of temperature for October and November with surface velocity vectors. Velocity vectors with a speed greater than 0.4m.s$^{-1}$ were removed for clarity. The thicker arrows represent the flow of removed vectors.**

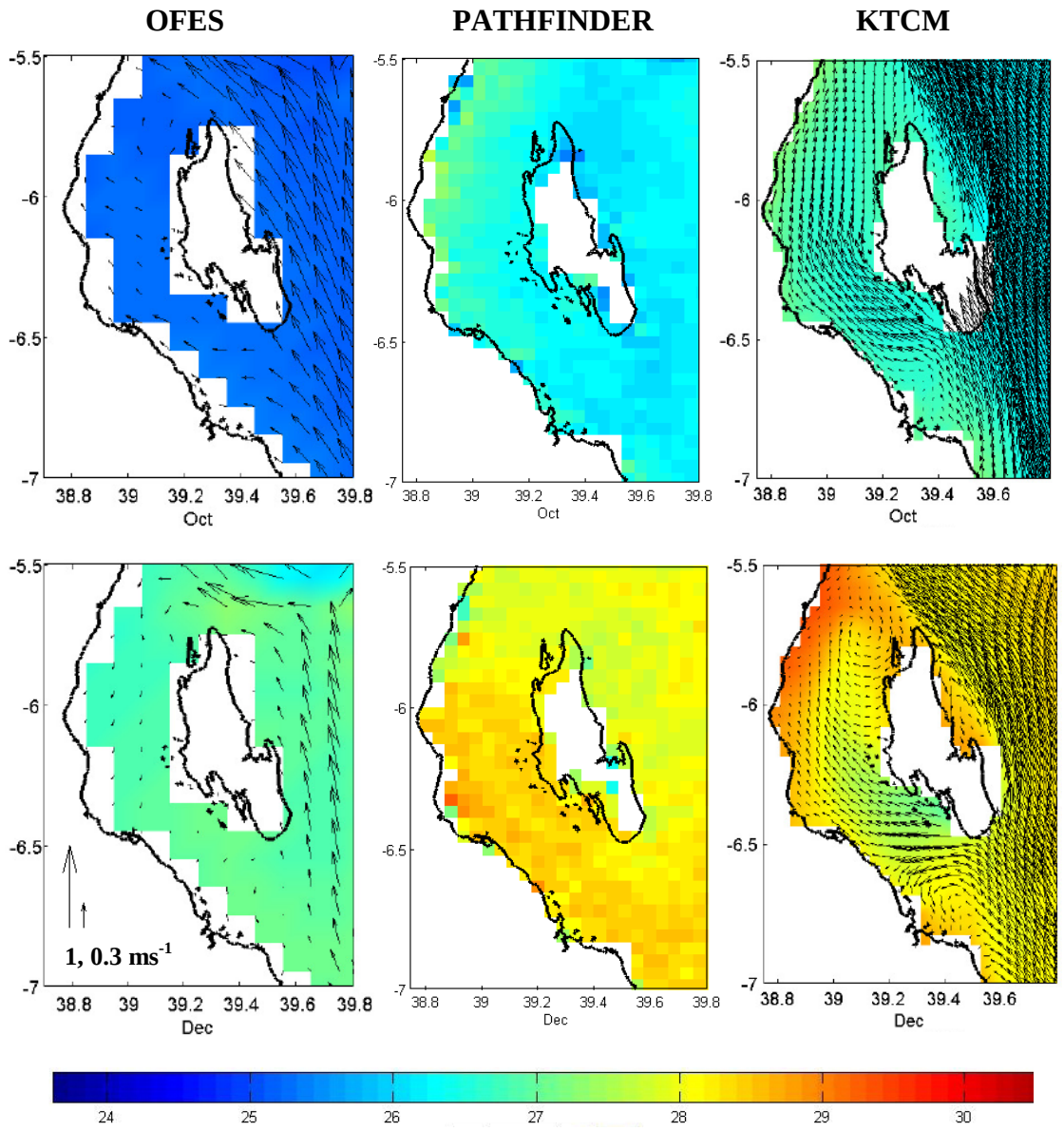


**Figure 20. SST around Zanzibar Island is shown in color for October (Top) and December (Bottom), from OFES, the Pathfinder satellite product and KTCM. Velocity vectors are shown at full resolution for both models. Scale arrows in the lower left panel apply to all panels.**

### *3.3. Model applications*

#### *3.3.1 Inter-annual variability*

The monthly wind stress forcing for 2000 is shown in Figure 21a and b. The observed patterns are similar to the climatological forcing field. The magnitude of the wind stress is stronger than in the climatology by ~0.1 dyn $m^2$ during most of the year, except during October to November. The volume transports through the three open boundaries during this year (Fig 22) are very similar to the patterns observed in the climatology, with more variability as expected for an individual year.

The circulation pattern in 2000 is very similar to the climatological results during the 1$^{st}$ half of the year (Figs 23a & 14a). Speeds are greater than in the climatological run in some locations. The confluence of the SC and the EACC is shifted southward during January, February and March. The anticyclonic eddy centered near 6$^o$S, 42$^o$E (Fig 14b) in the climatology during Nov-Dec, is present in the 2000 year simulation from Sep to Dec. The SG present in the climatology from July to October in the northeast corner of the domain during the 2nd half of the year is not present during 2000. During November and December the band of high SSH along the southern open boundary (SEC) is narrower than in the climatology. SST (Fig 24) is in general colder than the climatology (Fig 5c). The warmer months are January-February opposed to March in the climatology.

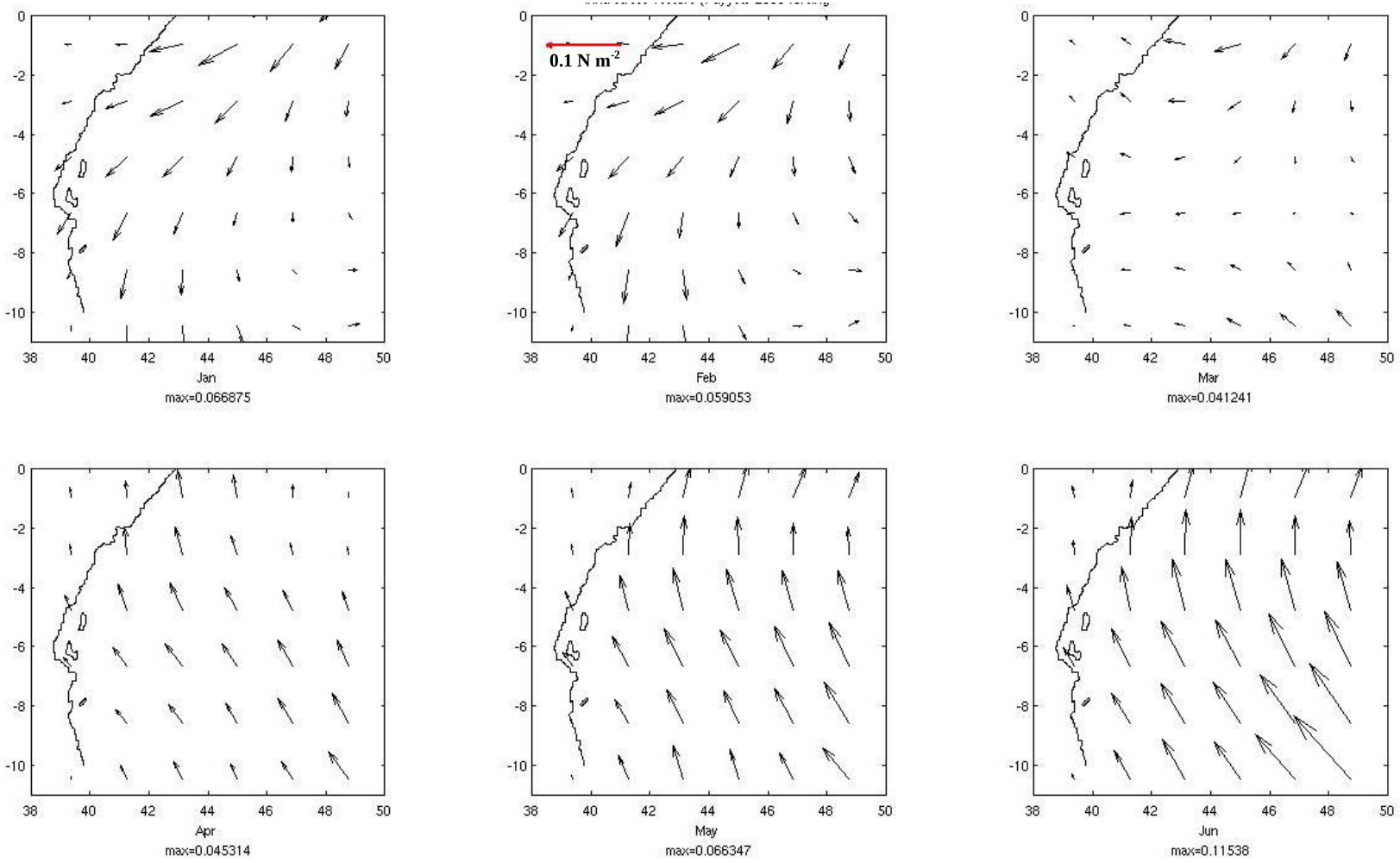


**Figure 21a. Monthly means of the NCEP wind stress forcing for Jan to Jun of 2000. The number below each panel is the maximum of the wind stress magnitude for each month in N $m^{-2}$. Scale vector on Feb apply to all panels.**

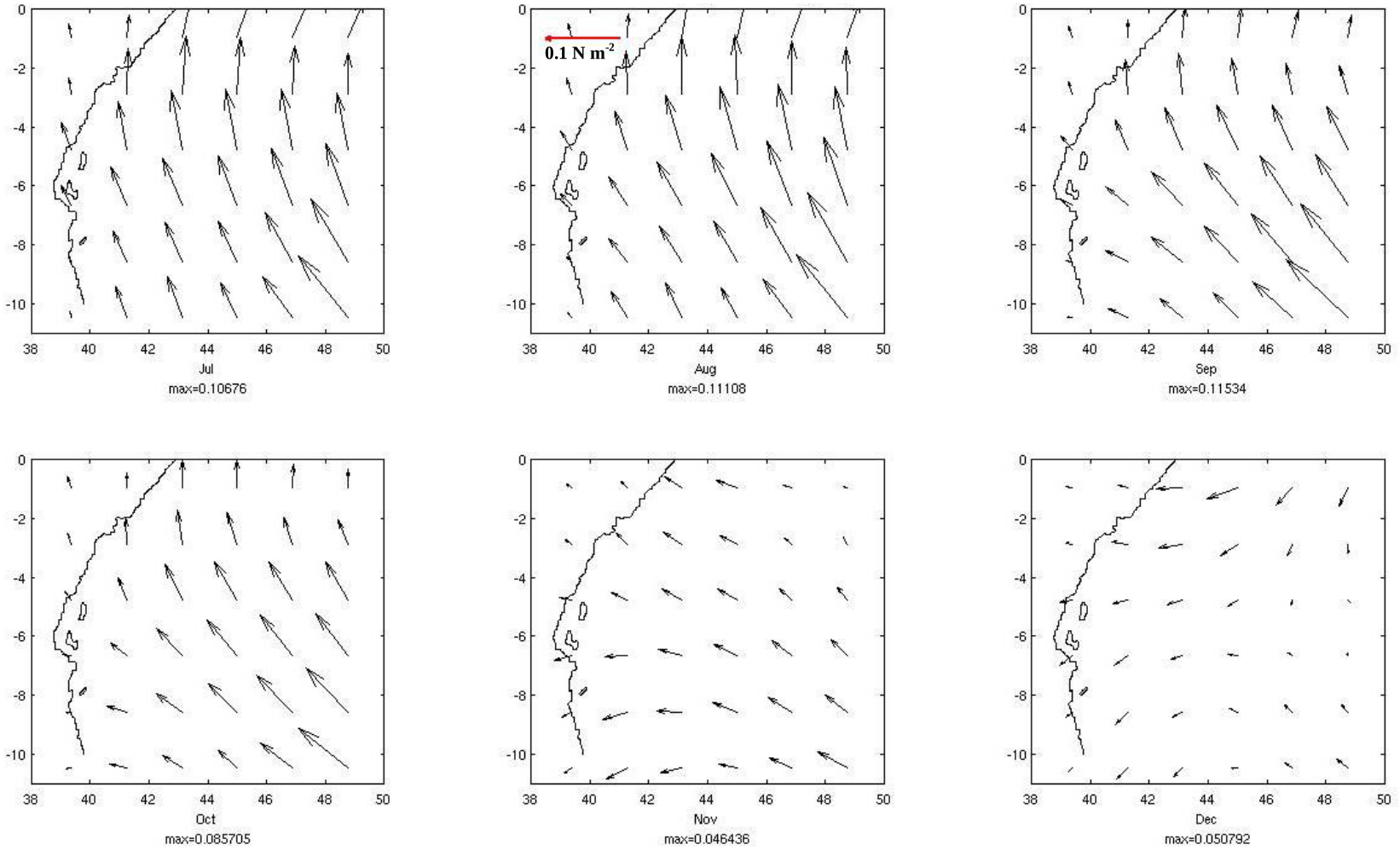


**Figure 21b. Monthly means of the NCEP wind stress forcing for Jul to Dec of 2000. The number below each panel is the maximum of the wind stress magnitude for each month in N $m^{-2}$. Scale vector on Aug apply to all panels.**

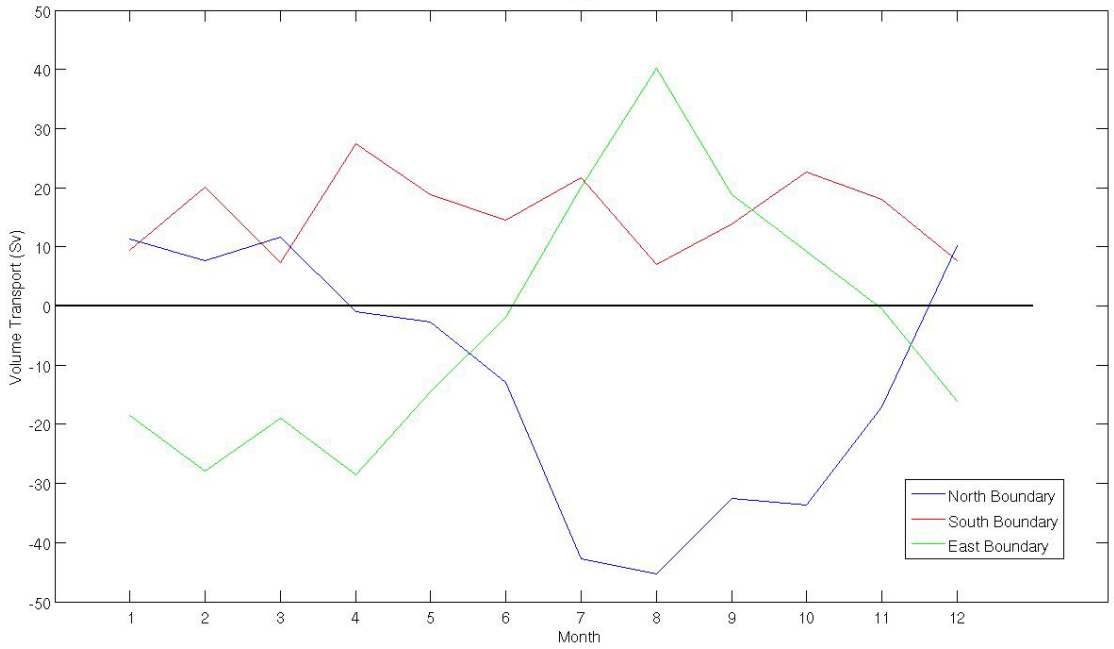


**Figure 22. Volume transport in Sverdrup's ($Sv=10^6 m3s^{-1}$) across the 3 open boundaries of the model domain for 2000. Positive values represent transport into the domain, and negative values transport out of the domain.**

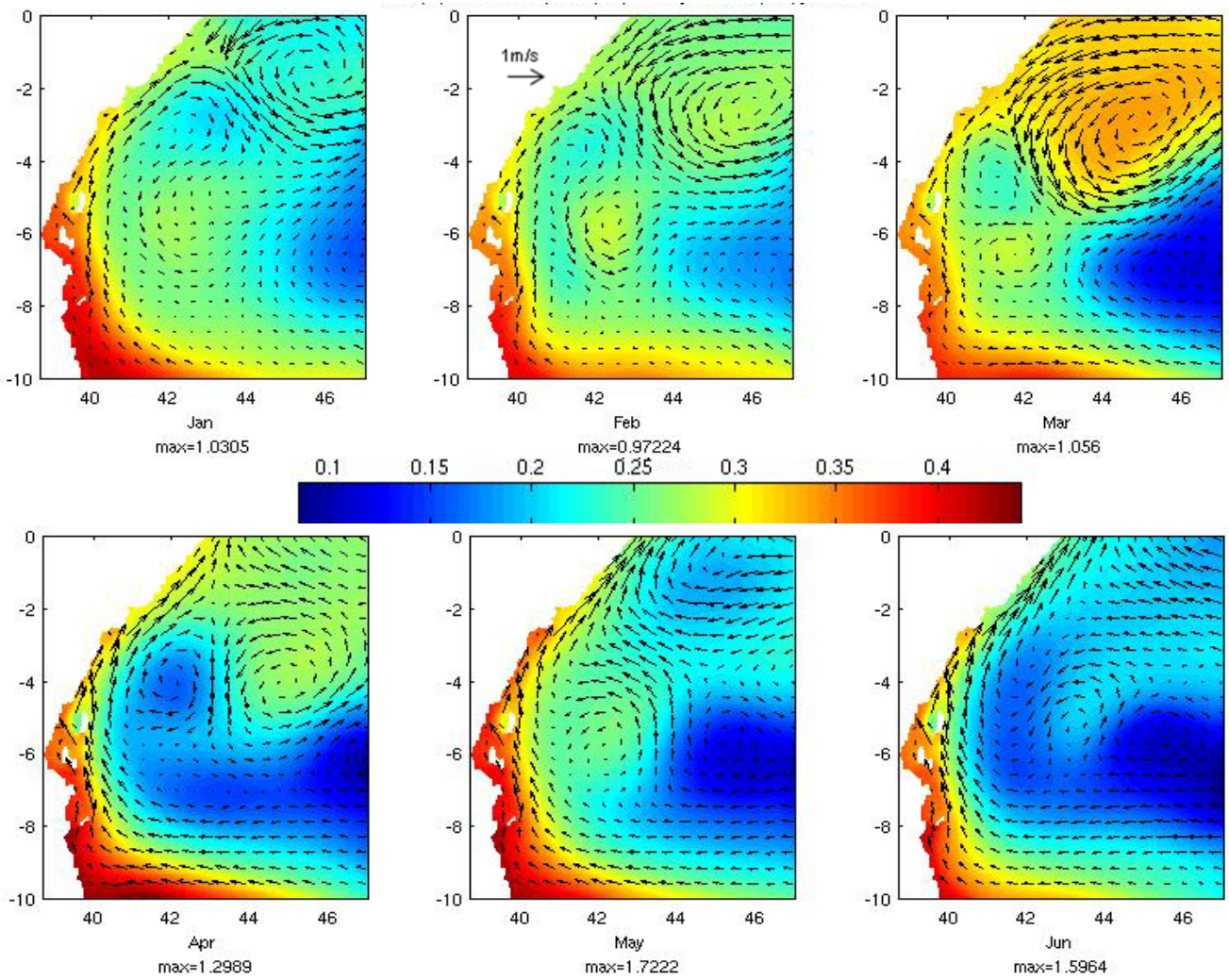


**Figure 23a. KTCM 'Bulk' monthly SSH in meters with vectors of surface velocity for Jan to Jun of 2000, maximum speed in m.s$^{-1}$ for each month is at the foot of each panel. Scale vector on Feb apply to all panels.**

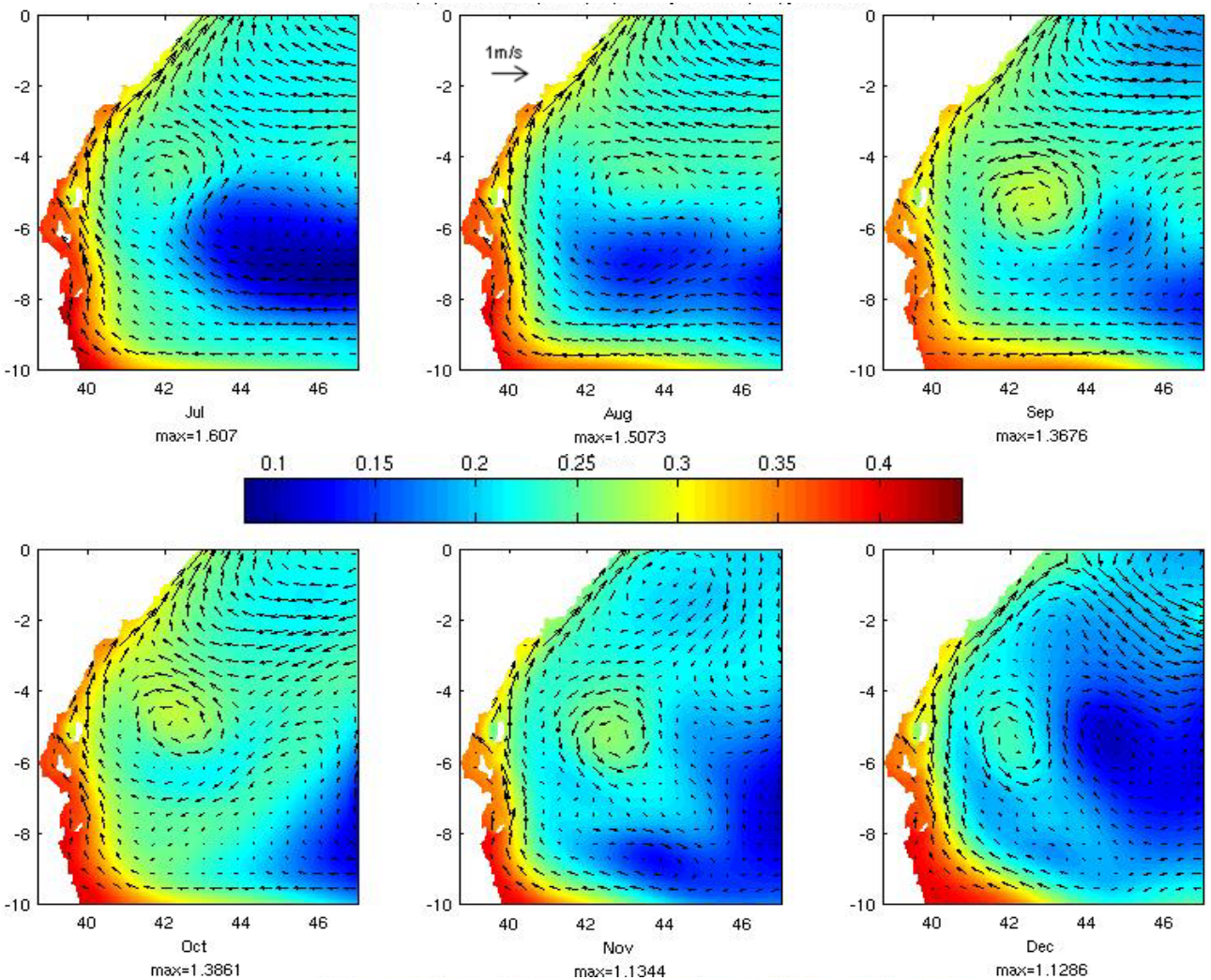


**Figure 23b. KTCM 'Bulk' monthly SSH in meters with vectors of surface velocity for Jul to Dec of 2000, maximum speed in m.s$^{-1}$ for each month is at the foot of each panel. Scale vector on Aug apply to all panels.**

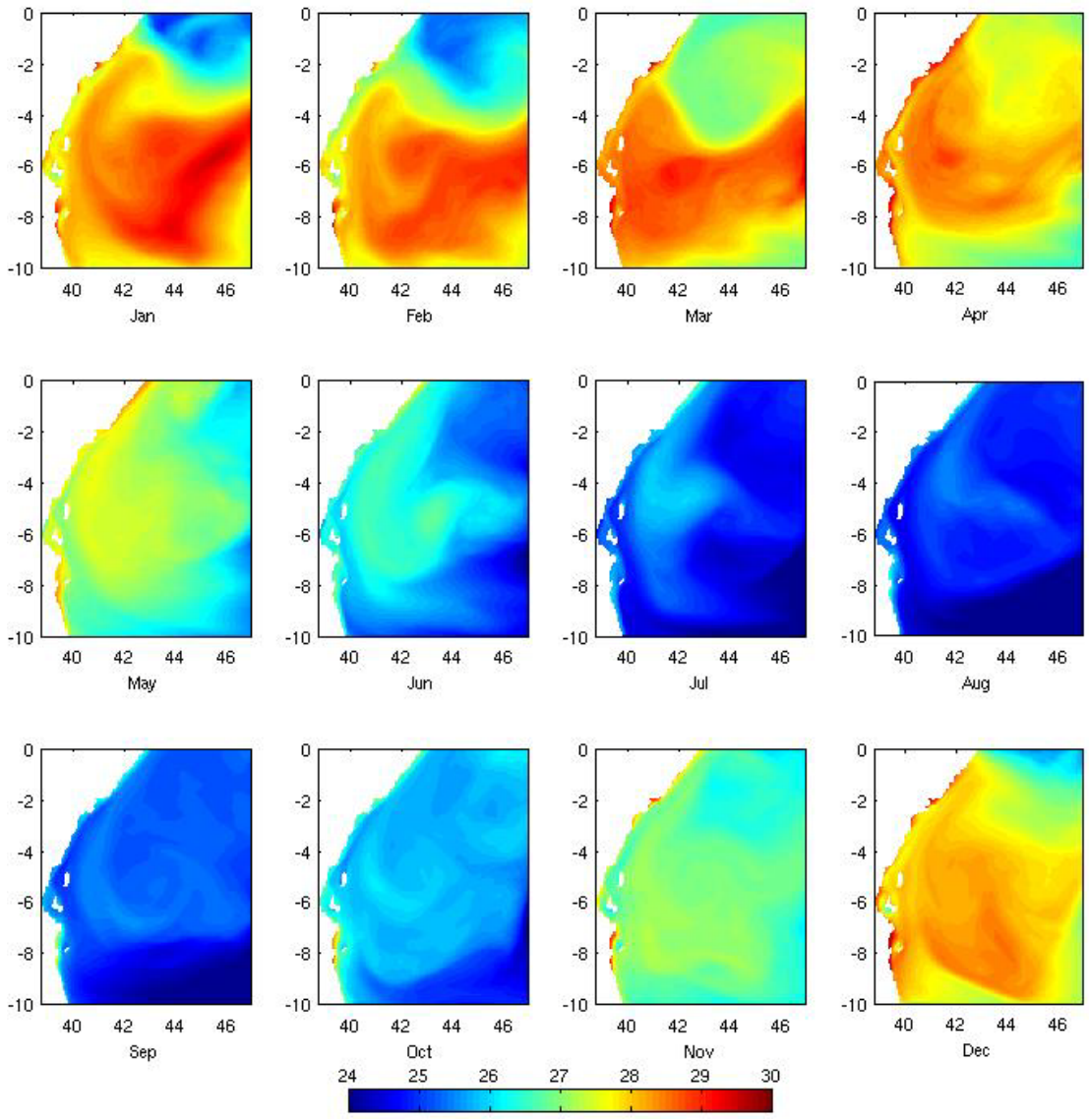


**Figure 24. Modeled monthly SST ($^{o}$C) for 2000.**

The monthly mean wind stress forcing used for 2007 is shown in Figure 25. The magnitude of the wind stress is stronger than in the climatology by ~0.2 dyn $m^2$ during most of the 2007 year, except during November when it is slightly weaker than in the climatology. The wind stress pattern is similar to the climatology during all the year, except in December when the wind is already aligned more alongshore, representing an earlier onset of the NE monsoon. The flow through the open boundaries during 2007 (Fig 26) show more variability than during 2000 or the climatology. The patterns are different mainly during the $1^{st}$ half of the year on the southern and eastern open boundaries. Outward transport of 20 Sv during April through the southern boundary differs markedly from the climatological case which has flow into the domain. There is less flow (volume transport < 5 Sv) through this boundary during December and February. The direction of the flow through the eastern boundary also switched direction in April. Less outward flow occurs during February and March and greater inward flow occurs during June, in comparison to the climatological and 2000 simulations.

The circulation patterns during the NE monsoon season in 2007 are very different compared to the climatological results (Figs 27a & 27b, 14a & 14b, Dec-Mar). The onset of the NE monsoon occurs very quickly, or very early in the previous year since by January 2007 the jet that results from the confluence of the SC and the EACC is already aligned in the north-south direction. The January 2007 circulation pattern is more similar to the March climatology. In February a second anticyclone

advects into the domain through the eastern open boundary. In March the mesoscale features seen in the February fields continue to be advected westward and are compressed against the coast in April by the incoming flow of the SEC. The circulation at this time is more similar to the climatological circulation from April to November. The SG is present in the NE corner of the domain. The anticyclone centered around $6^{o}$S, $42^{o}$E in the climatology during November is also present in November 2007. In December 2007, the NE monsoons begins relatively quickly again and the circulation pattern is more similar to a climatological February. SST (Fig 28) is in general warmer than the climatology (Fig 5c), and 1-2$^{o}$C warmer than the 2000 SST.

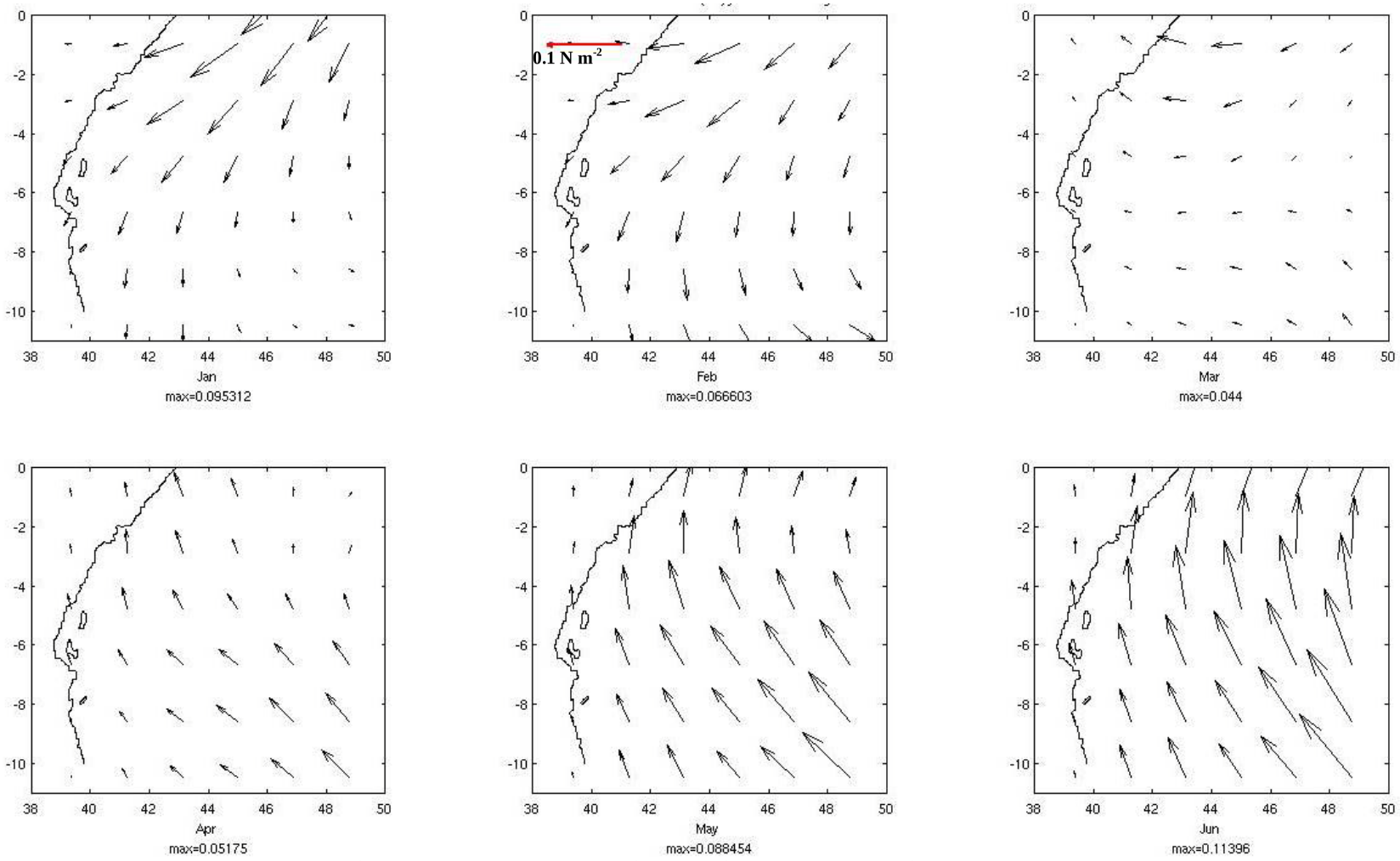


**Figure 25a. Monthly means of the NCEP wind stress forcing for Jan to Jun of 2007. The number below each panel is the maximum of the wind stress magnitude for each month in N $m^{-2}$. Scale vector on Feb apply to all panels.**

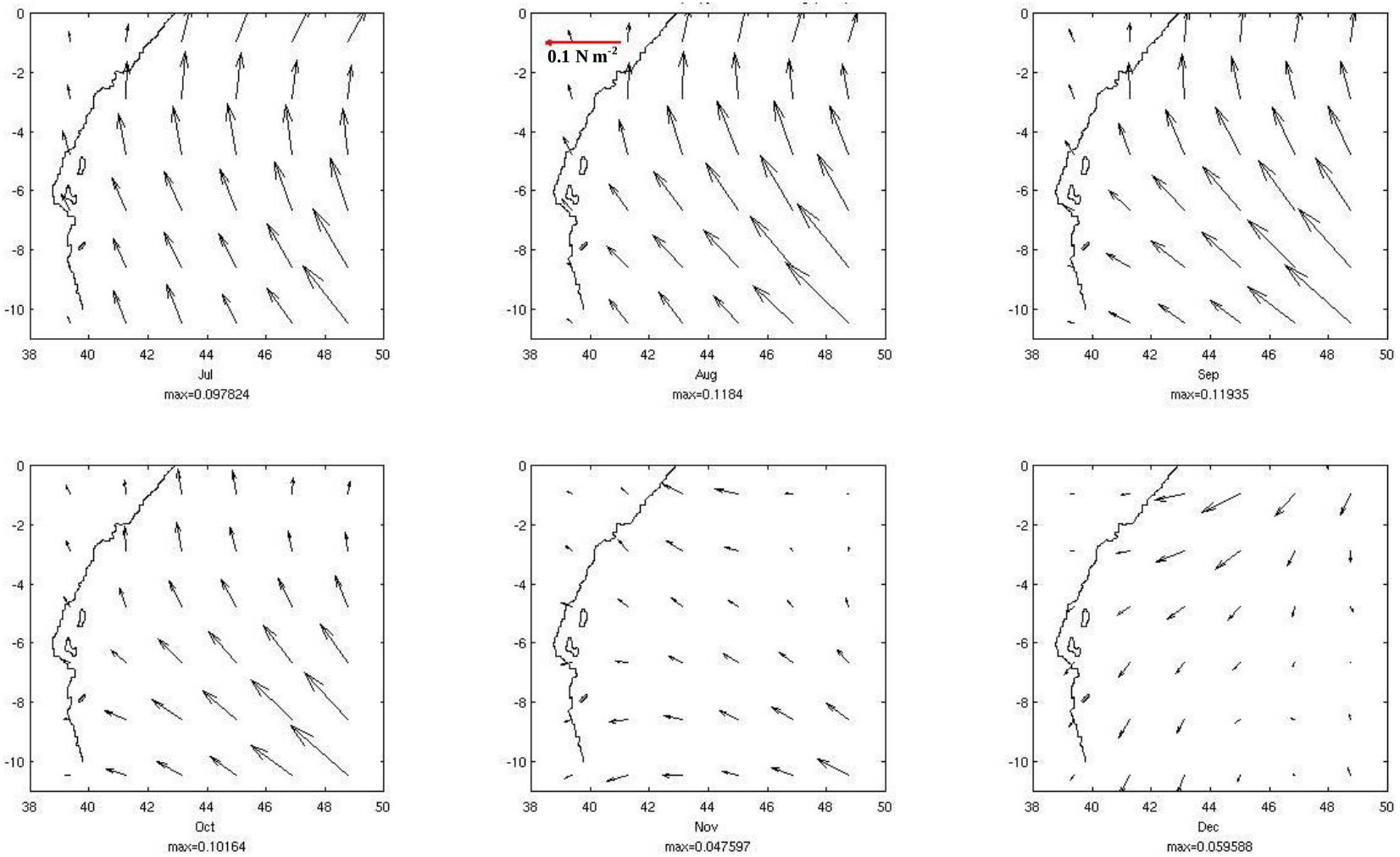


**Figure 25b. Monthly means of the NCEP wind stress forcing for Jul to Dec of 2007. The number below each panel is the maximum of the wind stress magnitude for each month in N $m^{-2}$. Scale vector on Aug apply to all panels.**

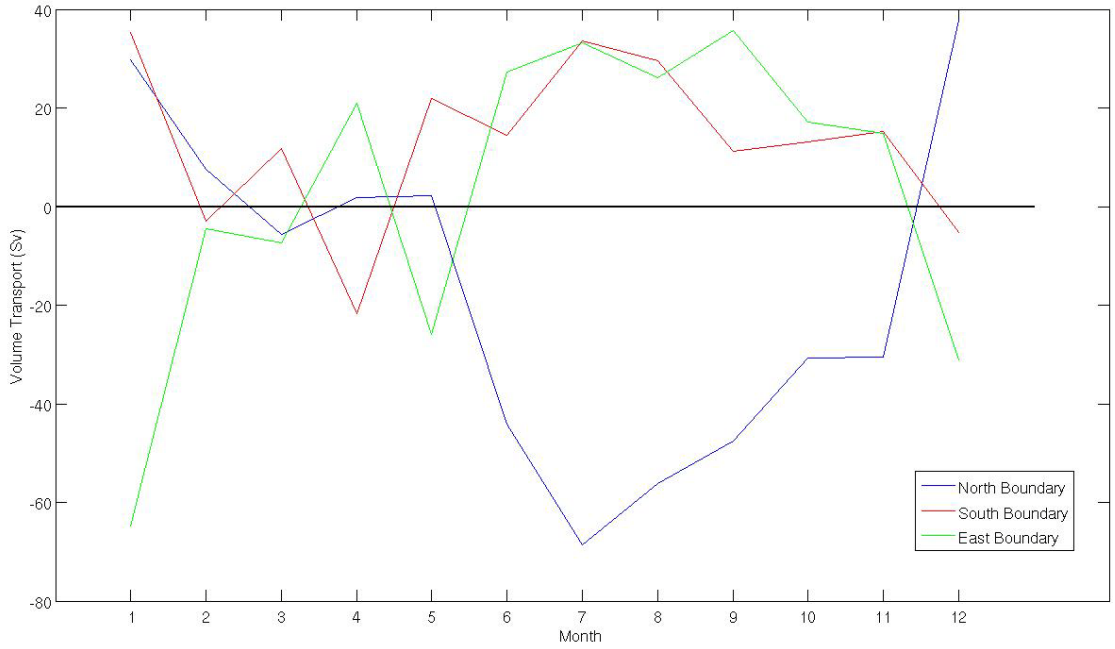


**Figure 26. Volume transport in Sverdrup's ($Sv=10^6 m^3 s^{-1}$) across the three open boundaries of the model domain for the 2007 year. Positive values represent transport into the domain, and negative values transport out of the domain.**

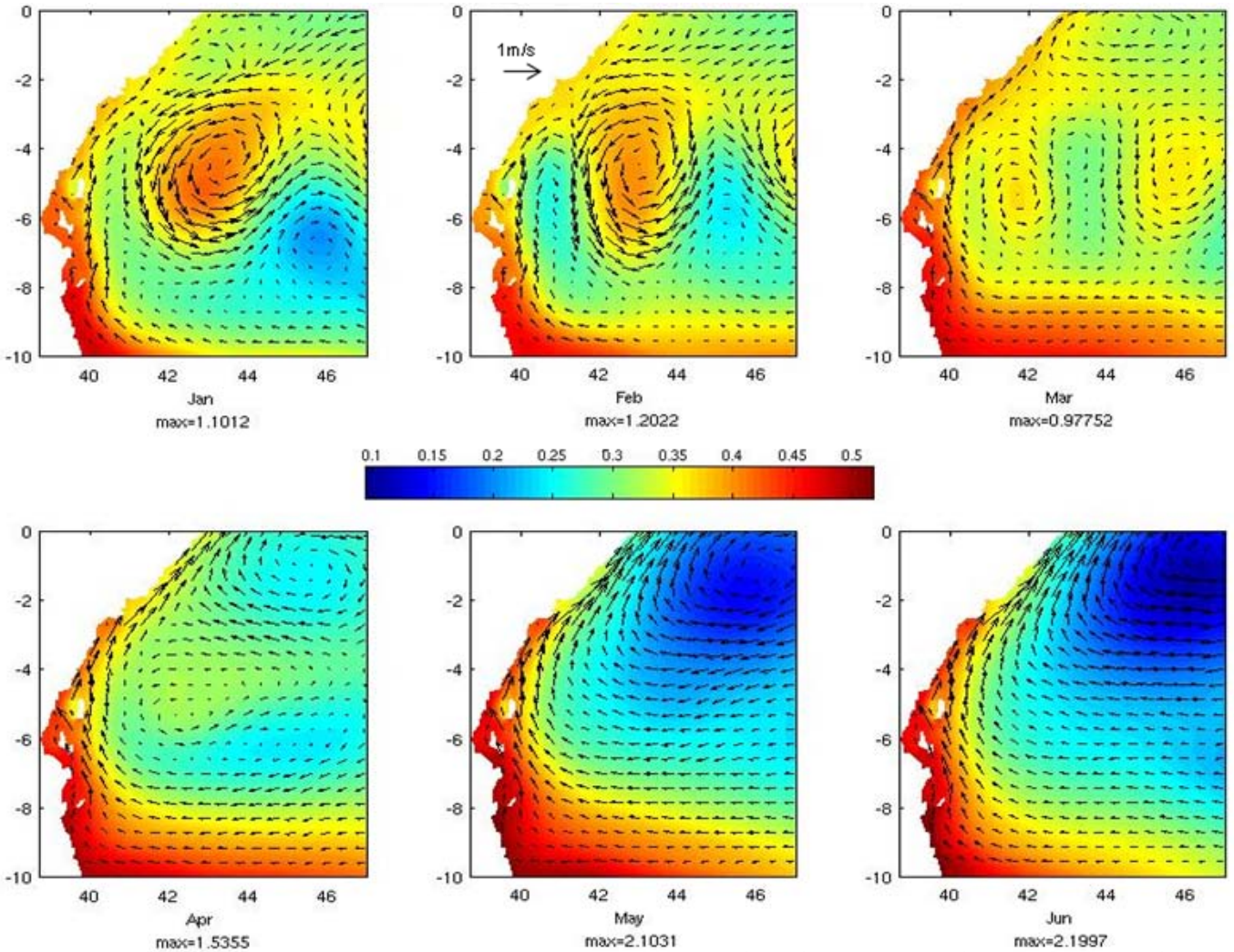


**Figure 27a. KTCM 'Bulk' monthly SSH in meters with vectors of surface velocity for Jan to Jun of 2007, maximum speed in m.s$^{-1}$ for each month is at the foot of each panel. Scale vector on Feb apply to all panels.**

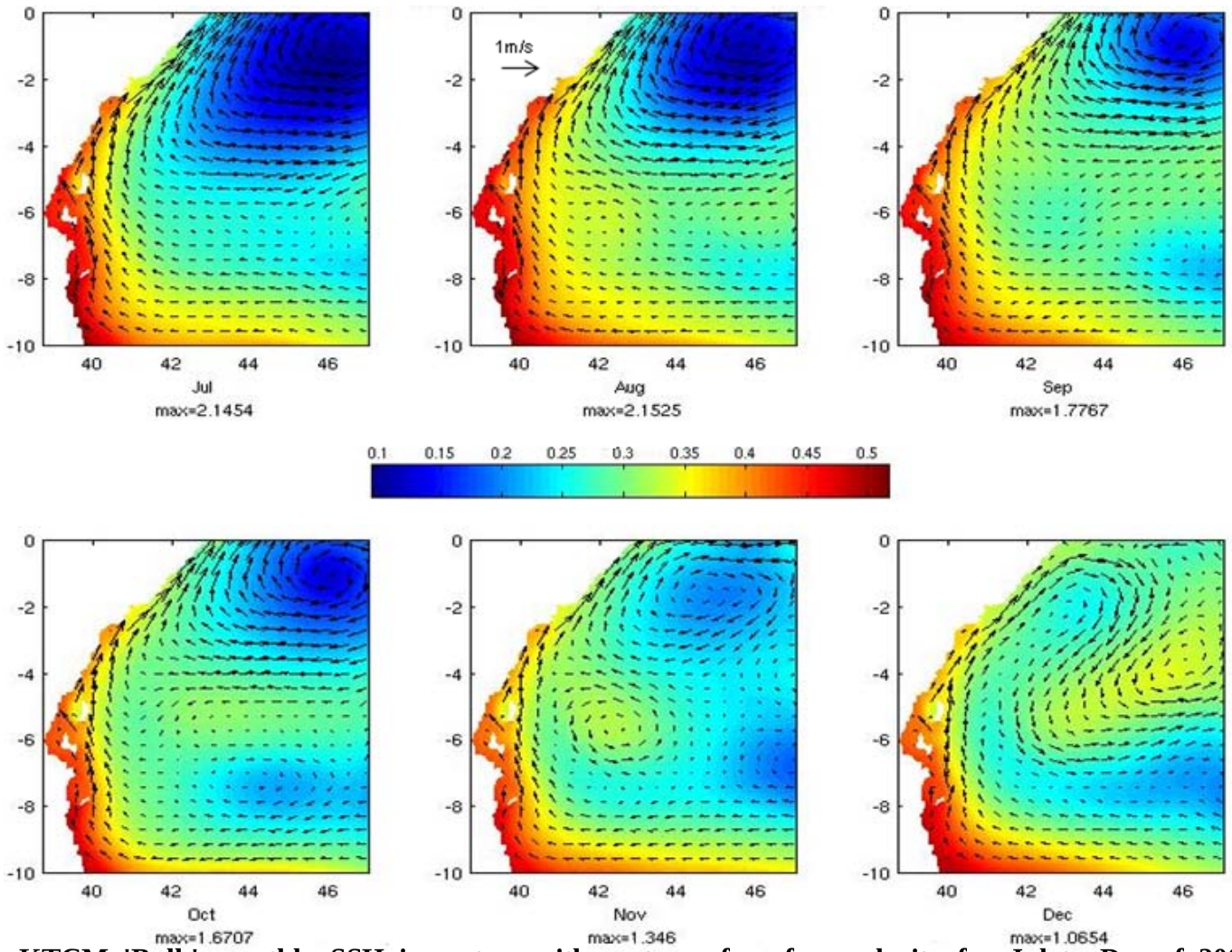


**Figure 27b. KTCM 'Bulk' monthly SSH in meters with vectors of surface velocity for Jul to Dec of 2007, maximum speed in m.s$^{-1}$ for each month is at the foot of each panel. Scale vector on Aug apply to all panels.**

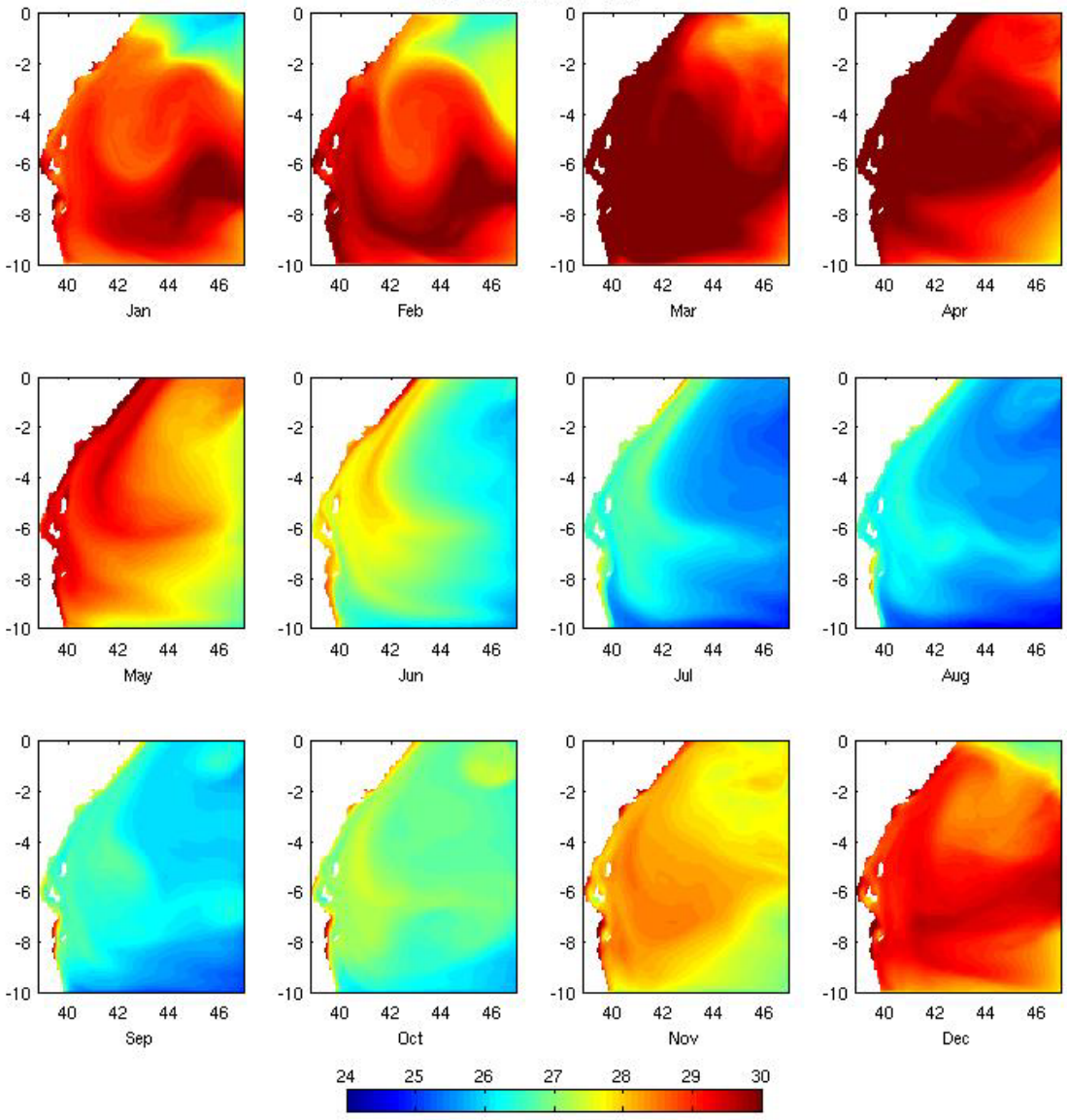


**Figure 28. Modeled monthly SST ($^{o}$C) for the year 2007.**

### *3.3.2 Lagrangian Particle Tracking Experiments*

The 60 day trajectories of surface Lagrangian particles released weekly in the climatological run from locations near coral reefs[6] (A through J; fig 29) were used to quantify the seasonal variability in flows, and to examine the potential connections among coral reef habitats. The 2 month period was chosen because it encompasses the pelagic larval duration of common benthic organisms that inhabit coral reef environments (Wellington and Victor, 1989). Although particles were released weekly, we focus here on the differences in transport distances, retention and connectivities during the NE monsoon (January-February) and the SW monsoon (June-July). The particle tracks demonstrate clearly the differences in transport from these nearshore environments between these two periods: the sluggish period, when the flow through the shallow channels (Zanzibar and Mafia) is minimal (December, January and February), and the strong northward flow regime during the rest of the year.

During December to February (only Jan-Feb shown) the near-shore region is very retentive (Figs 30a & 31a). Particles released from reefs locations within the Zanzibar Channel (A,B, D, E) are retained in the channel. Particles released on the west coast of Zanzibar Island (D & E) travel westward across the channel and spread both north and south from the release position. Particles released on the east coast of Zanzibar Island (C, I) are caught in a permanent anticyclone in Chwaka Bay on the east coast of the Island. Only one of the 16 particles from these two

stations made its way north and into the Pemba Channel. Particles released east of the northern tip of Zanzibar Island (F) travel westward and into the Zanzibar Channel, reaching the coast of mainland Tanzania at the end of 60 days. The particles released south and north of Mafia Island (G and H respectively) remain on the shelf and their net displacement is much less than during the rest of the year. Particles from the releases north of Mafia Island (H) travel westward to end their trajectories at the coast of mainland Tanzania. Some of these particles travel southward through the Mafia Channel and are caught in an anticylonic eddy, while others have a short (~60km) northward displacement. The particles released to the south of Mafia channel (G) travel around the north tip of the island and are caught in the same eddy. Some particles are transported to the north shores of Mafia Island while other particles escape the eddy and arrive at the coast of mainland Tanzania, approximately 60 km to the north of the Island.

During the rest of the year particles from all release locations are advected northward along the coast, reaching maximum speeds during June and July (Figs 30b & 31b). All particles released south of the Pemba Channel traverse through it. During the inter-monsoon periods (Mar-May and Oct-Nov) some of the particles released around Mafia Island make their way north through the Zanzibar Channel (not shown); the rest of the year they travel along the east coast of Zanzibar Island and into the Pemba Channel. Particles released in the northern coast of mainland Tanzania (J) travel northward along the coast all year-round.

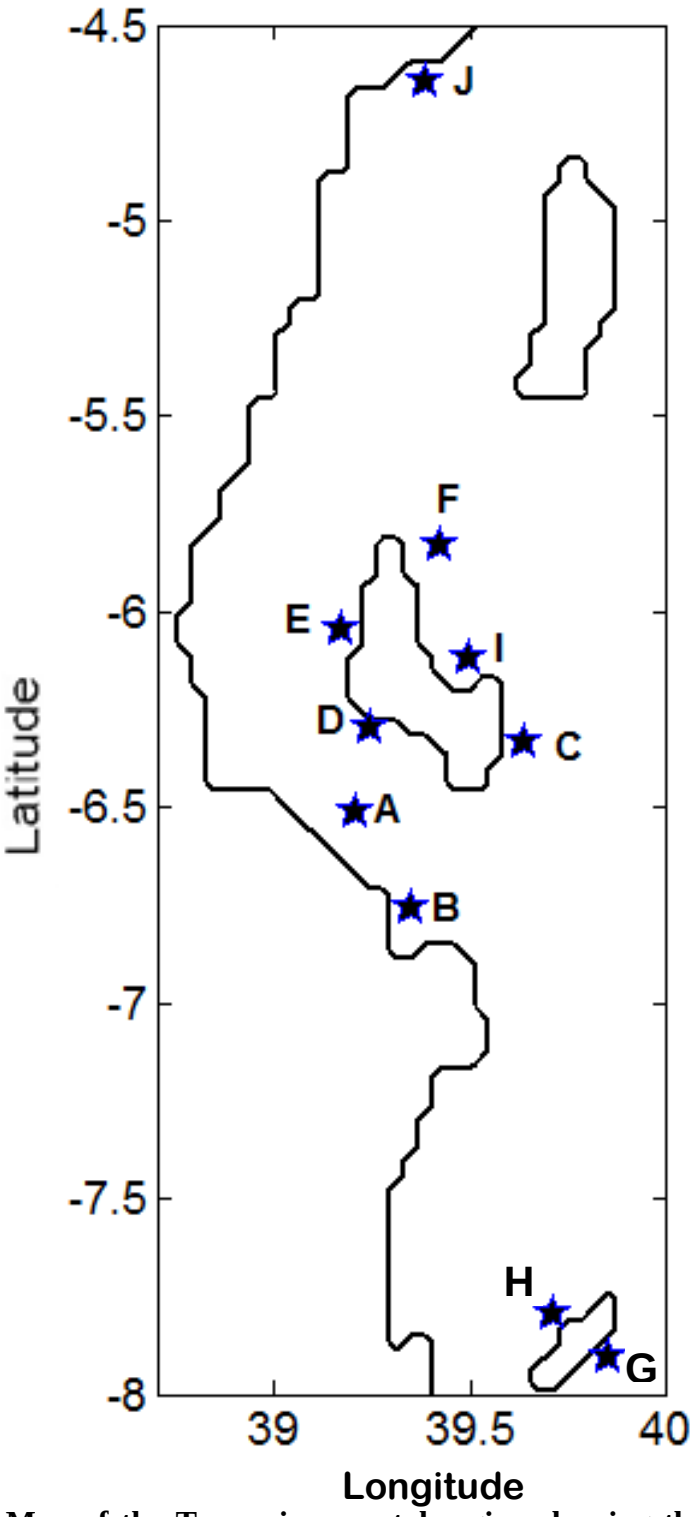


**Figure 29. Map of the Tanzanian coastal region showing the positions were surface Lagrangian particles where released. The Island from north to south are Pemba, Zanzibar and Mafia.**

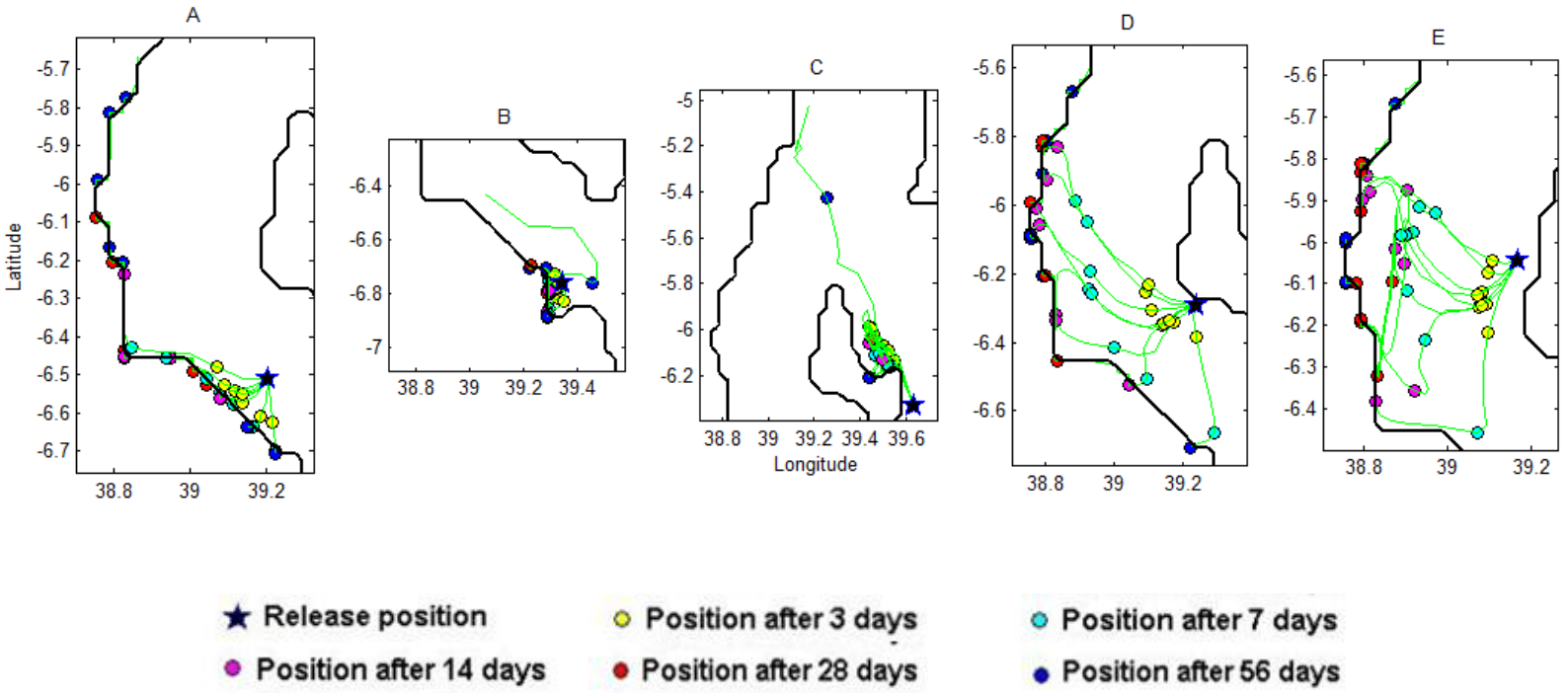


**Figure 30a. Trajectories particles released at positions A-E during January to February. Position through time is marked following the color key above. The eight trajectories (green lines) represent the releases from eight consecutive weeks.**

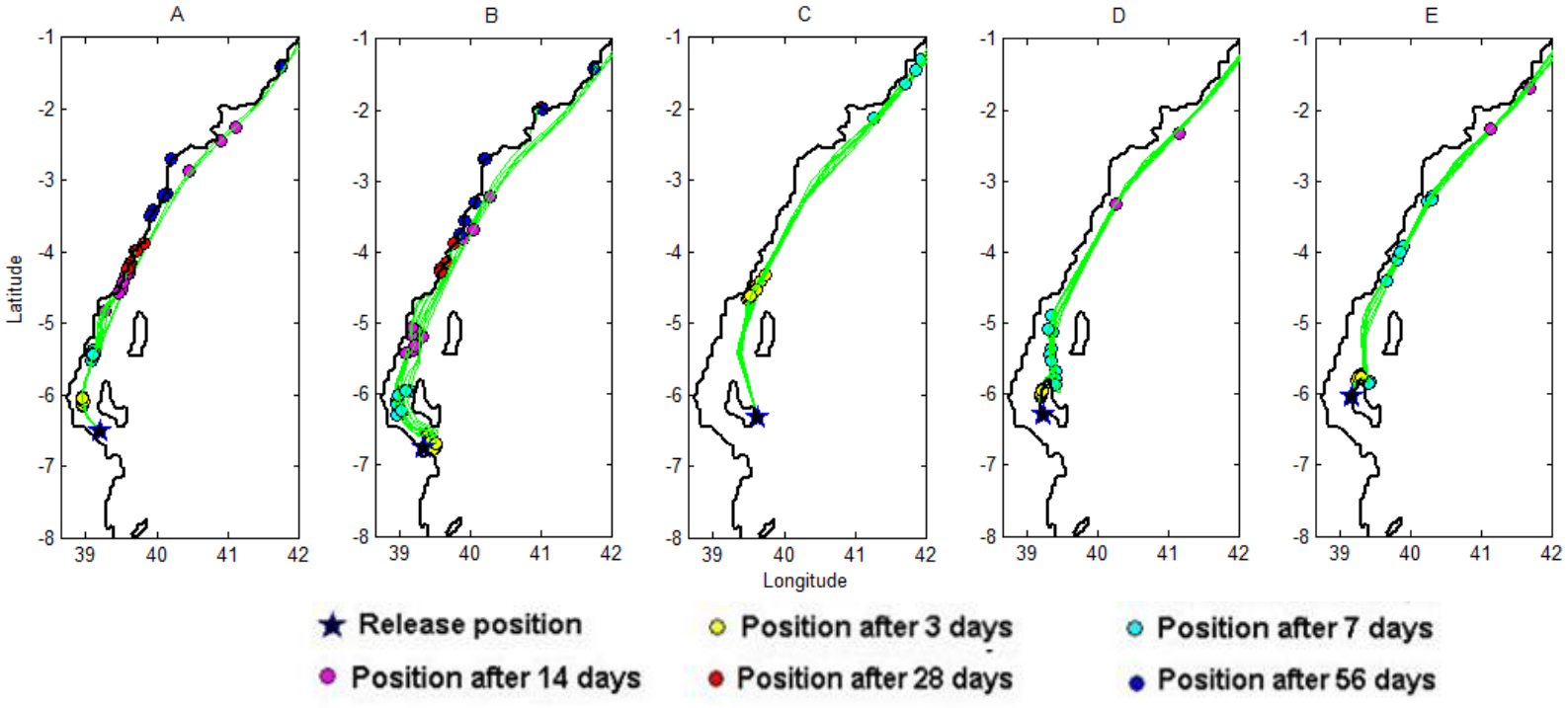


**Figure 30b. Trajectories of the particles released at positions A-E during June to July. Position through time is marked following the color key above. The eight trajectories (green lines) represent the releases from eight consecutive weeks.**

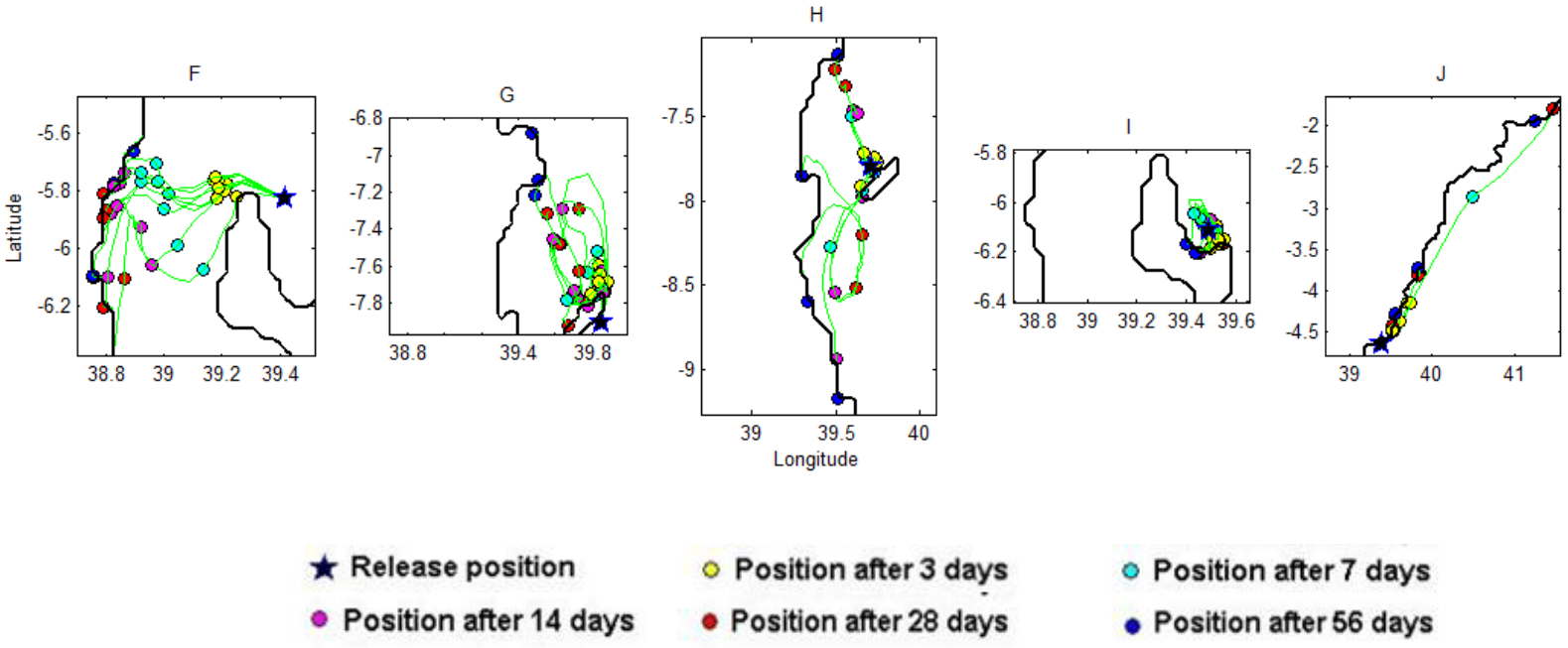


**Figure 31a. Trajectories of particles released at the positions F-J during January to February. Position through time is marked following the color key above. The eight trajectories (green lines) represent the releases from eight consecutive weeks.**

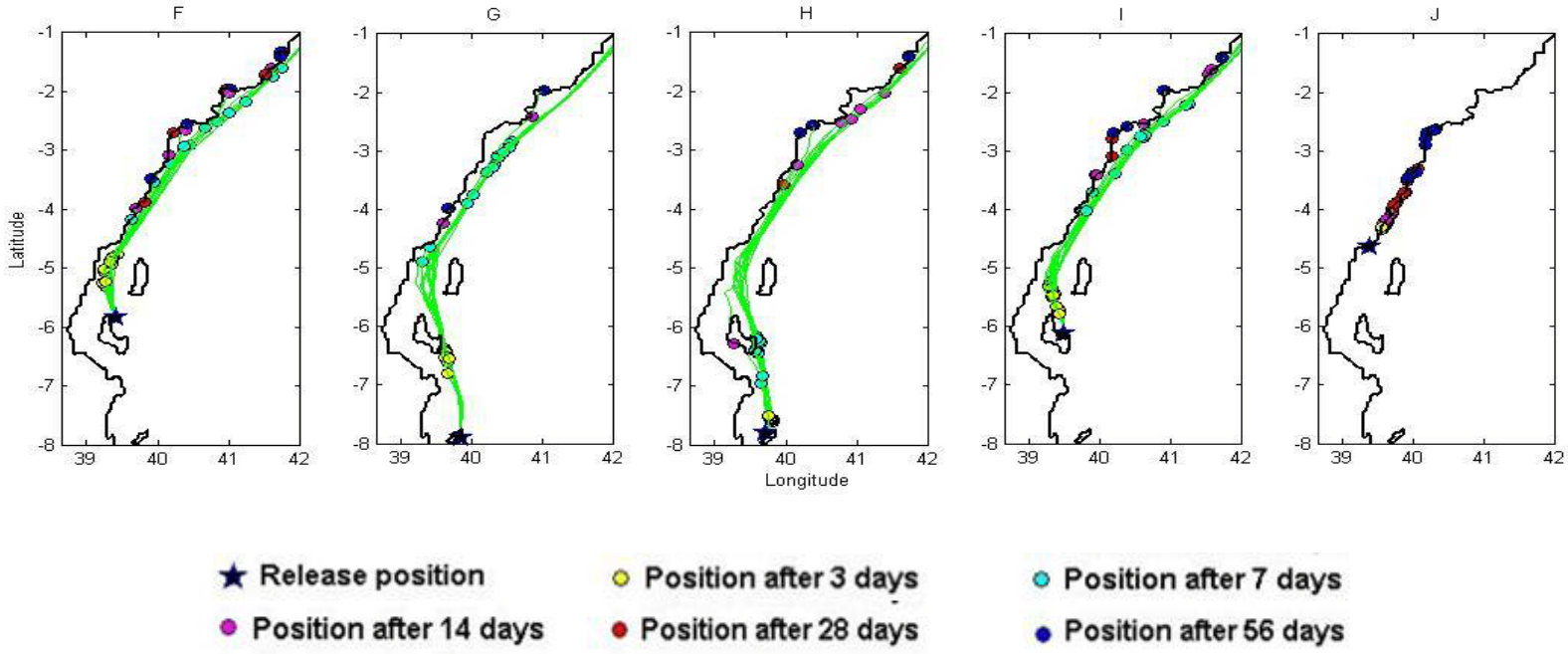


**Figure 31b. Trajectories of the particles released at positions F-J during June to July. Position through time is marked following the color key above. The eight trajectories (green lines) represent the releases from eight consecutive weeks.**

## 4. Discussion

The nested ROMS model using bulk heat fluxes calculated from model SST values ('KTCM Bulk' model) shows an improvement in the capability to hindcast SST, as represented by the Pathfinder satellite data, in comparison to the global model OFES that is in general 1 to 2$^{o}$C colder than the observations. Further studies at smaller spatial and temporal scales are needed to determine the ability of any of these models to reproduce the small scale SST patterns present in satellite observations and to gain more insight on the local upwelling and its effect on SST. Higher spatial resolution models with higher frequency surface and tidal forcing will be needed. Satellite SST observations can continue to be used to corroborate model results, but more *in situ* velocity and temperature measurements in the vicinity of the islands are needed to assess subsurface dynamics. So far the skill to hindcast temperature at depth as represented by WOD profiles is acceptable, but very similar to the skill of OFES. A better approach would be to assess the agreement in the spatial patterns of model temperatures and observations on specific depth horizons. This has not been done here. The offshore salinity range and its vertical and horizontal distribution is qualitatively in good agreement with values reported in the literature.

The seasonality of the EACC, the SC and the offshore jet that contributes to the ECC in the model are qualitatively in agreement with field studies (Swallow *et al*,1991, Schott and McCreary, 2001, Reid, 2003, Schott *et al*, 2009). Quantitative

comparisons with observations of these large scale features are difficult to carry out due to the lack of observations throughout the year or a long time series that will allow us to build an observation-based climatology. However there is agreement on the order of magnitude of the volume transport of the features and its seasonality as far as the observation and descriptions reported in the literature allow comparison. The prevalence of northward flow along the coast during January and February when the wind is blowing in the opposite direction is counterintuitive; however, it highlights the importance of the large-scale forcing on the regional circulation. Further analysis to determine the effects of local winds on coastal circulation will be of interest. A more detailed examination of the terms of the momentum equations solved by the KTCM model could provide additional insight but has not been done. Empirical Orthogonal Functions (EOF) analysis of the velocity and/or temperature fields will identify the dominant modes of variability and better characterize the seasonal and spatial variability of the regional circulation. EOF analysis of the velocity fields at the 3 open boundaries will be useful for determining the most important patterns and seasonality of the in/out flow driving the circulation.

The hydrodynamic model presented here is a tool that offers a wide range of possibilities to study physical phenomenon despite the lack of observations, and provides opportunities for making additional advances in our understanding of the regional ocean circulation and the effect of the circulation on marine ecosystems in the region. After a phenomena is studied with the model, optimal observational campaigns

that will yield the data needed to validate the model results could be designed, in order to maximize the use of the limited economical resources dedicated to the study of the East African Coastal Ocean. Assimilation of new physical data would increase the fidelity of the model fields. The model results also might be improved through the use of higher resolution and/or more realistic forcing fields. The use of scatterometer derived winds from QuickSCAT and future sensors with higher spatial and time resolution could improve the model realism. The model domain and its resolution (both vertical and horizontal) can be modified to better assess specific phenomena of interest. For example, to make a more thorough analysis of the interaction of the Somali Current and the EACC, a larger domain that encompasses both currents in their entirety should be used. The modeled time period can also be modified as required as long as data to create the forcing are available. OFES and NCEP provide the required boundary conditions and surface forcing, respectively, since the 1950s.

The simulations for 2000 and 2007 demonstrated a significant level of inter-annual variability in the circulation and water temperatures. Modeling experiments changing only the boundary conditions while keeping the same surface forcing or vice versa could be done to determine the relative importance of the remote forcing (advected temperature and momentum) vs. local forcing (local winds, surface heating/cooling) on the inter-annual variability of the circulation and SST patterns. Modeling additional years will give insight on the evolution of the ocean state during a wider range of conditions over a longer period. The hindcast ability of the model can

also address the effects of global climate changes in the ocean circulation of the region. Making a climatological model of a previous decade, and comparing it to the climatology presented here would give an idea of the effects of global climate change on the circulation and hydrography of the region. A similar nested model run within the IPCC's future models could extend the examination of regional changes in ocean circulation into the future.

The 'KTCM Bulk' model can also be used to provide boundary conditions for nested smaller scale, higher resolution, process oriented models that could be helpful to assess local environmental issues along the East African coast. The preliminary studies shown here could be refined to study specific local phenomena such as the effect of climate change on the circulation, sea level rise, coastal erosion, dispersion of pollutants, coral stress due to extreme temperatures, coral reef connectivity and the spillover effect of MPAs. Very high spatial resolution (grid spacing <=1km) small-scale models would be ideal to make these studies more realistic.

Adding tidal forcing to the model will be an important extension, since tidal currents at near-diurnal time scales may create small-scale circulation patterns in places with intricate bathymetric features (Shaghude *et al*, 2002). River runoff created buoyancy driven currents during the rainy seasons may also be important in generating circulation at smaller spatial scales. Rivers are the main source of sediments to coastal areas and should be included in examining sediment transports, as

well as in studies of coral stress monitoring, due to the high sensitivity of coral to turbidity.

ROMS and other models (e.g. FVCOM[7], ADCIRC[8]) offer increased levels of complexity, which allow the representation of realistic scenarios to assess a variety of targeted problems. Some process oriented models that could be helpful are already embedded into the ROMS code. The waves and sediment transport modules could be used to assess coastal erosion problems. The 'point source' capability could be configured to represent rivers and/or sewage discharges. The 'passive tracer' option could also be used to track pollutant dispersion. Modifications to the particle tracking code in ROMS could be made to represent different coral reef organisms and study their dispersal and connectivity patterns. The release of particle clusters from nearby positions would better represent the spawning of coral reef organisms. A random walk or other modifications could be added to the trajectories to account for dispersion due to subgrid scale turbulence. Statistics should be used to calculate the probability that particles released from a specific reef will reach a suitable habitat location to settle. For these studies parameters like pelagic larval duration, density, buoyancy control and/or swimming ability should be taken into account. Detailed maps of reefs location and geometry at a very fine spatial scale would be necessary to be included in the model bathymetry and to identify suitable habitat locations.

The resolution of the KTCM Bulk model highly increases the details of the circulation around the islands (e.g. Fig 20). The circulation patterns of the KTCM model are likely to be more realistic than those of the OFES model since bathymetry is represented more accurately, allowing nonlinear interaction between the flow and the bottom topography to be better resolved. However, velocity observations on the shelf are needed to corroborate the model circulation patterns.

Accurate high resolution circulation patterns in the near shore region are critical to assess environmental issues in the East African Coastal region. Observational studies of coral reef larval dispersal suggest that near-field circulation has a profound influence on dispersal and recruitment of coral larvae (Sammarco and Andrews, 1988). Implications of the described circulation regimes in the near-shore region on environmental issues such as pollution dispersal, mariculture, coral reef health and connectivity of coral reef organisms, can be inferred from the results of this purely physical model. The strong northward flow during March to November imply shorter residence time of the water in the Zanzibar and Mafia Channels compared to the sluggish circulation period during December, January and February. Locally the strong northward flow regime during most of the year is a positive factor for pollution dispersion, since the concentration of pollutants near the source will decrease due to rapid flushing. However, pollutant concentrations will impact larger (downstream) regions, but at lower absolute concentrations. Mixing is enhanced by strong flows which will also reduce plume concentrations. In general, lower concentrations of

pollutants in a larger area has less impact on the ecosystems than higher pollution concentrations in a smaller area, which will be the case during the sluggish circulation regime. Strong flows are also beneficial for mariculture and coral reef health due to the constant replacement of the oxygen- and nutrient-depleted water surrounding the organisms.

The particle tracking experiments confirm that particles released during the sluggish circulation period are retained in a small area. Unlike the negative effect on pollutant concentrations, the period of higher local retention may favor coral reef species recruitment. Retention in the region of the originating adult population will make it more likely that they will find a suitable subtract on which to settle, providing conditions that will allow them to reach adulthood. In general self recruitment (e.g., self-seeding) is an important replenishment mechanisms for reef ecosystems and the primary replenishment mechanism for coral larvae (Sammarco and Andrews, 1988). If larvae are advected passively, they will travel long distances during the northward flow regime. The probability of finding suitable habitat a long distance away from the parent population is much less. However, this scenario provides the possibility of longer range, one-way connectivity between southern and northern reefs.

Improvements in our understanding of larval dispersion and connectivity patterns are crucial to determine optimal management strategies to protect the coral reef ecosystems. For example if a population is shown to be mainly self-seeded, a

single marine protected area (MPA) could be successful. If considerable larval exchange between distant populations (i.e. southern and northern reefs) is shown to occur, multiple connected MPAs may enhance the survival and/or persistence of existing populations. Species specific biological factors such as seasonality of spawning, pelagic larval duration and behavior (swimming ability or buoyant control) can significantly alter the dispersion and connectivity patterns of coral reef organisms. Individual based biological modeling and other process-oriented models (ideally complemented with observations) should be used to extend the results obtained here from a purely physical model.

## 5. Summary

1. The Kenyan-Tanzanian Coastal Model (KTCM) is a 4km resolution oceanographic circulation model for the East African coastal region, 0-10° S, 38.7-46.98° E. It was developed using ROMS and forced by 8-year (2000-2007) average seasonal climatology of the forcing fields. Surface forcing fields were derived from the daily NCEP/NCAR products. The forcing fields along the boundaries of the KTCM model were provided by monthly fields from the Japanese global OFES model. A realistic bathymetry for the model was constructed by fusing ETOPO-2 and local bathymetric data.

2. Two different surface forcing configurations were tested. One ('Bulk') used atmospheric parameters from the NCEP fields to calculate the net heat flux using a bulk formulation. The other ('Qcorrected') used a model option to adjust the net heat flux from the NCEP fields to match model SST fields to the seasonal SST climatology constructed from the OFES fields.

3. Fields of SST and SSH anomalies from the two KTCM model configurations and OFES were compared to Pathfinder satellite SST and AVISO SSH climatologies. The KTCM Bulk model and OFES represented the annual patterns of monthly mean satellite SST with similar skill, which was superior than that attained with the Qcorrected model; this was true for both inshore (depths<300m) and offshore (depths>300m) regions of the model domain. The KTCM Bulk monthly mean SST

was also closer to the satellite observations throughout the year, while OFES and KTCM Qcorrected SSTs were in general too cold. Positive and negative SSH anomaly features observed in the AVISO altimeter product were qualitatively reproduced in all three physical models. However, gradient and mesoscale features in the models were shifted in space, which resulted in relatively poor agreement between the model and altimeter fields when calculating quantitative comparisons. The OFES SSHa field was more similar to AVISO SSH.

4. Comparisons of the three physical models to temperature profiles extracted from the World Ocean Dataset (WOD) showed that all three models represented the temperature patterns with depth equally well during all months. The correlation coefficients were all greater than 0.65, with no significant differences between the ability of the three models to hindcast subsurface water temperatures. A similar analysis looking at spatial agreement on specific depth horizons will be a more objective analysis to assess the ability of the models to hindcast subsurface hydrography.

5. The offshore range of modeled salinity agrees with literature values for the EACC. Quantitative comparisons with WOD salinity profiles resulted in low correlations, due to the limited number and high variability of the *in situ* measurements. The main features of the salinity vertical and cross-shore structure in the model results were similar to an April salinity section off Tanzania from the literature.

6. The seasonality of the circulation, SST and SSS patterns were described based on the climatological results of the KTCM Bulk model, given its more realistic representation of the SST fields.

7. The East African Coastal Current (EACC), Somali Current (SC) and Southern Gyre (SG) circulation features appear in the model results. The SC is only present during the NE monsoon, and the SG during the SE monsoon as reported in studies describing the large scale circulation of the Indian Ocean. The mean volume transport of the EACC at 4.5$^{o}$S was 13 Sv compared to 19.9 Sv reported by Swallow *et al* (1991) from a hydrographic section.

8. The increased resolution of the KTCM ROMS application provided more detailed circulation patterns on the shelf compared to the OFES model. The features are expected to be more realistic, since the bathymetry and morphology of the coast are better represented in the KTCM model. However, this region of the Southern

Indian Ocean has had relatively sparse *in situ* oceanographic observations, so it is currently difficult to assess the agreement of the model results with data.

9. Strong seasonality was observed in the shelf circulation. A sluggish period occurs during December, January and February, when the flow through the shallow channels (Zanzibar and Mafia) is minimal. During the other months of the year flow in the channels is strongly to the north.

10. Lagrangian particle tracking experiments were done using the float tracking code within ROMS and the climatological forcing. Passive surface particles were released every week from 10 separate reef locations, and tracked for 60 days. Particle trajectories showed strong seasonality in shelf retention time and particle dispersion. The December to February period is highly retentive, with particles remaining within the 100 $km^2$ area surrounding the release positions. During the rest of the year, strong northward advection along the coast transported particles up to 400 km in one week.

11. The seasonality of the retention time in the near shore region has implications for the dispersion of pollutants discharged into the ocean. During Dec-Feb, pollutants discharged into the Zanzibar Channel will remain concentrated and localized near the sources. Enhanced mixing and shorter residence times during the strong northward flow regime will decrease pollutant concentrations near the source, but carry pollution plumes to locations farther north.

12. Seasonality of the dispersion patterns will affect recruitment of populations of coral reef organisms. Longer retention periods on the shelf will increase the probability of self recruitment, while the non-retentive period may provide longer range, one-way connectivity between southern and northern reefs. This seasonality may impact population dynamics and the success of MPAs designed to preserve reef ecosystems. Results of the model may inform the design (placement and size) of adequate MPAs.

13. Simulations with specific forcing fields for 2000 and 2007 showed strong differences in circulation and SST patterns. The 2000 SSTs were in general colder than the climatology, while 2007 was warmer. In 2007 the circulation showed more eddy activity than the climatology or the first half of 2000. Equatorial dynamics appears to be responsible for the increased variability in the eddy field. This application to specific years with contrasting forcing shows the potential of the model for examining interannual variability and the effects of global climate changes on the circulation of the region.

14. The Eulerian and Lagrangian fields produced by the model can be used in future studies to answer more specific questions regarding the physical processes which drive the circulation in the region. They could also be used to investigate physical and biogeochemical processes, sediment and point source transports. The KTCM could provide boundary conditions for nested, higher resolution, process-oriented

models designed to address local environmental issues at smaller scales within the anthropogenically influenced regions between the islands and the mainland.

15. The hydrodynamic model presented here offers a wide range of possibilities to examine physical phenomena despite the lack of observations. It can also be used to design optimal observational systems and campaigns for specific process studies. The realism of these model studies could be improved by including tides and rivers, using more realistic wind forcing such as QuickSCAT and assimilating hydrographic or satellite measurements.

16. Results from the 'KTCM Bulk' model have yielded insight on the seasonality of the circulation patterns of the studied region. The work reported here provides a foundation or framework for better assessing environmental problems in the Kenyan and Tanzanian Coastal Ocean.

**Endnotes**

[1] OFES http://www.jamstec.go.jp/esc/ofes/eng/index.html

[2] HYCOM http://www.hycom.org/

[3] World Ocean Data Base. National Oceanographic Data Center (NODC). NOAA Satellite and Information Service http://www.nodc.noaa.gov/OC5/SELECT/dbsearch/dbsearch.html

[4] Pathfinder v5 http://www.nodc.noaa.gov/SatelliteData/pathfinder4km/userguide.html

[5] AVISO http://www.aviso.oceanobs.com/en/data/products/sea-surface-height-products/global/msla-mean-climatoloy/index.html#c7275

[6] Ocean Data and Information Network from Africa. http://www.odinafrica.org

[7] FVCOM http://fvcom.smast.umassd.edu/FVCOM/index.html

[8] ADCIRC http://adcirc.org/

**Bibliography**

Anderson, D.L.T., Carrington, D.J., Corry, R., Gordon, C. 1991. Modeling the variability of the Somali Current. Journal of Marine Research, 49, 659-696.

Aoki, S., Hariyama, M., Mitsudera, H., Sasaki, H., Sasai, Y. 2007. Formation regions of Subantarctic Mode Water detected by OFES and Argo profiling floats, Geophys. Res. Lett., 34, L10606, doi:10.1029/2007GL029828.

Chambwera, M., MacGregor, J. 2009. Cultivating success: the need to climate-proof Tanzanian agriculture. International Institute for Environment and Development briefing papers. September 2009. 2 pp.

Da Silva, J.C.B., New, A. L., Magalhaes, J.M. 2009. Internal solitary waves in the Mozambique Channel: Observation and interpretation. Journal of geophysical Research, 114, C5, doi:10.1029/2008JC005125.

Fay, M. 1992. Maziwi Island off Pangani (Tanzania): History of its destruction and possible causes. UNEP Regional Seas Report and Studies, 139. 43pp.

Fieux, M. 2001. Indian Ocean Equatorial Currents. Academic Press. 1298-1308 DOI: 10.1006/rwos.2001.0367

Haidvogel, D.B., Arango, H., Budgell, W.P., Cornuelle, B.D., Curchitser, E., Di Lorenzo, E., Fennel, K., Geyer, W.R. A.J. Hermann, A.J., Lanerolle, L., Levin, J., McWilliams, J.C., Miller, A.J, Moore, A.M., Powell, T.M., Shchepetkin, A.F., Sherwood, C.R., Signell, R.P, Warner, J.C., Wilkin, J. 2008. Ocean forecasting in terrain-following coordinates: Formulation and skill assessment of the Regional Ocean Modeling System. Journal of Computational Physics, 227, 3595–3624.

Hamner, W. M., Hauri, I.R. 1981. Effects of island mass: Water flow and plankton pattern around a reef in the Great Barrier Reef lagoon, Australia. Limnol. Oceanogr., 26, 1084-1102.

Hermes, J.C., Reason, C.J.C. 2008. Annual cycle of the South Indian Ocean (Seychelles-Chagos) thermocline ridge in a regional ocean model. Journal of Geophysical Research, 113, C4, doi:10.1029/2007JC004363.

Masumoto, Y., and Coauthors, 2004: A fifty-year eddy-resolving simulation of the World Ocean -Preliminary outcomes of OFES (OGCM for the Earth Simulator). J. Earth Simul., 1, 31–52

Matano, R.P., Beier, E.J., Strub, P.T. 2002. Large-Scale Forcing of the Agulhas Variability: The Seasonal Cycle. Journal of Physical Oceanography, 32, 1228-1241.

Matano, R.P., Beier, E.J., Strub, P.T. 2008. The seasonal variability of the circulation in the South Indian Ocean: Model and observations. Journal of Marine Systems, 74, 315-328.

Mayorga-Adame, C. G. 2007. Ocean Circulation of the Zanzibar Channel: A Modeling Approach. 8pp. http://www.zanzibarproject.org/students/mayorga-adame/mayorga-adame_final_report.pdf

Mishra, A.P., Rai, S., Pandey, A.C.. 2007. Ocean Model Simulation of Southern Indian Ocean Surface Currents. Marine Geodesy, 30, 345-354.

Moulton, M.R., Mayorga-Adame, C. G., Garcia- Reyes, M., Nadeau,P.C., Zavala-Garay, J., Theiss, J. 2010. Modeling Seasonal Dynamics in the Zanzibar Channel. Poster presented at Ocean Science Meeting, Portland, OR, 2010.

Nauw, J.J., van Aken, H.M., Webb, A., Lutjeharms, J.R.E ., De Ruijiter, W.P.M. 2008. Observations of the southern East Madagascar Courrent undercurrent and countercurrent system. *J. Geophys. Res,* 113, C8, doi:10.1029/2007Jc004639.

Odido, M., Mazzilli, S. (Eds). 2009. African Oceans and Coasts. IOC Information Document. 1255 pp. UNESCO-IOC Regional Bureau for Sciences and Technology in Africa. Kenya.

Reid, J.L. 2003. On the total geostrophic circulation of the Indian Ocean: flow patterns, tracers, and transports. Progress in Oceanography, 56, 137-186.

Richmond, M. D. (Ed). 1997. A Guide to the Seashores of Eastern Africa and The Western Indian Ocean Islands. Swedish International Development Cooperation Agency (SIDA). 448 pp. ISBN 91-630-4594-X.

Roman, R.E., Lutjeharms, J.R.E. 2009. Red Sea Intermediate Water in the source regions the Agulhas Current. Deep-Sea Research I, 56, 939-962.

Sammarco, P. W., Andrews, J. C. 1988. Localized Dispersal and Recruitment in Great Barrier Reef Corals: The Helix Experiment. Science, 239, 1422-1424.

Shaghude, Y. W., Wannas, K.O., Mahongo, S. B. 2002. Biogenic Assemblage and Hydrodynamic Settings of the Tidally Dominated Reef Platform Sediments of the Zanzibar Channel. Western Indian Ocean J. Mar. Sci. 1(2): 107–116.

Schott, F. A., McCreary, J. 2001. The monsoon circulation of the Indian Ocean. Progress in Oceanography, 51, 1-123.

Schott, F.A., Xie, S.P., McCreary J.P. 2009. Indian Ocean circulation and climate variability. Reviews of Geophysics, 47, 1,doi:10.1029/2007RG000245.

Sen Gupta, R., Desa, E (Eds). 2001. The Indian Ocean: a perspective. Vol 1. 396 pp. A.A. Balkema Publishers.

Smith, S. L. (Ed) 1998. The 1994-1996 Arabian Sea Expedition: An integrated, interdisciplinary investigation of the response of the northwestern Indian Ocean to Monsoonal Forcing, Part 1. Deep-Sea Research II,45 (10-11), pp 1905- 1915.

Smith, S. L. (Ed) 1999. The 1994-1996 Arabian Sea Expedition, Part 2. Deep-Sea Research II, 46 (8-9), pp 1531-1964.

Smith, S. L. (Ed) 2000. The 1994-1996 Arabian Sea Expedition, Part 3. Deep-Sea Research II. 47 (7-8), pp 1177-1677.

Snoussi, M., Kitheka, J., Shaghude, Y., Kane, A., Arthurton, R., Le Rissier, M., Virji, H. 2007. Downstream and coastal impacts of damming and water abstraction in Africa. Environmental Management 39, 587-600.

Swallow, J.C., Schott, F., Fieux, M. 1991. Structure and Transport of the East African Coastal Current. Journal of Geophysical Research, 96, 22245-22257.

Taylor, K.E. 2001. Summarizing multiple aspects of model performance in a single diagram. J. Geophys. Res., 106, 7183-7192.

Temple, P. H., Sundborg, A. 1972. The Rufiji River, Tanzania Hydrology and Sediment Transport. Geografiska Annaler. Series A, Physical Geography. Studies of Soil Erosion and Sedimentation in Tanzania. 54 (3-4), 345-368.

Van der Werf, P. M., van Leeuwen, P. J., Ridderinkhof, H., de Ruijter, W. P. M. 2010. Comparison between observations and models of the Mozambique Channel transport: Seasonal cycle and eddy frequencies, *J. Geophys. Res*, 115, C2, doi:10.1029/2009JC005633.

Vimal Kumar, K.G., Dinesh Kumar, P.K., Smitha, B.R., Habeeb Rahman. , Jacob Josia., Muraleedharan, K.R., Sanjeevan,V.N., Achuthankutty, C.T. 2008. Hydrographic characterization of southeast Arabian Sea during the wane of southwest monsoon and spring intermonsoon. Environmental Monitoring and Assessment, 140, 231- 247.

Wellington, G. M., Victor, B. C. 1989. Planktonic larval duration of one hundred species of Pacific and Atlantic damselfishes (Pomacentridae). Marine Biology, 101, 557-567.

Whittick, A. (Ed). 2007. Western Indian Ocean Marine Science Association Annual Report 2006. WIOMSA. 26 pp.

Wiggert, J.D., Murtugudde, R. G., Christian, J.R. 2006. Annual ecosystem variability in the tropical Indian Ocean Results of a coupled bio-physical ocean general circulation model. Deep-Sea Research II, 53, 644-676.

**Appendix A.**

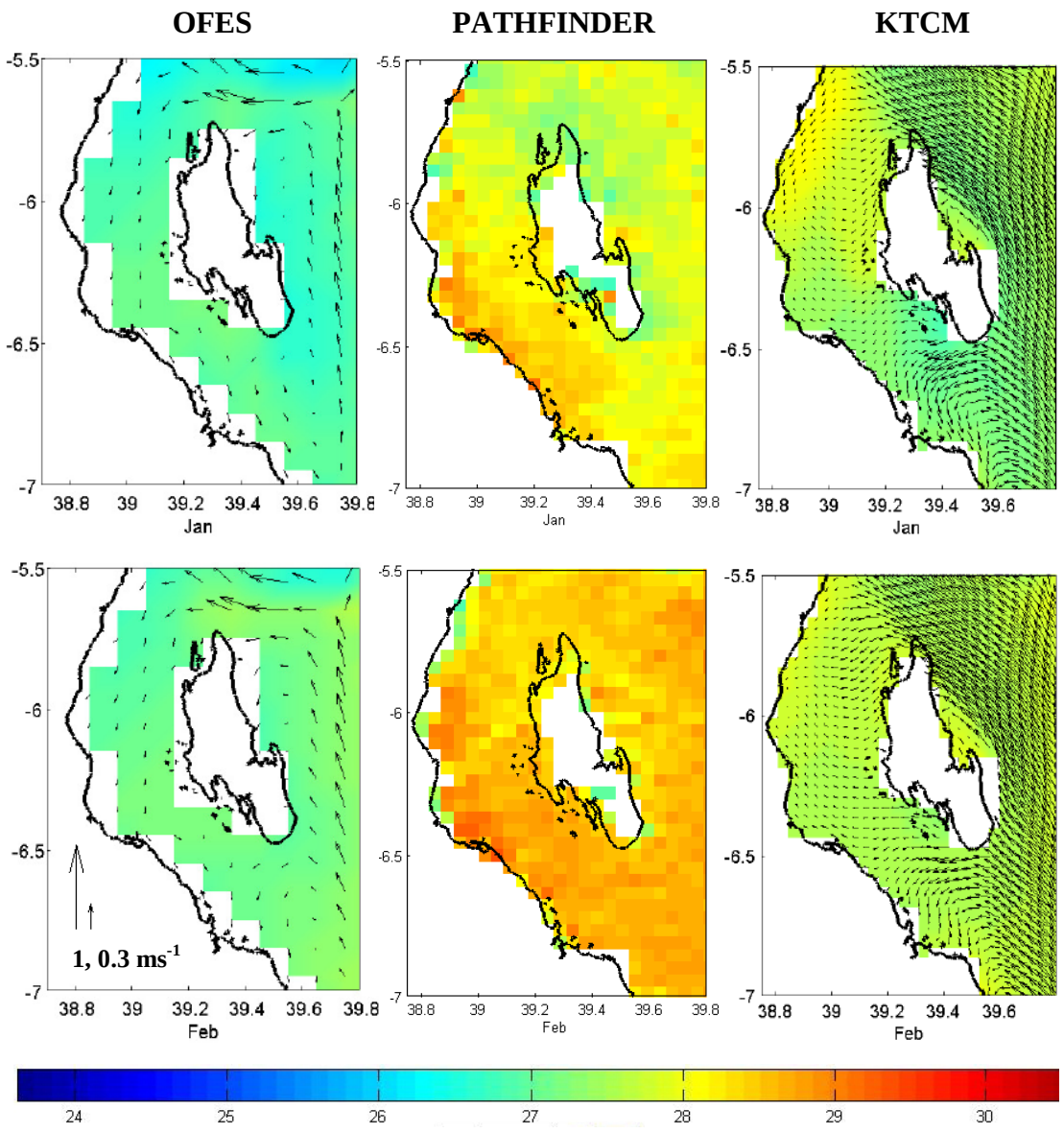


**Figure A1. SST around Zanzibar Island is shown in color for January (Top) and February (Bottom), from OFES, the Pathfinder satellite product and KTCM. Velocity vectors are shown at full resolution for both models. Scale arrows in the lower left panel apply to all panels.**

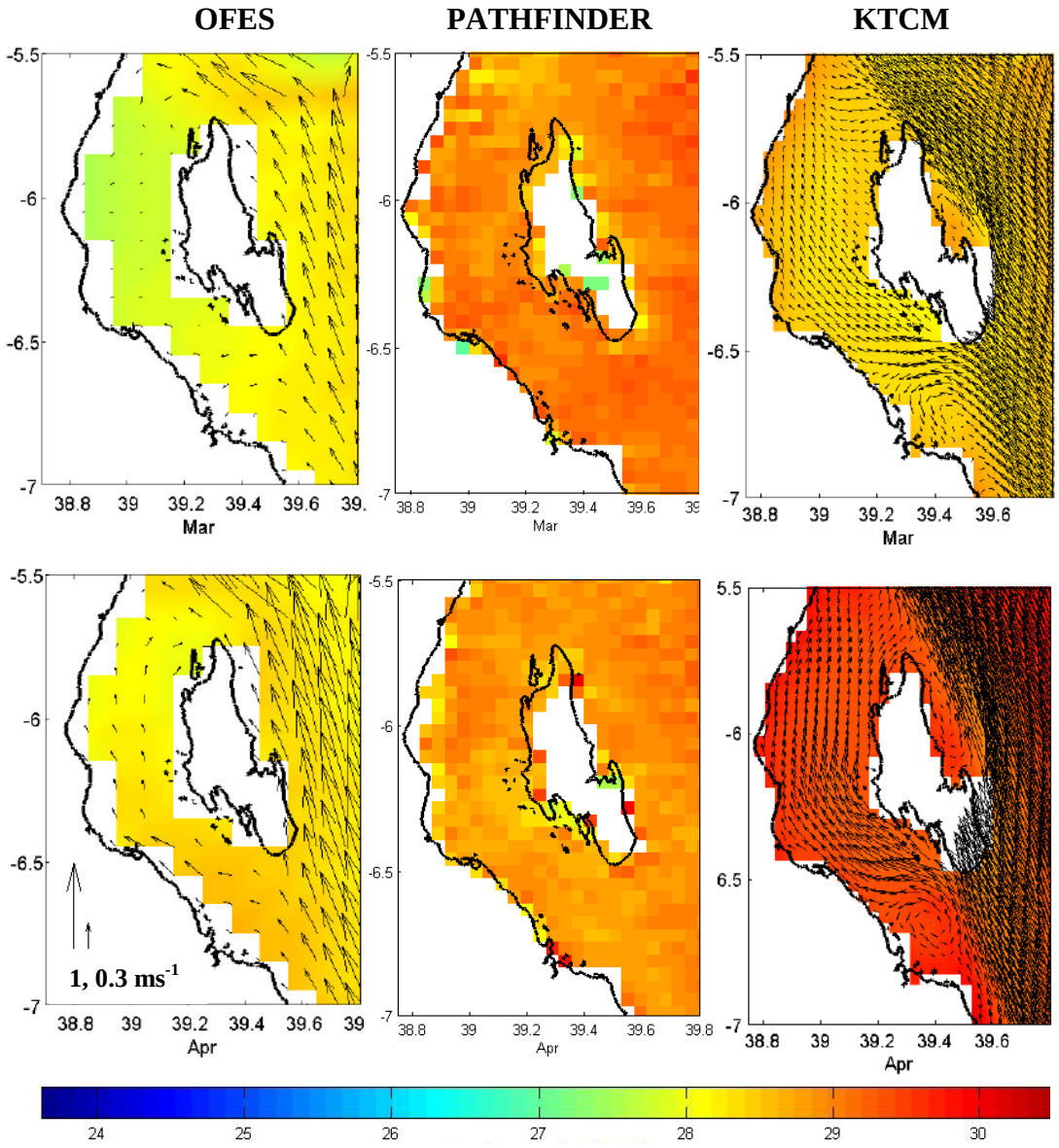


**Figure A2. SST around Zanzibar Island is shown in color for March (Top) and April (Bottom), from OFES, the Pathfinder satellite product and KTCM. Velocity vectors are shown at full resolution for both models. Scale arrows in the lower left panel apply to all panels.**

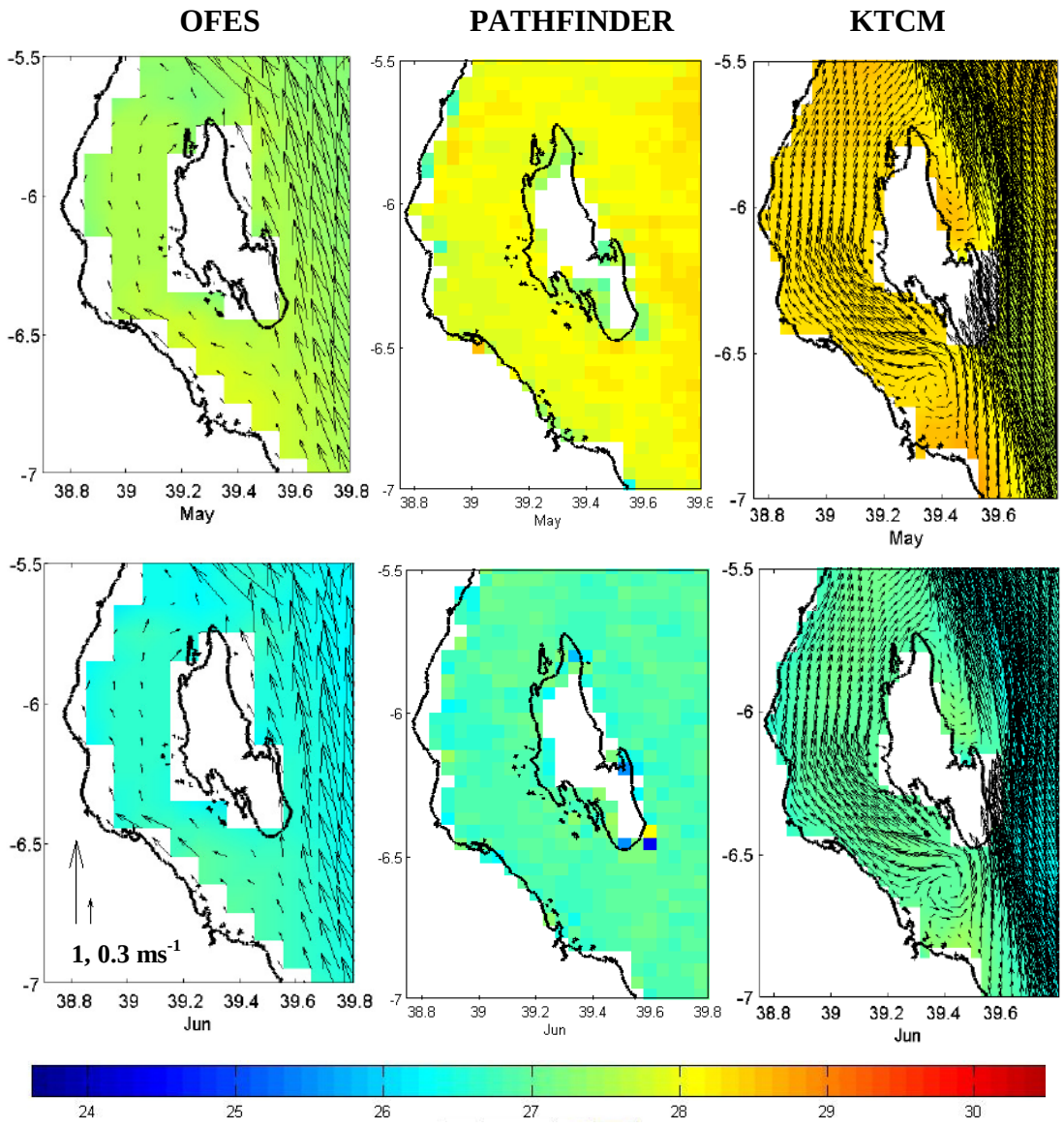


**Figure A3. SST around Zanzibar Island is shown in color for May (Top) and June (Bottom), from OFES, the Pathfinder satellite product and KTCM. Velocity vectors are shown at full resolution for both models. Scale arrows in the lower left panel apply to all panels.**

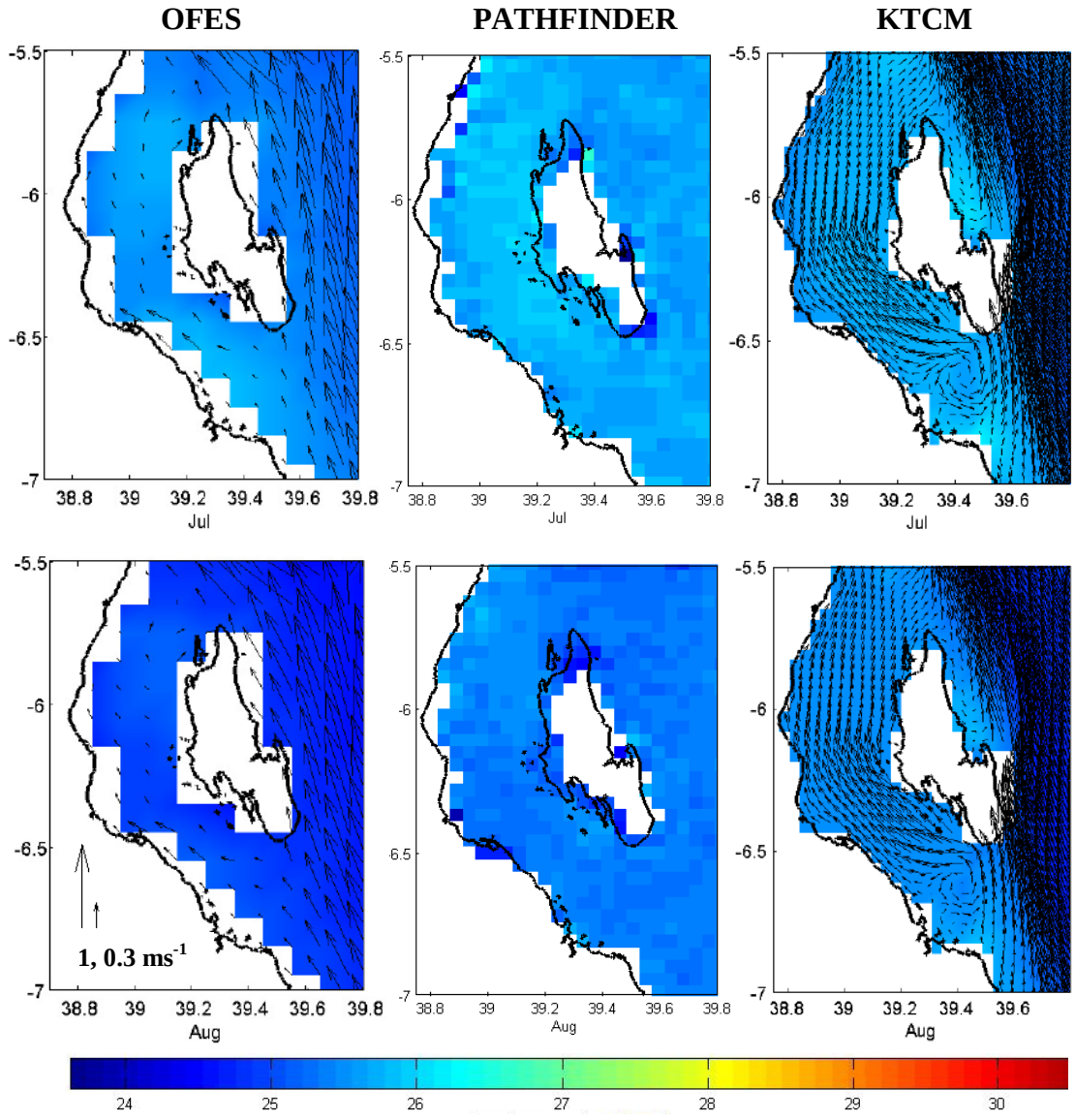


**Figure A4. SST around Zanzibar Island is shown in color for July (Top) and August (Bottom), from OFES, the Pathfinder satellite product and KTCM. Velocity vectors are shown at full resolution for both models. Scale arrows in the lower left panel apply to all panels.**

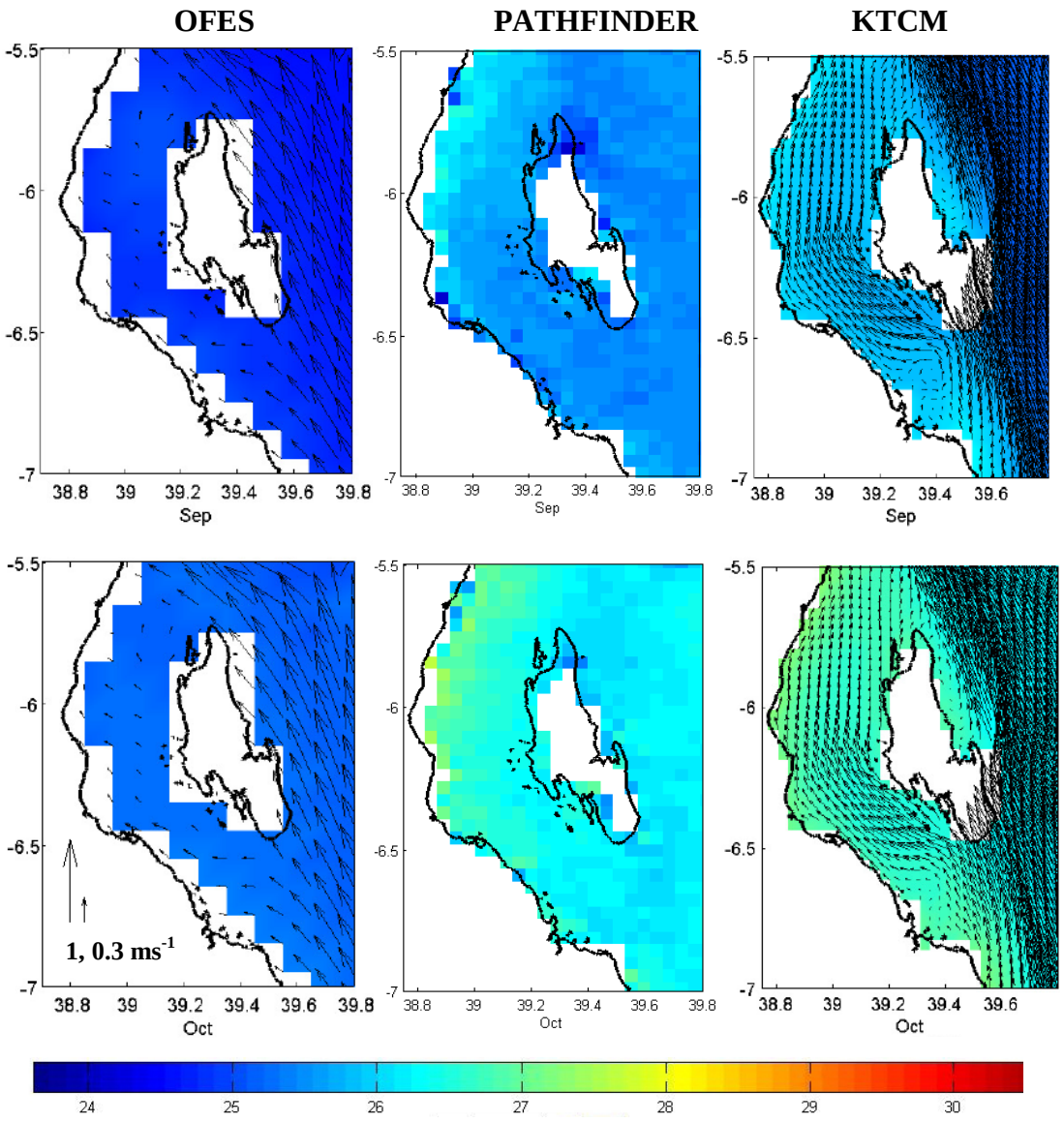


**Figure A5. SST around Zanzibar Island is shown in color for September (Top) and October (Bottom), from OFES, the Pathfinder satellite product and KTCM. Velocity vectors are shown at full resolution for both models. Scale arrows in the lower left panel apply to all panels.**

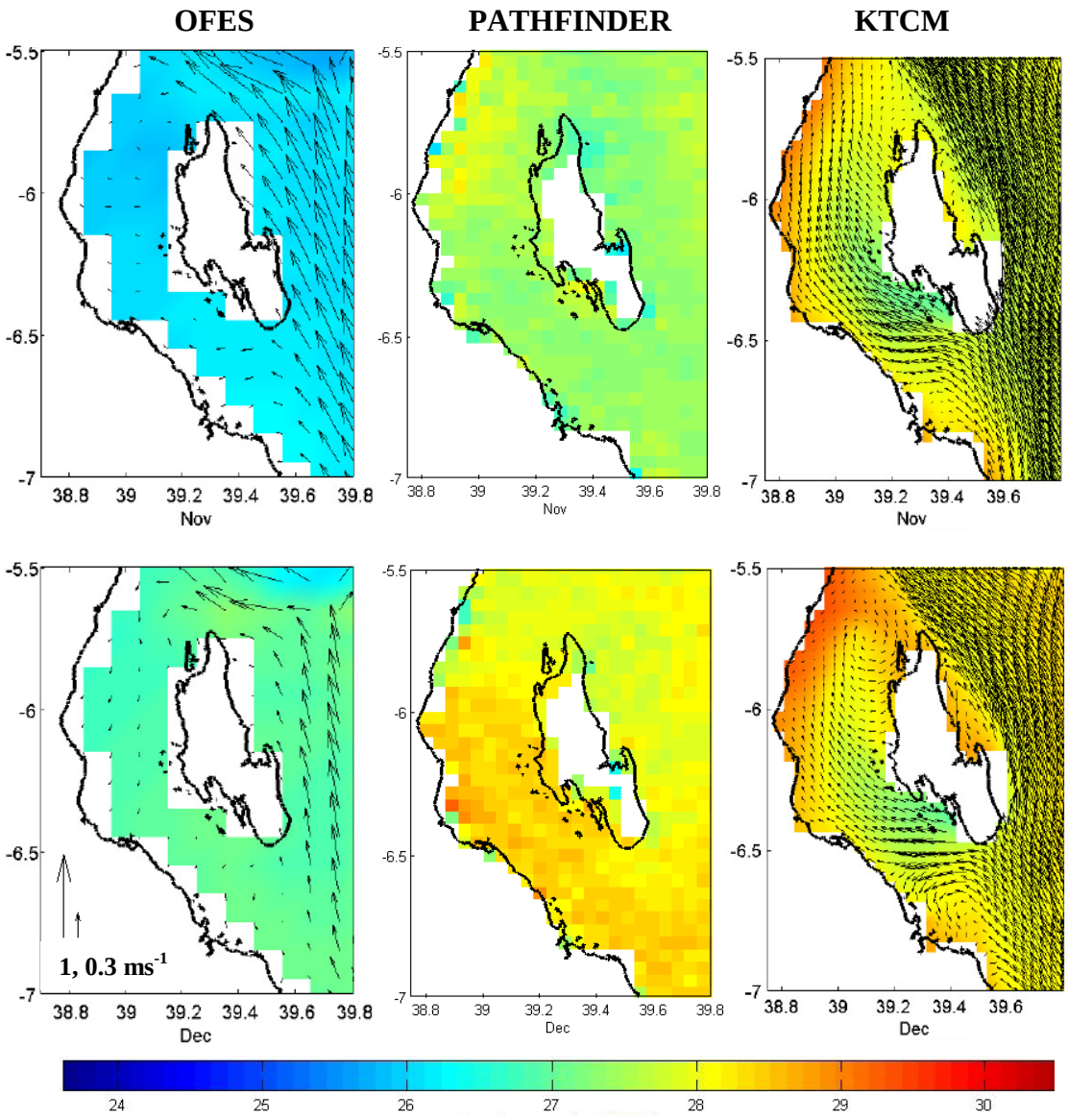


**Figure A6. SST around Zanzibar Island is shown in color for November (Top) and December (Bottom), from OFES, the Pathfinder satellite product and KTCM. Velocity vectors are shown at full resolution for both models. Scale arrows in the lower left panel apply to all panels.**